

CHARACTERIZATION AND UTILIZATION OF INJECTABLE HYDROGELS FOR TISSUE ENGINEERING APPLICATIONS

**A Thesis Submitted to
the Graduate School of Engineering and Sciences of
İzmir Institute of Technology
in Partial Fulfillment of the Requirements for the Degree of**

MASTER OF SCIENCE

in Bioengineering

**by
Meltem GÜZELGÜLGEN**

**July 2020
İZMİR**

ACKNOWLEDGMENTS

Firstly, I would like to express my sincere and deep gratitude to my supervisor Assoc. Prof. Dr. Ahu ARSLAN YILDIZ for all of her patience, counseling, encouragement, and support throughout my graduate studies. The opportunities she provided to me are very precious and the reason for my academic career has begun.

I gratefully acknowledge the support by the “İzmir Institute of Technology, Biotechnology and Bioengineering Research and Application Center” and “İzmir Institute of Technology, Center for Materials Research” for their technical supports and high-tech laboratories. I would like to express my special thanks to the Assoc. Prof. Dr. Ümit Hakan YILDIZ for AFM facilities and their support.

I especially warmly express my thanks to my family, friends and co-workers for their endless support and encouragement.

ABSTRACT

CHARACTERIZATION AND UTILIZATION OF INJECTABLE HYDROGELS FOR TISSUE ENGINEERING APPLICATIONS

Tissue engineering combines the knowledge of the engineering aspects with life sciences to improve human health. Recent studies in tissue engineering have focused on investigating biocompatible scaffold materials and design. Quince seed hydrogel (QSH) has been used in traditional and modern medicine for skin wound and burn treatments, synovial lubrication, cough and asthma removal, and oral drug delivery with its antioxidant potential and biocompatible aspects. This thesis focuses on developing QSH and evaluating its potential as an injectable hydrogel in treating bone tissue defects as a totally new tissue scaffold and also as a promising tissue filling material.

For this purpose, QSH scaffold optimization was carried out using various concentrations of hydrogel and crosslinkers which were glutaraldehyde (GTA) and 1-Ethyl-3-(3-dimethylaminopropyl)carbodiimide (EDC) / N-hydroxysuccinimide (NHS). Morphological and chemical analysis of QSH was done using SEM, FTIR, AFM, and protein adsorption test. Thus, porosity, swelling ratio, degradation rate and surface characteristics were evaluated. NIH-3T3 and SaOS-2 cell lines were utilized for 3D cell culture formation. Afterward, 3D spheroids were analyzed for cell viability and proliferation by using AlamarBlue and LiveDead assays, and also cell imaging technics. Results showed that QSH scaffolds did not show any cytotoxic effect on NIH-3T3 and SaOS-2 cells. The optimum results were achieved with 2 mg/mL of QSH and 0.03 M GTA concentrations; where 76.59 μm average pore size, 56.8 fold water holding capacity and at least 80% cell viability was observed. Therefore, it was concluded that QSH has a high potential to promote tissue engineering applications with its injectable texture as a filling material.

ÖZET

ENJEKTE EDİLEBİLİR HİDROJELLERİN KARAKTERİZASYONU VE DOKU MÜHENDİSLİĞİ UYGULAMALARINDA KULLANIMI

Doku mühendisliği, insan sağlığını iyileştirmek için yaşam bilimlerinin mühendislik temelleriyle bir araya getirilmesidir. Bu alanındaki güncel çalışmalar, biyoyumlu doku iskelesi malzemelerinin üretimi ve geliştirilmesi alanına odaklanmıştır. Ayva çekirdeği hidrojeli (AÇH), geleneksel ve modern tipta cilt üstü yara ve yanık tedavileri, eklem arası yüzey kayganlaştırması, öksürük-astım tedavisi ve antioksidan potansiyeli, biyoyumlu özellikleri sayesinde oral ilaç taşınımı sistemlerinde kullanılmıştır. Bu tez, AÇH'nin geliştirilmesi ve elde edilen jelin kemik dokusu hasarlarında kullanılmak üzere, enjekte edilebilir hidrojel formunda tamamen yeni bir malzeme ve doku dolgu materyali olarak kullanım potansiyelinin incelenmesi konusuna odaklanmıştır.

Bu amaçla, AÇH doku iskelesi, çeşitli jel ve çapraz bağlayıcı (GTA veya EDC/NHS) konsantrasyonları kullanılarak optimize edilmiştir. AÇH; SEM, FTIR ve AFM kullanılarak karakterize edilmiş, protein adsorpsiyonu, gözenekliliği, su tutma kapasitesi ve degradasyon kapasitesi değerlendirilmiştir. Ardından, NIH-3T3 ve SaOS-2 hücre hatları üzerinde AlamarBlue, LiveDead testi ve hücre görüntüleme teknikleri kullanılarak *in vitro* canlılık analizleri gerçekleştirilmiştir. Elde edilen sonuçlar, AÇH iskelelerinin NIH-3T3 ve SaOS-2 hücre hatları üzerinde herhangi bir sitotoksik etkiye neden olmadığını göstermiştir. Karakterizasyon ve canlılık analizine bağlı olarak optimum sonuçlar 2 mg/mL hidrojel ve 0.03 M GTA çapraz bağlayıcı konsantrasyonu ile elde edilmiş olup, 76.59 μm ortalama por boyutu, 56.8 kat su tutma kapasitesi ve inkübasyon süresinin genelinde % 80'in üzerinde hücre canlılığı elde edilmiştir. Tüm bunlara bağlı olarak, AÇH'nin, enjekte edilebilir özelliği ile kemik dokusu hasarlarında dolgu malzemesi olarak kullanılabilme potansiyeli olan, doku mühendisliği uygulamalarında büyük umut vadeden bir malzeme olduğu sonucuna varılmıştır.

TABLE OF CONTENTS

ACKNOWLEDGEMENTS	ii
ABSTRACT	iii
ÖZET	iv
TABLE OF CONTENTS	v
LIST OF FIGURES	vii
LIST OF TABLE	ix
CHAPTER 1 INTRODUCTION	1
1.1. Scope of the Thesis	1
1.2. Tissue Engineering	1
1.2.1. Extracellular Matrix	3
1.3. Biomaterials for Scaffold Fabrication	5
1.3.1. Synthetic Polymers	5
1.3.2. Natural Polymers	6
1.3.2.1. Hydrogel Forming Natural Polymers	7
1.3.2.2. Injectable Hydrogels	8
1.3.2.3. Quince Seed Hydrogel	9
CHAPTER 2 MATERIALS AND METHODS	11
2.1. Materials	11
2.2. Methods	12
2.2.1. QSH Scaffold Fabrication	12
2.2.1.1. QSH Crosslinking with GTA	13
2.2.1.2. QSH Crosslinking with EDC/NHS	14
2.2.2. Characterization of QSH Scaffolds	14
2.2.2.1. Macro Imaging and SEM Analysis	14
2.2.2.2. Pore Size and Distribution Analyses	15

2.2.2.3.	Swelling Analysis.....	15
2.2.2.4.	Degradation Analysis	15
2.2.2.5.	FTIR Analysis	16
2.2.2.6.	AFM Analysis	16
2.2.2.7.	Protein Adsorption Assay.....	17
2.2.3.	3D Cell Culture Studies	17
2.2.3.1.	2D Cell Culture and Maintenance	18
2.2.3.2.	Cell Viability and Proliferation Analyses	18
2.2.3.3.	Live/Dead Analysis	20
2.2.3.4.	Cellular Imaging.....	21
CHAPTER 3	RESULTS AND DISCUSSION	23
3.1.	Optimization of QSH Scaffold Fabrication.....	23
3.2.	Characterization of QSH	32
3.2.1.	Structural and Morphological Analysis	32
3.2.2.	Swelling Analysis	34
3.2.3.	Degradation Analysis	35
3.2.4.	FTIR Analysis	37
3.2.5.	AFM Analysis	39
3.2.6.	Protein Adsorption Assay	41
3.3.	3D Cell Culture Studies, Cell Viability and Proliferation.....	42
3.3.1.	Cell Viability and Proliferation Analyses	42
3.3.2.	3D Cell Culture Morphology and ECM Secretion Analyses....	53
3.3.2.1.	SEM Analyses	53
3.3.2.2.	ECM Formation Analyses	54
CHAPTER 4	CONCLUSION	56
REFERENCES	58

LIST OF FIGURES

<u>Figure</u>	<u>Page</u>
Figure 1.1. Association of three elements of tissue engineering	3
Figure 1.2. Extracellular matrix structure in contact with the cell membrane.....	4
Figure 1.3. Main criteria of injectable hydrogel design.....	9
Figure 3.1. The experimental production and design steps of the QSH scaffold	24
Figure 3.2 QSH production method comparison macro images.....	25
Figure 3.3. QSH production method comparison SEM images	26
Figure 3.4. FTIR spectrum of Wang et al. (2017) method, Wang et al. (2018) method, Ashraf et al. (2018) method in lyophilized and oven-dried forms, our novel method in 2 mg/mL seed concentration	27
Figure 3.5. Directly crosslinked QSH samples without lyophilization	28
Figure 3.6. SEM images of QSH samples via directly crosslinking method	29
Figure 3.7. The experimental production and design steps of the injectable QSH scaffold.....	30
Figure 3.8. Crosslink achievement by sample types of QSH for EDC/NHS crosslinking	31
Figure 3.9. Morphological characterization of QSH scaffolds. Macro images, SEM images and average pore size distribution histograms.....	32
Figure 3.10. Cross-section SEM images of QSH	33
Figure 3.11. Morphological characterization of EDC/NHS crosslinked QSH scaffolds via SEM analysis	34
Figure 3.12. Water holding capacity graphs of QSH samples.....	35
Figure 3.13. Degradation profiles	36
Figure 3.14. FTIR spectrum of non-crosslinked, lightly GTA crosslinked, and heavily GTA crosslinked QSH scaffolds.....	37
Figure 3.15. FTIR spectrum of non-crosslinked, 100 μ L EDC/NHS crosslinked, and 150 μ L EDC/NHS crosslinked QSH scaffolds	39
Figure 3.16. AFM analysis showing the surface characteristics of QSH surface topography and force-distance profiles	40

<u>Figure</u>	<u>Page</u>
Figure 3.17. Protein adsorption graph of QSH	41
Figure 3.18. Cell viability results of NIH-3T3 cells, cell viability against crosslinking parameters and cell number	42
Figure 3.19. Cell viability results of NIH-3T3 cells, cell viability for long term culturing.....	43
Figure 3.20. Cell viability results of SaOS-2 cells, cell viability against cell number ...	44
Figure 3.21. Cell viability results of SaOS-2 cells, cell viability for long term culturing.....	45
Figure 3.22. Cell viability results of SaOS-2 cells evaluated by MTT and AlamarBlue assay in shaking method	45
Figure 3.23. Cell viability results of SaOS-2 cells on EDC/NHS crosslinked injectable QSH scaffolds	47
Figure 3.24. Fluorescence microscope images of Live/Dead assay of NIH-3T3 cells...	48
Figure 3.25. Fluorescence microscope images of Live/Dead assay of SaOS-2 cells from day 1 to 7.....	49
Figure 3.26. Fluorescence microscope images of Live/Dead assay of SaOS-2 cells from day 9 to 15.....	50
Figure 3.27. Fluorescence microscope images of Live/Dead assay of SaOS-2 cells from day 21 to 63.....	51
Figure 3.28. Fluorescence microscope images of Live/Dead assay of SaOS-2 cells on EDC/NHS crosslinked injectable QSH scaffolds	52
Figure 3.29. SEM images of NIH-3T3 cells for long term incubation	54
Figure 3.30. DAPI staining images of NIH-3T3 cells for long term incubation	55
Figure 3.31. Collagen staining images of NIH-3T3 cells for long term incubation	55

LIST OF TABLE

<u>Table</u>	<u>Page</u>
Table 2.1. The molar extinction coefficients for AlamarBlue analysis	20

CHAPTER 1

INTRODUCTION

1.1. Scope of the Thesis

The present study aims to develop a novel, highly porous, and biocompatible natural biomaterial as a scaffold that can mimic ECM structure for tissue engineering applications. Here, quince seeds were used as a natural source to obtain polysaccharide-based natural hydrogel, and the quince seed hydrogel (QSH) was used for 3D cell culture studies. QSH scaffolds were fabricated through the following steps; *(i)* gelation, *(ii)* lyophilization and *(iii)* crosslinking with GTA for preformed scaffolds while injectable hydrogels were fabricated through the *(i)* gelation, and *(ii)* crosslinking with EDC-NHS. Later gelation and crosslinking parameters were optimized. Prior to 3D cell culture application morphological, chemical, and biocompatibility-related properties were evaluated. Finally, QSH was utilized as a scaffold to culture either NIH-3T3 or SaOS-2 cells in 3D microenvironment. Highly porous convenient structure and biocompatible features of QSH with its cost-effectiveness compared to similar commercial products makes it a potent scaffold material that can be used in tissue engineering.

1.2. Tissue Engineering

Tissue engineering focuses on improving the functions of tissues and organs in the body or repairing them [1]. It aims to eliminate waiting lists for organ transplants by fabricating organs from the patient's own cells [2]. The three basic components of the tissue engineering strategy are living cells, biocompatible and biodegradable biomaterials, and bioactive molecules that control cell behavior. Biocompatible and

biodegradable biomaterials are aimed to inhabit living cells and bioactive molecules to improve proliferation and cell viability [3]. There are two basic approaches to tissue engineering described as “top-down” and “bottom-up”[4]. In the traditional top-down approach, porous scaffolds are created and cells are seeded onto prefabricated scaffolds. Optimization of the design parameters such as porosity, pore size, material strength, and biodegradability are important. The material should have suitable porosity to allow neovascularization while providing sufficient mechanical support.

The top-down approach allows the utilization of a wide range of materials including polymers, ceramics, and metals for scaffold fabrication while providing high control over porosity and mechanical properties. Tissues such as skin, bladder, and cartilage which are more similar to two-dimensional tissues can be produced via this approach.[4].

On the other hand, the "Bottom-up" approach follows an opposite methodology than the top-down approach, where modular single units are used to construct complex tissue structures. The bottom-up techniques include 3D bioprinting, cell sheeting and cell-laden microfabrication methods to create tissue from modular units [4]. The bottom-up method is preferred when the aim is to increase the density and/or the metabolic properties of cells to form complex tissues,. Hydrogels can be produced in both ways, and, in this study, the top-down methodology was followed.

Culturing cells *in vitro* is one of the main steps of tissue engineering studies. Traditional 2D culture methodologies provide opportunities for stem cell differentiation [5], tissue morphogenesis [6], and cell-microenvironment interactions [7; 8]. However, recent studies showed that the potential of these methods is limited since the cell behavior changes when the cells are isolated from their 3D microenvironment and seeded on 2D culturing surfaces [3]. Abnormalities in cell behavior such as differentiation to tumor cells may be observed unexpectedly in 2D culturing methods [9]. These challenges have pushed the researchers to search for new materials that can be used as scaffolds for 3D culture studies. 3D cultures can mimic *in vivo* conditions and make it possible to create multilayered complex tissue structures more successfully [10; 11].

As described in Figure 1.1, the tissue engineering approach mainly comprises three main components. These are; *(i)* scaffold to support the cells and provide them with a surface to adhere to,*(ii)* a rich cell source suitable to the target tissue, and *(iii)* the growth factors that control cell behavior [12]. When selecting scaffolds, attention must be drawn to two points, which are the biocompatibility and biodegradability of the

material [13-16]. One of the key interests of tissue engineering is maintaining continuity of the living and functional tissue by preserving the native structure of the tissue and facilitating the regeneration of the cells. The structure of the scaffold should be porous enough to allow the diffusion of the substances such as the nutrients and the gases for the cells within the matrix [13; 15].

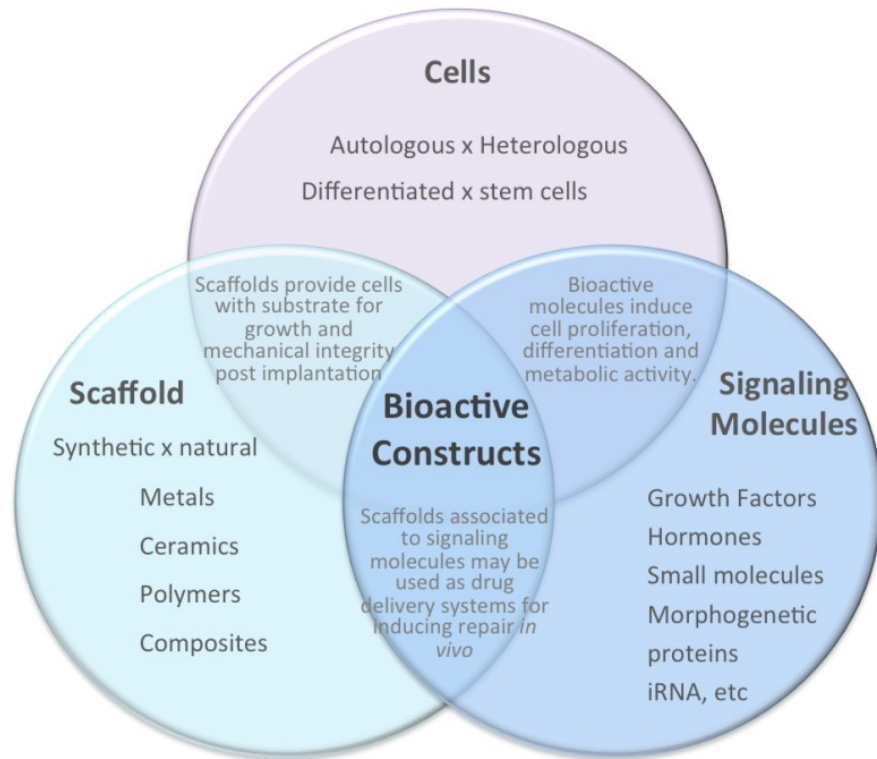


Figure 1.1. Association of three elements of tissue engineering
 (Source: Lott et.al., 2013)[4]

1.2.1. Extracellular Matrix

Extracellular matrix (ECM) is a non-cellular component that surrounds the cells. It is a complex network of water and macromolecules that are fibrous proteins, proteoglycans, and glycosaminoglycans (GAGs) as described in Figure 1.2 [17]. ECM is rich in fibrous proteins such as collagen, fibronectin, elastin, and laminin. ECM components have strong interactions in between and they create a rigid skeleton [18]. Also, cell surface

receptors, such as integrin, act as adhesives between cells and ECM [19; 20]. ECM is a dynamic system, in which the content and the structure is continuously remodeled. In a general aspect, ECM gives mechanical support to the cells, contributes to homeostasis, regulates the cell functions, such as growth and differentiation, harbors growth factors for the cellular receptors, senses and converts mechanical signals, and facilitates cellular communication [18; 21; 22]. Moreover, recent studies proved that ECM plays an active role in wound healing [23].

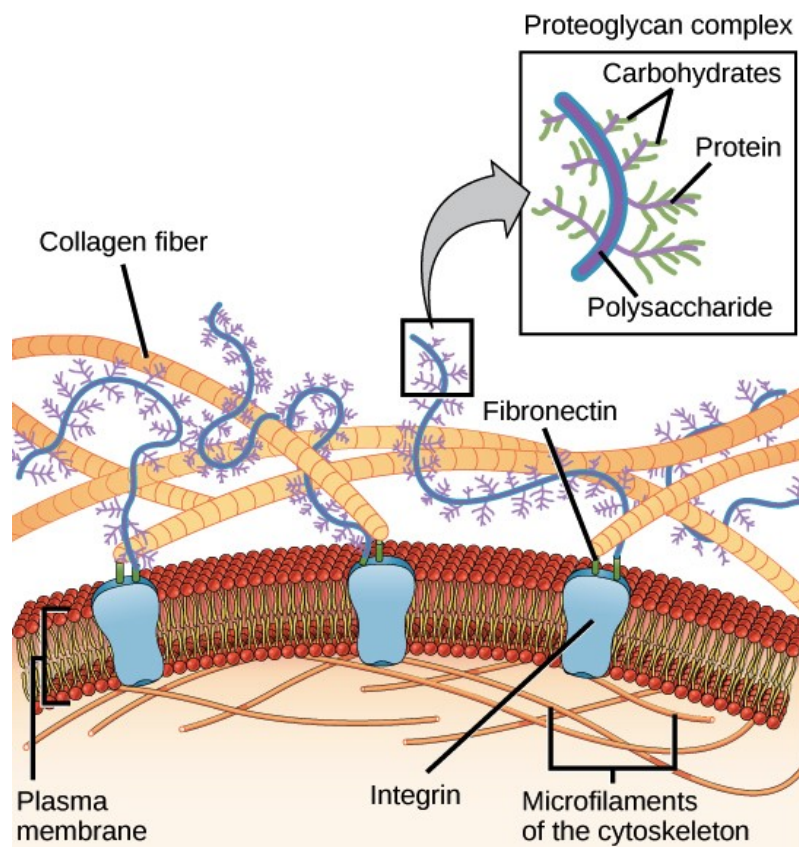


Figure 1.2. Extracellular matrix structure in contact with the cell membrane (Source: Bose, 2018) [5]

As ECM has a key role in regeneration processes, it is quite important also in tissue engineering studies [24]. The scaffold material should substitute native ECM during tissue formation while allowing cells to secrete their own ECM, and finally degrade and leave the environment gradually as the neo-ECM forms [16].

1.3. Biomaterials for Scaffold Fabrication

Biocompatibility and biodegradability are the key factors in biomaterial selection when designing scaffolds [13-15]. Metals, ceramics, polymers, and their composites are biomaterials that can be used for scaffold fabrication [16]. However, metals and ceramics have two main drawbacks; both have limited processability, and are non-biodegradable except for a few cases such as bio-ceramics [25]. Therefore, polymers are the most commonly used class of biomaterials for scaffold fabrication, and will be discussed in detail in the upcoming parts.

1.3.1. Synthetic Polymers

Synthetic polymers are industrially produced substances that are designed and synthesized according to the need. Their physical and chemical properties can easily be modified and tailored for the desired application.

Poly(glycolic acid) (PGA), poly(lactic acid) (PLA), and their copolymers; polycaprolactone (PCL) and polyethylene-glycol (PEG) are the most common synthetic polymers that are used in tissue engineering [15].

PGA has high porosity that allows cells to attach and proliferate in it, and its degradation products are resorbed without toxic effects. Yet, it starts to degrade within the first 1-2 months and degrades completely after around 6 months [26], and this short period limits its potential for implantation [25; 27].

PLA is a Food and Drug Administration (FDA) approved material and generally degrades in the body between 1 to 2 years following the implantation [28]. Due to its low elastic modulus and tensile strength, it is difficult to use by its own, and thus it is generally blended with other polymers [15; 25]. Both PLA and PGA have weak mechanical properties which are not suitable for hard tissue engineering studies without blending[27].

PCL is another synthetic biodegradable polymer. Its physical and mechanical properties are suitable for hard tissue engineering studies. Since it has a rapid degradation profile, it is more suitable to blend PCL with other materials [25].

PEG is one of the newest members of synthetic polymers that have good biocompatibility and high hydrophilicity. It has appropriate hydrophilicity that promotes protein adsorption, resulting in a high cell attachment profile. Moreover, this high hydrophilicity minimizes foreign body reaction *in situ*. As PEG has a high compressive modulus, it is generally used in blends with other materials, often with the aforementioned synthetic polymers to achieve better mechanical properties [25; 29].

1.3.2. Natural Polymers

Natural polymers are isolated from animals, plants, or microorganisms. They generally have good biocompatibility and thus lead to minimal immune rejection. As natural polymers are already isolated from living organisms, cytotoxicity is not a problem for this material class [30]. Furthermore, due to their bioactivity, these materials can stimulate cellular attachment and influence cell fate [29]. The main challenge of working with the natural biopolymers is their limited processability due to their sensitivity to harsh conditions, such as high temperature. Other problems include limitations in obtaining them in the required amounts or the high prices of the raw materials [25].

Natural polymers can be classified as (i) polysaccharides, (ii) proteins, and (iii) polynucleotides.

Polysaccharide-based natural polymers are divided into 4 categories by their origins as [30]:

- Higher plant polysaccharides (cellulose, starch, guar gum)
- Algal polysaccharides (alginate, carrageenan, agar-agar)
- Animal polysaccharides (chitosan, glycosaminoglycans (GAGs), and hyaluronic acid)
- Microorganism polysaccharides (bacterial cellulose, xanthan gum, gellan gum)

Protein-based natural polymers are classified as [27; 29; 31]:

- Animal-derived proteins (collagen, gelatin, elastin, silk, keratin, fibrinogen)
- Plant-derived proteins (soybean)

Finally, the last class of natural polymers, polynucleotides, has two members which consist of DNA or RNA [29].

1.3.2.1. Hydrogel Forming Natural Polymers

Hydrogels are one of the most commonly used materials in tissue engineering to mimic ECM [32]. Among various biomaterials, natural-based hydrogels, such as alginate [33] and collagen [34; 35] are promising candidates due to their tunable properties. However, the existing natural-based hydrogels have challenging properties, such as immunogenicity, poor mechanical strength, limited tissue-specific adhesion and inadequacy of presenting signaling molecules, which limit their application areas [34; 35]. Moreover, the majority of such materials are not affordable on a commercial scale. Therefore, there is a need for novel and natural-based hydrogels in biomaterials field.

Alginate is the sodium salt of alginic acid, which is extracted from brown algae or seaweed. It is a commonly used natural linear copolymer composed of mannuronic acid (M) and guluronic acid units (G) [36]. Alginate is biocompatible, biodegradable, and easy to process material, which has low immunogenicity due to its water-solubility and inherent hydrophilicity [27; 36]. Alginate is used in drug delivery [37], as well as in bone [38] and cartilage [39] tissue regeneration applications. On the other hand, alginate degrades slowly, and its cell adhesion capability is limited. Therefore, it results in poor tissue formation [25].

Collagen is a protein that is present in the ECM naturally and used in various fields, including tissue engineering [27; 40], medical applications [41], and cosmetics [42-44]. This major protein class has 28 types, and Collagen I, II, III, and IV are the most common collagen types [27; 45]. Collagen type I is the main component of bone, tendon, and skin. Cartilage mainly consists of collagen type II, while collagen type III is found in skin and blood vessels and type IV in basal lamina [46; 47]. Collagen is a biocompatible and biodegradable material with a porous structure and appropriate permeability [45]. Its weak mechanical properties make it hard to handle and produce. Furthermore, its biodegradability is not controllable, and immune response may occur depending on its origin [48].

Gelatin is a denaturized and partially hydrolyzed derivative of collagen, and it is less immunogenic than collagen [27; 49]. It is used in a wide range of applications including pharmaceuticals [50], tissue engineering [51-53], and food industry [27; 50]. Gelatin is a biocompatible and biodegradable material with a low-cost [27]. As a drawback, it is generally heterogeneous in terms of fiber size in its final form [54].

Chitosan is an abundant and cost-effective polysaccharide that is isolated from the hard exoskeletons of *crustaceans*, such as shrimps and crabs [27]. It can be used as a drug delivery agent [30; 55], dietary supplement [30; 56], and tissue engineering scaffold [57]. Chitosan leads to low foreign body reaction, and has high antibacterial activity, biodegradability, easy processability, and tunable mechanical properties [27; 58-62]. On the other hand, due to its poor mechanical strength and low water-solubility, chitosan has brittle characteristic [27]. To overcome this problem, chitosan is generally used in composite form with other materials [27].

1.3.2.2. Injectable Hydrogels

Tissue engineering constructs can be fabricated in a pre-defined geometry or in an injectable form that can be injected into the application site. Compared to scaffolds with defined geometry, injectable biomaterials fit better into the defect area, are minimally invasive, and can be used as an adhesive between the host tissue and the preformed scaffold material [63]. Moreover, while cell incorporation is difficult to achieve in preformed scaffolds, injectable hydrogels allow homogeneous cell distribution within the gel matrix [64]. Injectable biomaterials are made from hydrogel-based or ceramic-based materials to produce scaffolds. They are often used in bone and cartilage tissue engineering.

The main criteria for injectable hydrogel production are described in Figure 1.3. Briefly, an injectable hydrogel should lead to minimal or no immune response, degrade synchronously with neo-tissue formation without creating toxic by-products, fit into the injected area, and have appropriate mechanical properties for the host tissue, while allowing ECM secretion and exogenic cell transfer in and out of the matrix [63]. On the other hand, mechanical weakness is the main challenge of injectable hydrogels [65].

Temperature, ion mediation, self-assembling, enzymatic triggering, Schiff-base mediation, and shear-thinning-reinforced systems are used for the phase modulation of injectable hydrogels. These phase modulations are called gelling [66].

Also, injectable hydrogels are used as space fillers in plastic and cosmetic surgery applications, and as cardiac emboli agents without the aim of cell encapsulation as in tissue engineering applications.

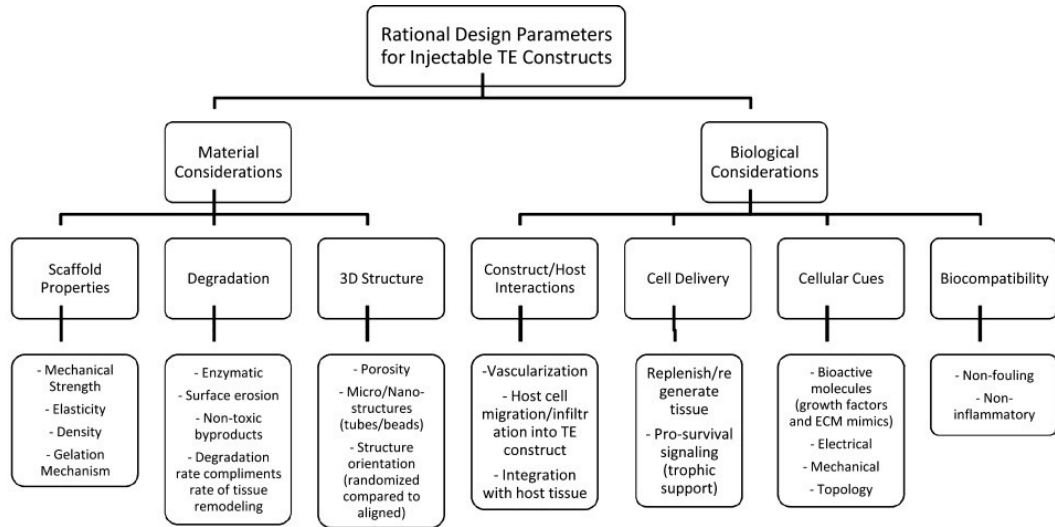


Figure 1.3. Main criteria of injectable hydrogel design

(Source: Overstreet et.al., 2012) [36]

1.3.2.3. Quince Seed Hydrogel

Quince (*Cydonia oblonga*, Rosaceae family) is a small plant that is generally 5-8 meters long, with pink blossom in spring and has bright yellow fruits with a characteristic aroma. It is native to Turkey and Iran but also can be cultivated even in South Africa [67]. Different parts of quince, such as its fruits, leaves, pulp, and, seeds have antimicrobial [68; 69], anti-oxidant[70; 71], and anti-ulcerative [72] properties. Brown and oval-shaped seeds are found in the middle of the fruit and, have been widely used on Iranian and Chinese traditional medicine with significant impact. Since most of the synthetic antioxidants have cytotoxicity [73], quince seed is a promising candidate as a natural antioxidant source with a high antioxidant capacity [70; 71; 74-76]. Furthermore, quince seeds are rich in phenolic compounds and flavonoids [77; 78].

Quince seeds rapidly adsorb water and create a gel-like lubricious liquid [73]. Previously, numerous studies have been done on the potential of quince seed extracts or hydrogels in regenerative medicine applications and biotechnology [71; 75; 79-82]. Quince seed hydrogel (QSH) was evaluated for its use in wound healing as a topical cream enhancer. In a study conducted on rabbits, 10% QSH addition to eucerin-based cream resulted in a better healing profile than eucerin base cream [79; 80]. In another

study, 15% QSH addition accelerated wound healing in T-2 toxin-induced dermal toxicities in rabbits [81]. QSH is also used as a food packaging material due to its antioxidant properties. There are also follow-up studies to make it antibacterial via the addition of thyme essential oil [71; 75]. Although there are several studies for QSH, there have been no study regarding the use of QSH as scaffold materials. Therefore, in this thesis, fabrication and optimization of QSH scaffolds will be the main focus, and the use of QSH scaffold as an injectable hydrogel for bone tissue engineering will be investigated thoroughly.

CHAPTER 2

MATERIALS AND METHODS

2.1. Materials

Quince fruits obtained from local markets of Western Turkey were used for extraction and preparation of QSH. GTA (Glutaraldehyde solution G6257, Sigma Aldrich), HCl (Hydrochloric Acid 3071, Sigma Aldrich), Acetone (VWR Life) were used for crosslinking reaction. Lyophilized BSA powder (Bovine serum albumin A9418, Sigma Aldrich), PierceTM BCA protein assay kit (23225, Thermo Scientific), 10X PBS (Phosphate buffer saline pH 7.4 70011-044, Gibco-Thermo Fischer) and SDS powder (Sodium dodecyl sulfate, Bioshop) were used for protein adsorption tests. For cell culture analyses, NIH-3T3 (ATCC® CRL-1658TM) and SaOS-2 (ATCC® HTB-85TM) cell lines were used. The cell media consisted of DMEM high glucose (Dulbecco's Modified Eagle Medium 41965-039, Gibco), FBS (Fetal bovine serum 10270-106, Gibco) and Penicillin-Streptomycin (P4333, Sigma-Aldrich). Trypsin EDTA solution (25200-056, Gibco) was used for detaching the cells. Resazurin sodium salt (R7017, Sigma Aldrich), MTT salt (3-(4,5-dimethylthiazolyl-2)-2,5-diphenyltetrazolium bromide, Sigma Aldrich), and Live/Dead cell viability test (CytoCalcein AM and Propidium Iodide 22789, AAT Bioquest) were used for cell viability analyses. Anti-collagen Type I-FITC Antibody (FCMAB412F, Milli-Mark) and DAPI (D9542, Sigma-Aldrich) were used for collagen immunostaining and nucleus staining respectively.

2.2. Methods

2.2.1. QSH Scaffold Fabrication

Quince fruits were obtained from Western Turkey. Quince seeds were cored out from the fruit. The fruit impurities were removed and seeds were air-dried for approximately 7 days at room temperature. Excess amounts of seeds were refrigerated at +4°C until further use.

The seeds were cracked, and brown colored outer shells were dissected from the white core that does not have gelation ability. Brown outer shells were mixed with ultra-pure water (UP H₂O) to prepare different concentrations (1, 1.5, 2, 3.3, 5, and 10 mg seed/mL) of QSH. The mixtures were left for incubation for 24 hours at room temperature. After incubation, the mixture was filtered through cotton gauze cloth to obtain QSH. Filtered QSH was frozen at -80°C. Finally, QSH samples were lyophilized for approximately 72 hours.

Quince seed hydrogel extraction and production methods from the literature; hot water-based [82] and alcohol-based [76; 83] hydrogel extraction methodologies were tested, and results were compared with the novel technique developed in our laboratories.

As explained in the hot water extraction method that was developed by Ashraf et al.[82]; whole-grain quince seeds were cleaned and soaked in deionized (DI) water for 6 hours to obtain 200 mg/mL concentration. Then, the mixture was transferred onto a hot plate for 30 minutes at 50°C and mixed with a magnetic stirrer. The QSH was separated from the seeds via filtration after the hydrogel reached room temperature. 1:1 and 1:5 volumes of QSH and n-hexane were added to the separation funnels, and QSHs were washed 3 times with n-hexane. Afterward, QSHs were washed with the same volume of DI water. After centrifuging the hydrogel at 3030×G for 3×10 minutes, QSHs were collected from the sediment. QSHs were dried in a vacuum oven at 60°C for 48 h and in freeze-dryer subsequently.

Alcohol-based extraction methods were performed based on the methodology described by Wang et al. [76; 83] with small modifications. In the first method [76], whole quince seeds were air-dried and then ground in a milling machine. The meal obtained from quince seeds was extracted by hexane method instead of subcritical butane to eliminate

the oil and then dried for 12 hours at 50°C. The crude polysaccharides obtained from quince seed meal were extracted via hot water (1:10, w/v) in an oil bath at 80°C under continuous mixing during 3 hours. When the extraction was accomplished, the water extract was cooled to 25°C, filtered via polyamide cloth and centrifuged at 2540×G for 10 minutes. The supernatant was precipitated with 95% ethanol and then 3 times rinsed with 75% ethanol to produce QSH, then lyophilized.

In the second method [83], the seeds were completely dried in 50°C oven and after that, immersed in ultra-pure water in 60 mg/mL concentration under gentle stirring at room temperature. The hydrogel was centrifuged, and then two volumes of anhydrous ethanol was mixed with the supernatant completely. Subsequently, the mixture was centrifuged (3000×G, 10 minutes) and the recovered precipitate was dissolved in 3 volumes of ultra-pure water. Finally, the material was lyophilized.

2.2.1.1. QSH Crosslinking with GTA

Lyophilized QSHs were subsequently crosslinked by immersion method with GTA to optimize crosslinking parameters. Different concentrations of GTA (0.03, 0.05, 0.1, 0.3 and 0.5 M) were prepared with 0.05 M hydrochloric acid (HCl) in acetone medium. QSHs were incubated in crosslinking solutions for different time frames; 30 minutes, 1, 2, and 3 hours. The crosslinked QSHs were rinsed with UP H₂O to remove the crosslinking solution residues for 2 minutes, 5 minutes, 1 hour, overnight, and 2 days at room temperature and 4°C to optimize the best rinsing period that can eliminate all GTA residues without creating any surface degradation on the hydrogel. Prepared samples were kept lyophilized to achieve long shelf life if not used right after production.

Furthermore, filtered non-lyophilized QSHs were subsequently crosslinked with GTA to optimize the controlled shapeable crosslinking capability of hydrogels in liquid form. QSHs were crosslinked in 0.03M, 0.1M, 0.5M GTA solutions with 0.05 M hydrochloric acid (HCl) in acetone medium. Gels were injected into the crosslinking solution in liquid form without freezing or lyophilization steps. After 30 minutes of incubation in crosslink solution, gels were rinsed with UP H₂O to remove the excess amount of crosslink solution residues.

2.2.1.2. QSH Crosslinking with EDC/NHS

Filtered, non-lyophilized QSHs were subsequently crosslinked by EDC/NHS to obtain injectable hydrogel. 0.4 M EDS and 0.1 M NHS solutions were prepared with UP H₂O. 500 µL and 1mL QSHs in varied concentrations (2, 10, 20, 50 mg seed/mL UP H₂O) mixed with EDC and NHS solutions in varied volumes (5, 10, 15, 20, 25, 50, 75, 100, 200, and 300 µL EDS and NHS). EDC and NHS solutions added to the hydrogels separately, mixed right after adding. QSHs were incubated up to 4 hours for total crosslinking.

2.2.2. Characterization of QSH Scaffolds

Characterization of QSH was accomplished via macro imaging, SEM, pore size and distribution, swelling, degradation, FTIR, AFM and protein adsorption analysis as explained in detail in this chapter.

2.2.2.1. Macro Imaging and SEM Analysis

Macro imaging and SEM analysis methods were used to fulfill the morphological characterization of QSH on macro and micro scale. For SEM measurements, the QSH samples were coated with a gold layer under argon gas. A scanning electron microscope (FEI QUANTA, 250 FEG) was used for imaging. QSHs were prepared according to different protocols, as described in chapter 2.2.1. Furthermore, to remove residual GTA, QSHs were rinsed 3 times in UP H₂O, and samples were oven-dried or lyophilized. Samples that were crosslinked with EDC/NHS lyophilized directly right after the production as described in chapter 2.2.1.2. The samples were analyzed using SEM to obtain optimum production parameters.

2.2.2.2. Pore Size and Distribution Analyses

2mg/mL QSH samples were kept non crosslinked or crosslinked in low-concentration of crosslinker (0.03M GTA, lightly crosslink) and high-concentration of crosslinker (0.5 M GTA, heavily crosslink) included crosslinking solutions for 30 minutes incubation periods for pore size and distribution analyses. SEM images were processed to determine average pore size and pore size distribution via ImageJ (NIH) image processing software and OriginPro (Northampton, MA) data processing software.

2.2.2.3. Swelling Analysis

The water uptake capacity of the QSH samples was analyzed using swelling analysis. The dry weight (W_D) of the samples were measured prior to wetting. The samples were then immersed into UP H₂O and incubated for varied periods (2, 8, and 48h). Afterward, the samples were weighed again for wet weight (W_W) value. Swelling ratio was calculated using the following equation:

$$\text{Swelling Ratio} = \frac{W_W - W_D}{W_D} \times 100 \quad (\text{Eq 2.1.}) [84; 85]$$

The QSH samples with 2mg/mL concentration were crosslinked in 0.03, 0.05, 0.1, 0.3, 0.5 M GTA-containing crosslinking solutions for 30 minutes incubation period for swelling analysis.

2.2.2.4. Degradation Analysis

The degradation analysis of QSH samples was performed by incubating the hydrogels in complete DMEM medium (10% FBS, 1% penicillin/streptomycin (V/V) in DMEM High Glucose basal medium) at 37°C. Analyses were carried out to evaluate the material's own degradation dynamics, the effects of the crosslinking conditions, and the

sterilization step. QSHs were sterilized via UV irradiation at different periods from the top and the bottom sides of the material before testing. The samples were evaluated only for total degradation. The weight loss by the time was not tested to conserve sterility. The data were analyzed using OriginPro software (Northampton, MA). 2mg/mL QSH samples, crosslinked in 0.03 and 0.1 M GTA solutions for 30 minutes, and 1 hour incubation periods, were used for degradation analysis.

2.2.2.5. FTIR Analysis

Fourier Transform Infrared (FTIR) analysis was used for the chemical characterization of QSHs. The analyses were done in Fourier Transform Infrared Spectroscopy Attenuated Total Reflection (FTIR-ATR) mode (PerkinElmer, USA). QSH samples that were crosslinked with GTA were prepared in 2 mg/mL concentration and lyophilized. Varied crosslinking parameters were investigated to define the effects of GTA on QSH structure and crosslinking mechanism. Non-crosslinked, lightly crosslinked (0.03M GTA) and heavily crosslinked (0.5M) QSHs were analyzed from 4000 to 1000 cm^{-1} . Also, for the EDC/NHS crosslinking, QSH samples were prepared in 20 mg/mL seed concentration and crosslinked with varied concentrations of EDC and NHS solutions. FTIR data were plotted and analyzed using OriginPro software (Northampton, MA).

2.2.2.6. AFM Analysis

Atomic force microscopy (AFM) was used for the mechanical characterization of QSH. Surface topography and force-distance profiles of QSHs were obtained using the FlexAFM System (Nanosurf CoreAFM, Switzerland). Thick, homogeneous, and dried gels were located on the microscope slide and were measured in the AFM with a beam shaped cantilever in contact mode (Stad 0.2 LAuD, NanoAndMore GMBH, Germany) with a nominal spring constant of 0.2 N/nm and tip radius of 7 nm. For each image, 512 lines were acquired at a speed of 2 s per line and 55 nN set point. Root mean square (RMS) roughness and Young's Modulus values were determined using the Gwyddion

Version 2.45 open source SPM data analysis program. A series of 256 force-distance curves were measured for $50 \times 50 \mu\text{m}^2$ regions and fit up to 1 μm tip deflections with a Hertz (sphere) model. QSHs were notched at a rate of about 1 $\mu\text{m}/\text{s}$, which is typically sufficient to investigate elastic characteristics of cells and matrices instead of viscoelastic characteristics. The analysis was triplicated for each sample and at least three independent analyses were done for each sample type.

2.2.2.7. Protein Adsorption Assay

Protein adsorption assay was used to obtain the absorbed protein amount on the surface of QSH. 2mg/mL QSHs were crosslinked with 0.03 M GTA and lyophilized in a cylindrical configuration. Bovine serum albumin (BSA) protein stock solutions were prepared in varying concentrations (0, 100, 250, 500, 1000, 2000 $\mu\text{g}/\text{mL}$) in PBS. The QSHs were immersed in BSA solutions for 2 hours at 37°C. Then QSHs were washed 3 times with 1X PBS solution and immersed into 5% (w/v) SDS solution for 1 hour at 37°C. The initial samples were collected from BSA stock solutions, and the final samples were collected from the supernatants of QSHs that were incubated in BSA solutions. The SDS samples were collected from the supernatants of QSHs incubated in SDS. BCA Protein Assay Kit was used to detect the adsorbed protein amount on the samples. The working reagent was prepared in proportion to 50:1 (Reagent A:B). 200 μL working reagent were added on 25 μL sample volume for each initial, final, and SDS samples in 96 well plates and incubated at 37 °C for 30 minutes. Finally, absorbance was measured at 562 nm using a microplate spectrophotometer (Fisher Scientific™accuSkan™GO UV/Vis) at room temperature. The standard curve was prepared with the applied BSA concentrations. Concentrations of adsorbed and solubilized proteins were quantified via the standard curve.

2.2.3. 3D Cell Culture Studies

Mouse embryonic fibroblast cell line; NIH/3T3 (ATCC® CRL-1658™) and human

osteosarcoma cell line; SaOS-2 (ATCC® HTB-85™) were used for *in vitro* models to test the QSH scaffolds.

2.2.3.1. 2D Cell Culture and Maintenance

Mouse embryonic fibroblast cell line (NIH/3T3) and human osteosarcoma cell line (SaOS-2) were maintained in complete growth medium containing 5% FBS and 1% Penicillin-Streptomycin solutions in DMEM High Glucose medium. Cells were incubated in a humidified incubator at 5% CO₂, 37°C. Both cell lines were passaged using trypsin-EDTA solution when they reached 80-90% confluence, generally twice a week.

2.2.3.2. Cell Viability and Proliferation Analyses

QSHs were prepared for cell culture analyses in 2 mg/mL concentration, left for gelation for 24 hours, and then filtered. The filtered hydrogels were filled into 24 well plates in 1300 µL or 48 well plates in 650 µL constant volume. The gels were frozen into -80°C freezer and lyophilized for 3 days. Dried samples crosslinked in GTA solution and rinsed 3 times with cold UP H₂O (2 minutes, 5 minutes, and overnight) to eliminate GTA residues. Minimum (0.03 M) and maximum (0.5 M) GTA concentrations were selected to observe the toxic effects of GTA on cell viability in addition to possible self-toxic effects of QSH. Both sides of the crosslinked QSHs were sterilized under UV light for 15 minutes then transferred to 48 well plates for conditioning. Conditioning was done for 2 hours into DMEM complete medium that contains 3% (V/V) Penicillin-Streptomycin and 10% (V/V) FBS solution.

Cell viability and proliferation analyses were done via the AlamarBlue assay for the NIH-3T3 cells. Low density ($1 \times 10^5 / 650 \mu\text{L}$ QSH) and high density ($1 \times 10^6 / 650 \mu\text{L}$ QSH) of cells were seeded on QSHs, and the cells were cultured for 7 days for cell number optimization. In the second experimental set, short and long term cellular behaviors were monitored with the cells cultured for up to 7 and 14 days. Long term

experiment was done only with the lightly crosslinked QSH samples and low cell seeding density.

AlamarBlue and MTT assays were done for SaOS-2 cells. In the first assay, low density (1×10^5 /650 μL QSH) and high density (1×10^6 /650 μL QSH) cells were seeded on QSHs which were crosslinked with 0.03 M GTA. The cells were cultured for 7 days for cell number optimization. In the second experiment set, 4×10^5 cells were seeded onto 650 μL QSHs which were crosslinked with 0.03 M GTA and cultured up to 15 days. In the third experiment set, MTT analysis and AlamarBlue analysis were done in parallel for method optimization. 5×10^5 cells were seeded onto QSHs and cultured for 7 days. Differently from a standard static method, after AlamarBlue reagent addition, these samples were incubated in a thermo shaker at 37°C and 50 rpm for 3.5 hours.

In all analyses, cells were seeded onto mid-point of gels with a minimum volume of complete DMEM medium. Fresh complete medium was added onto samples after cell attachment was done, approximately 3 hours later. The positive control was prepared with cells and medium. The negative control was prepared with QSH scaffolds and medium.

Later on, AlamarBlue analysis was done for SaOS-2 cells with EDC/NHS crosslinked QSH samples. QSH prepared in 20mg/mL seed concentration and filtered after 24 hours of incubation. EDC and NHS solutions were prepared in 0.4 M and 0.1 M concentrations respectively. QSH, EDC and NHS solutions were sterilized under UV. Experiments were done in two different protocols to optimize the experiment setup. In the first protocol, QSH mixed with the same amount of EDC and NHS solutions in various proportions. Cells (2×10^5 /1mL QSH) with minimum amount of DMEM complete medium were added to the mixture immediately after mixing and mixture transferred to the well plates. Crosslinking occurred while the cells were in the hydrogel. Fresh complete medium was added onto samples after crosslinking was mostly done, approximately 3 hours later. In the second protocol, QSH mixed with the same amount of EDC and NHS solutions in various proportions and mixture transferred to the well plates. Plates allowed to incubation for 3 hours to ensure the crosslinking. Cells (2×10^5 /1mL QSH) were seeded onto crosslinked hydrogels with fresh complete medium. The positive control was prepared with cells and medium as 2D control and with cells, medium and QSH as 3D control. Also, another control group was settled with cells, EDC/NHS solution and medium to observe effects of EDC/NHS only. The

negative control was prepared with medium only as 2D control and QSH and medium as 3D control. All samples were incubated for 48 hours prior to AlamarBlue analysis. The cell culture medium was changed every second day. Before analyses, fresh complete DMEM medium containing 0.01% (v/v) resazurin sodium salt were prepared and the scaffolds were transferred into the new medium, then incubated for 4 hours. Absorbances were measured at 570 and 600 nm by microplate spectrophotometer (Fisher Scientific™accuSkan™GO UV/Vis). The scaffold samples were duplicated and the absorbance measurements were triplicated for each sample. OriginPro software (Northampton, MA) software was used to analyze the viability results. Eq 2.2. was used for calculations where A indicates absorbance values of test or positive control samples and N indicates absorbance values of negative control samples.

$$\text{Cell Proliferation, \%} = \frac{(O_2 \times A_1) - (O_1 \times A_2)}{(R_1 \times N_2) - (R_2 \times N_1)} \times 100 \quad (\text{Eq 2.2.})$$

Table 2.1. The molar extinction coefficients for AlamarBlue analysis

Wavelength (nm)	Reduced state (R)	Oxidized state (O)
570 (1)	155677	80586
600 (2)	14652	117216

2.2.3.3. Live/Dead Analysis

The Live/Dead assay was used to determine cell spreading on the scaffold and analyze possible toxic effects of GTA and EDC/NHS on cells. QSH scaffolds were prepared in the same method with cell viability and proliferation analyses samples as described in section 2.2.3.2.

For the NIH-3T3 cells, low density (1×10^5) and high density (1×10^6) cells were seeded on 650 μL QSH scaffolds and cultured for 14 days to observe short-term and long-term cellular behaviors. Both low-crosslinked (0.03 M GTA) and high-crosslinked (0.5 M GTA) QSHs were analyzed to investigate the potentially toxic effects of GTA. For SaOS-2 cells, 4×10^5 cells were seeded onto 650 μL QSHs, which were crosslinked with

0.03 M GTA and cultured up to 9 weeks.

In all analyses, cells were seeded onto the mid-point of the gels with a minimum volume of complete DMEM medium. Fresh complete medium was added onto the samples after cell attachment was accomplished, approximately 3 hours later. The positive control was prepared using only cells and medium. The negative control was prepared with QSH scaffolds and medium. The cell culture medium was changed every second day.

Following to GTA crosslinked QSH experiments, Live-Dead assay was done for SaOS-2 cells with EDC/NHS crosslinked QSH samples. Samples were prepared in the same protocol as described in chapter 2.2.3.2. All samples were incubated for 48 hours prior to the Live/Dead assay.

Before the analyses, freshly prepared complete DMEM medium containing an equal volume of CytoCalcein and Propidium Iodide were mixed in Live/Dead assay buffer solution applied to the QSH scaffolds on the experiment days and protected from light. After 30 minutes of incubation, samples were observed via the fluorescent microscope (Zeiss Observer Z1).

2.2.3.4. Cellular Imaging

Spreading of cells and cellular spheroids on scaffolds were observed by SEM analysis and fluorescence imaging. NIH-3T3 cells were cultured for long-term (60 days) on QSH scaffolds to observe spheroid formations. For SEM analysis, scaffolds were rinsed 3 times with 1X PBS to get rid of unwanted residues and culture medium, then fixated in 4% paraformaldehyde (PFA) solution. Later on fixation, secondary rinsing was done with 1X PBS for 3 times and DI water for 2 times to eliminate PFA residues. Scaffolds were gold-coated under vacuum and argon gas prior to analysis and then, were analyzed by SEM (FEI QUANTA, 250 FEG).

Additionally, ECM formation and structural integrity in the NIH-3T3 cells were confirmed via DAPI and Collagen staining. Anti-collagen Type-I FITC antibody and DAPI staining reagents were used for fluorescence staining. The QSH scaffolds were fixated with the same protocol as cellular SEM analysis. The fixated scaffolds were rinsed with 1X PBS and transferred into either anti-collagen Type-I FITC antibody (1:5

(V:V)) or DAPI (1:1000(V:V)) solutions in PBS separately. Incubation of scaffolds was done at 4 °C, overnight for anti-collagen Type-I FITC solution; and at RT, 10 minutes for DAPI solution, both protected from light. The scaffolds were gently rinsed in 1X PBS solution after the incubation period and observed under a fluorescent microscope (Zeiss Observer Z1).

CHAPTER 3

RESULTS AND DISCUSSION

3.1. Optimization of QSH Scaffold Fabrication

In this thesis, a new method for quince seed hydrogel production was developed. The production pathway is summarized in Figure 3.1. Quince seeds were dissected from the fruit, the dried outer brown seed shells were mixed with UP H₂O in certain concentrations and left for 24 hours incubation at room temperature. After the incubation period, the hydrogel was filtered with cotton gauze and filled into polystyrene cylindrical containers and frozen overnight. Afterward, hydrogels were lyophilized and crosslinked with GTA to obtain preformed scaffolds or directly crosslinked with EDC/NHS without lyophilization for injectable hydrogel production. If the preformed scaffolds were not used right after production, they were lyophilized again to increase the shelf life after rinsing of the material to eliminate GTA residues. As described in Figure 3.2, with this protocol (Figure 3.2a), better hydrogel is produced in terms of viscosity, transparency and biocompatibility through uncomplicated and rapid process when compared with the previously reported methods in Figure 3.2b,c and d. Besides, Figure 3.3 and Figure 3.4 demonstrate that, there is no structural difference in micro-level and chemical composition compared to previously reported methods [76; 82; 83]. In addition to all, no toxic solvent was used in the gelation step and general use of toxic solvents was minimized making the protocol more biocompatible and eco-friendly.

In gelation optimization, 2 mg/mL seed concentration in UP H₂O gave the most appropriate results regarding the texture, stiffness, and porosity of the material. Lower concentrations (1 and 1.5 mg /mL) could not give a proper structure after the lyophilization, and material tended to degrade and collapse rapidly upon air contact. Higher QSH concentrations (3.3, 5, and 10 mg /mL) produced too firm texture while having a proper porosity, as seen in Figure 3.3.a-b. In the crosslinking step with GTA, 30 minutes of incubation period in 0.03 M GTA solution created a strong, adequately

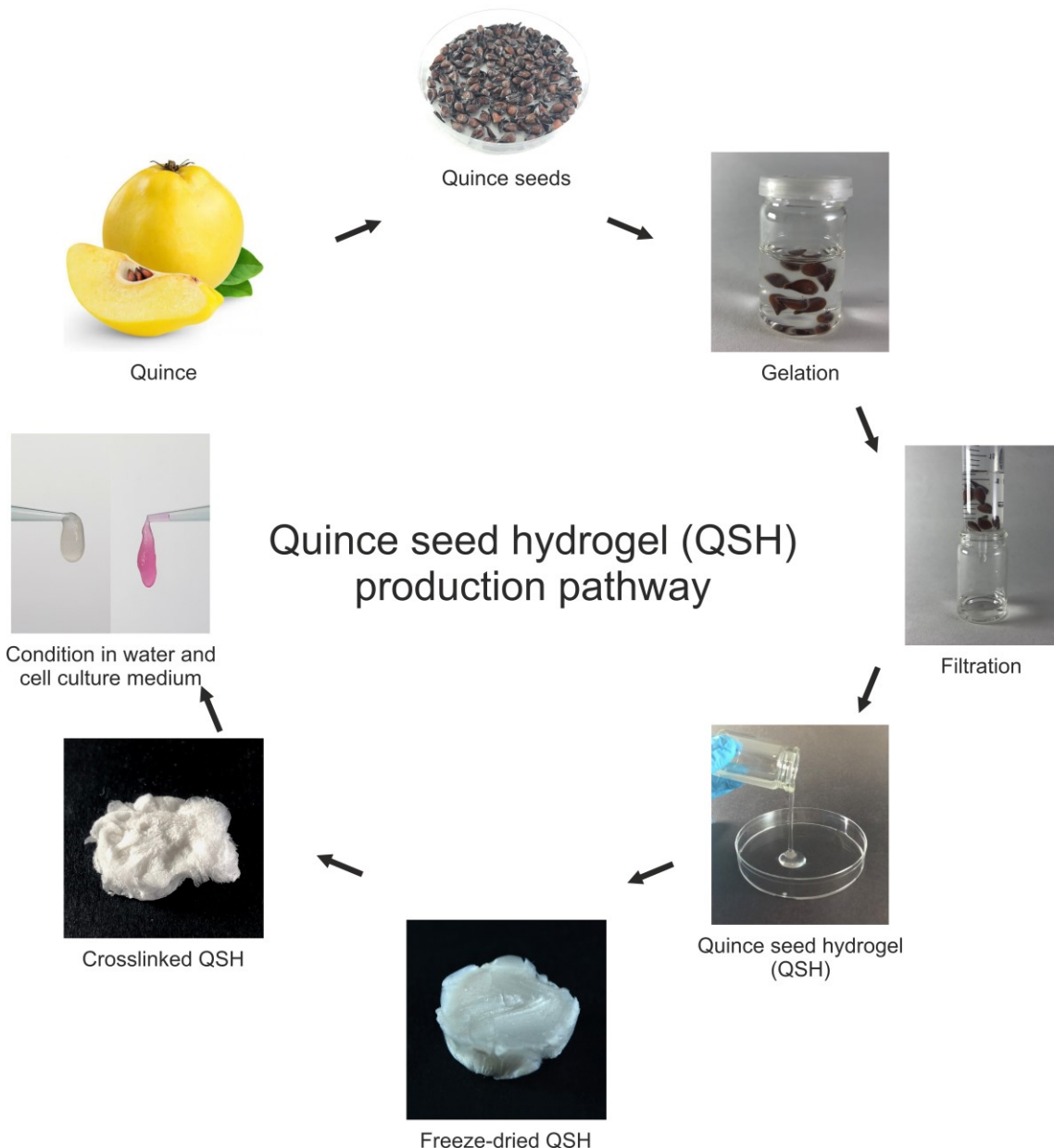


Figure 3.1. The experimental production and design steps of the QSH scaffold; the quince fruits were collected, the seeds cored out from the fruits, gelation was achieved in water after 24hours. The gels were filtered, lyophilized, crosslinked and given their final form with conditioning in water and cell culture medium respectively

crosslinked structure. As the crosslinker concentration increases, the material becomes brittle which is not a desirable property for hydrogel scaffolds [86-88]. Subsequently, QSHs were rinsed with UP H₂O to remove GTA properly. In this step, rinsing with cold

water helped to preserve the final crosslinked form of hydrogel, while hot or warm water caused disruption and QSHs were dissolved in water rapidly. The most consistent results were obtained from rinsing of the QSHs 3 times with cold UP H₂O (2 minutes, 5 minutes, and overnight) to eliminate undesired GTA residues in the scaffold. Longer or more repeated rinsing steps did not provide higher viability and extra washing steps resulted in undesirable consequences like early degradation of the material due to over-rinsing. Crosslinked hydrogels had a more durable and stable structure, and their mechanical properties improved, parallel to the studies that were used chemical crosslinking in the literature[89].

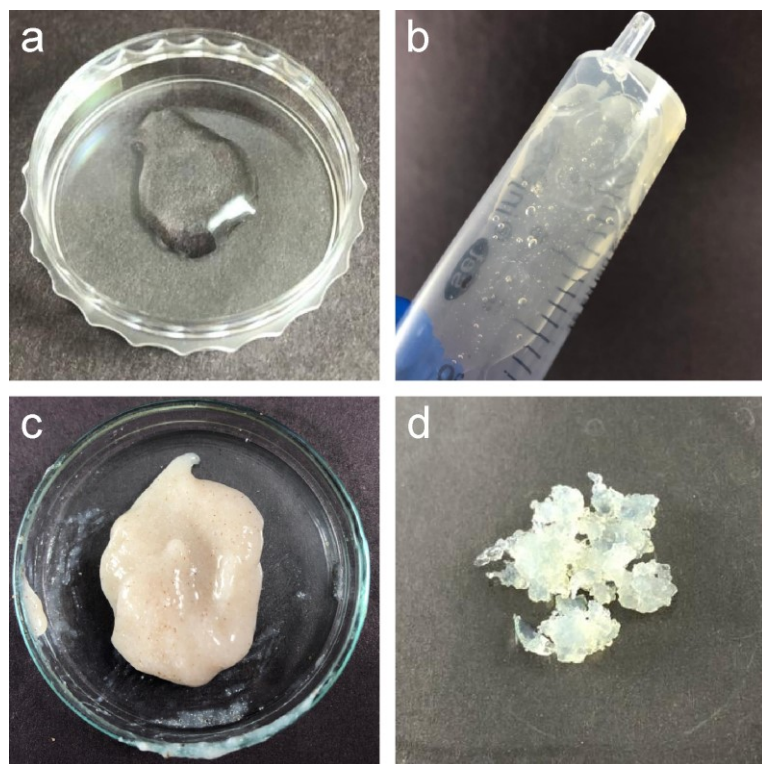


Figure 3.2 QSH production method comparison macro images of a) our method 2 mg/mL concentration, b) Ashraf et al. (2018) method, c) Wang et al. (2017) method, and d) Wang et al. (2018) method

The QSH preparation method developed in this study was compared with previously published methods in the literature. The hot water-based method from Ashraf et. al. [82] and alcohol-based methods from Wang et. al. [76; 83] were reproduced for comparison. As seen in Figure 3.2., our method created easy-to-use hydrogels very rapidly that have

optimum fluidity and transparency without any impurities. Compared to methods of Wang et. al. both 2017 and 2018, sticky paste or crystal-like materials were obtained that are not suitable for tissue engineering applications due to material form and mechanical properties.

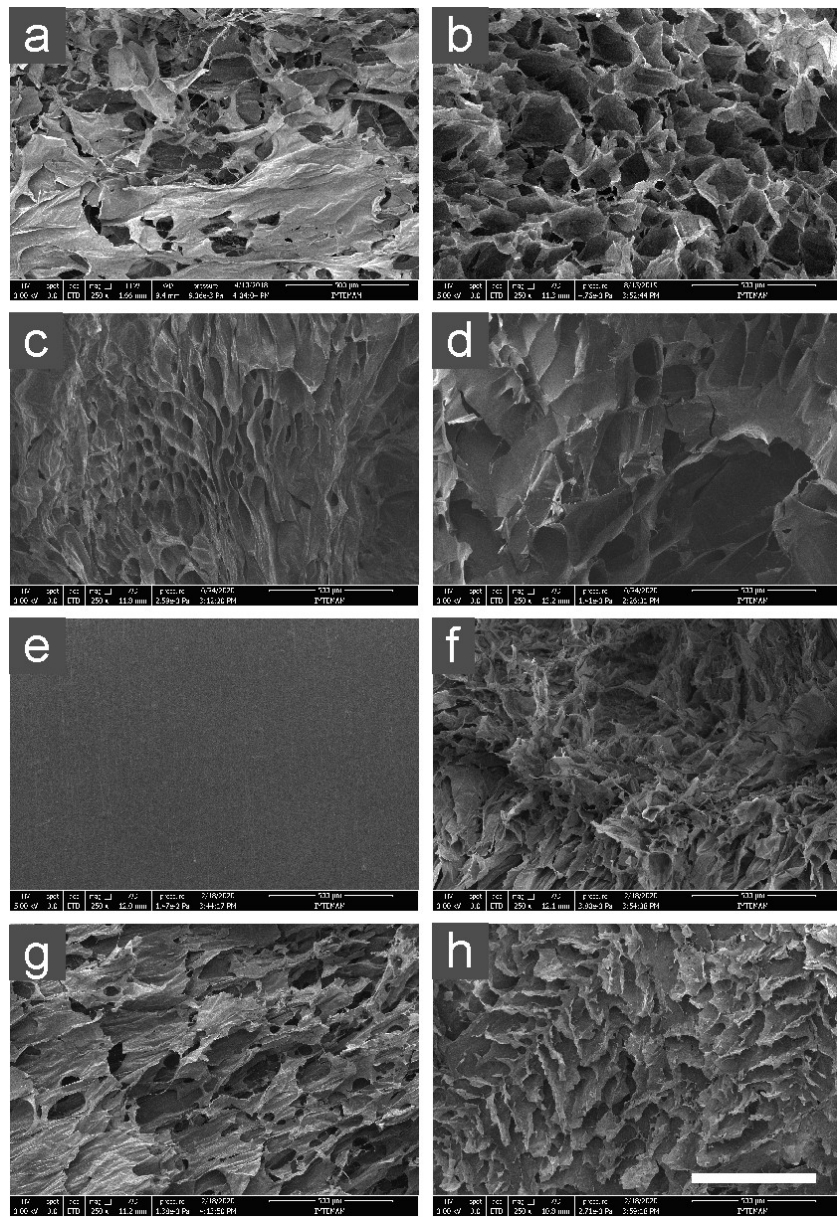


Figure 3.3. QSH production method comparison SEM images of our novel method a) 2 mg/mL b) 10mg/mL c) 20 mg/mL and d) 50mg/mL seed concentration, e) oven-dried Ashraf et al. method f) lyophilized Ashraf et al. method g), Wang et al.,2017 method h) Wang et al.,2018 method (scale bar 500 μm)

SEM images of all scaffolds obtained from each method were given in Figure 3.3. Firstly, the material obtained from Ashraf et. al. method was prepared via oven-drying as described in the reference paper. However, the results were quite different from our method as given in Figure 3.2(a,b). Desired porosity cannot be gained via oven-drying in the Ashraf et. al. method thus lyophilization also applied to these samples. From the SEM images (Figure 3.3), it was concluded that all the remaining methods other than Ashraf et. al. provide similar results with our methodology in terms of porosity and

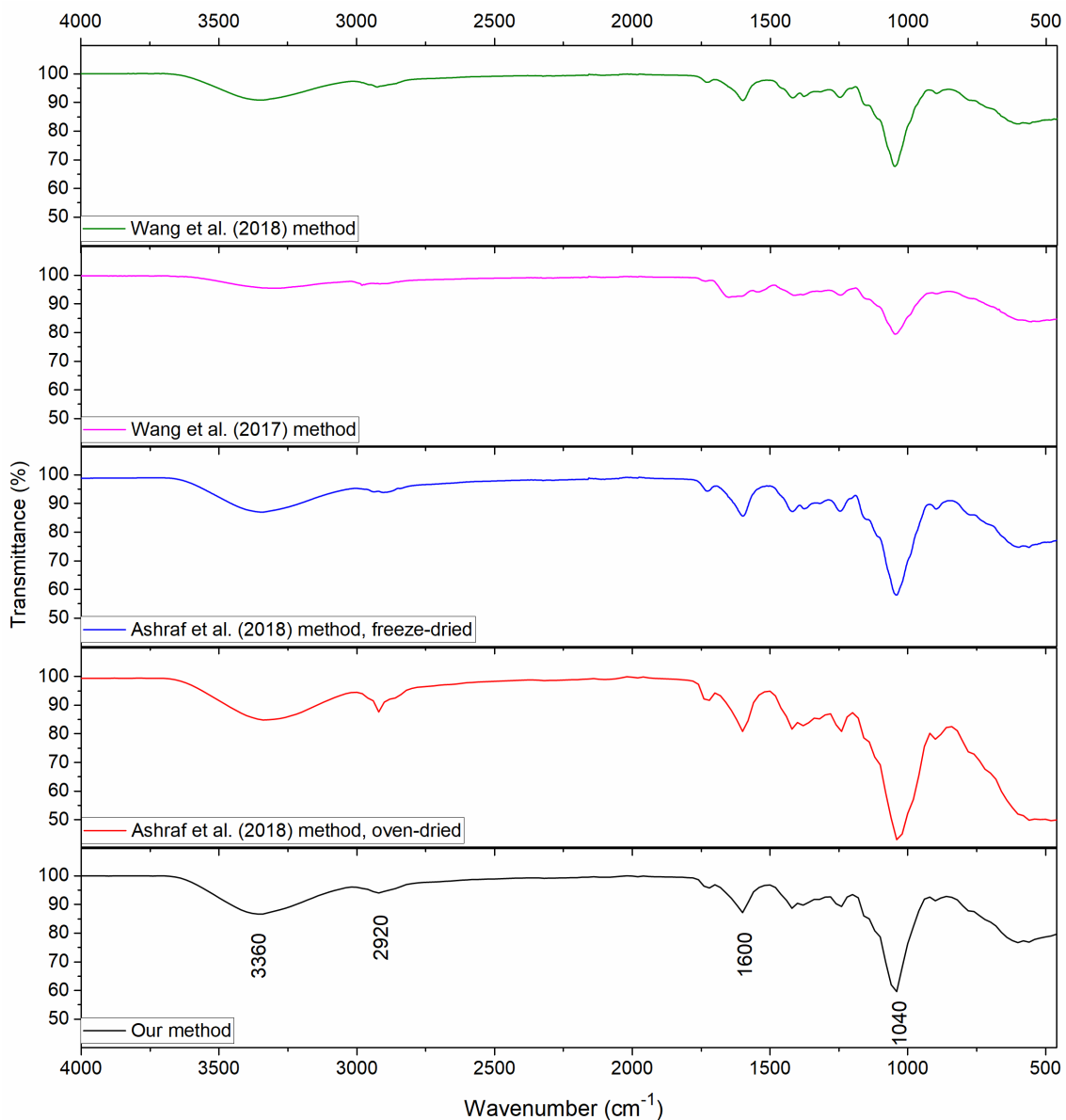


Figure 3.4. FTIR spectrum of Wang et al. (2017) method, Wang et al. (2018) method, Ashraf et al. (2018) method in lyophilized and oven-dried forms, our novel method in 2 mg/mL seed concentration

overall microstructure.

Afterward, FTIR analysis was done for all scaffolds obtained from each method as given in the Figure 3.4. The main peaks that are determinant for QSH were obtained for all samples. The presence of broad band around 3360 cm^{-1} shows the $-\text{OH}$ stretching ($3800\text{--}3100\text{ cm}^{-1}$) and peak around 2920 cm^{-1} is referred to CH ($3100\text{--}2700\text{ cm}^{-1}$). Peak around 1600 cm^{-1} is characteristic for carbonyl group (C=O) ($1620\text{--}1420\text{ cm}^{-1}$) which indicates uronic acid in structure [90; 91]. And the last characteristic peak in the structure for QSH indicates glycosidic linkage in the polysaccharide which is detected as a sharp peak around 1040 cm^{-1} ($1200\text{--}1000\text{ cm}^{-1}$) [90]. Also, these peaks are evidence of the polysaccharide structure of the QSH [92].

Our method produced a hydrogel that has similar properties to those of the samples in the literature through the most straightforward production procedure with relatively short production time also an eco-friendly and organic solvent-free process.

Based on the GTA crosslinking analysis of non lyophilized 2mg/mL concentrated QSH samples, crosslinking did not occur in standard 30 minutes crosslinking time frame. Thus crosslinking period prolonged to overnight. Even though the hydrogels were seemed to be crosslinked right after application of the GTA solution, they were degraded during standard rinsing steps. Thus, crosslinking incubation was prolonged to 24 hours and the washing step was shortened to 5 minutes. Fluidic and injectable

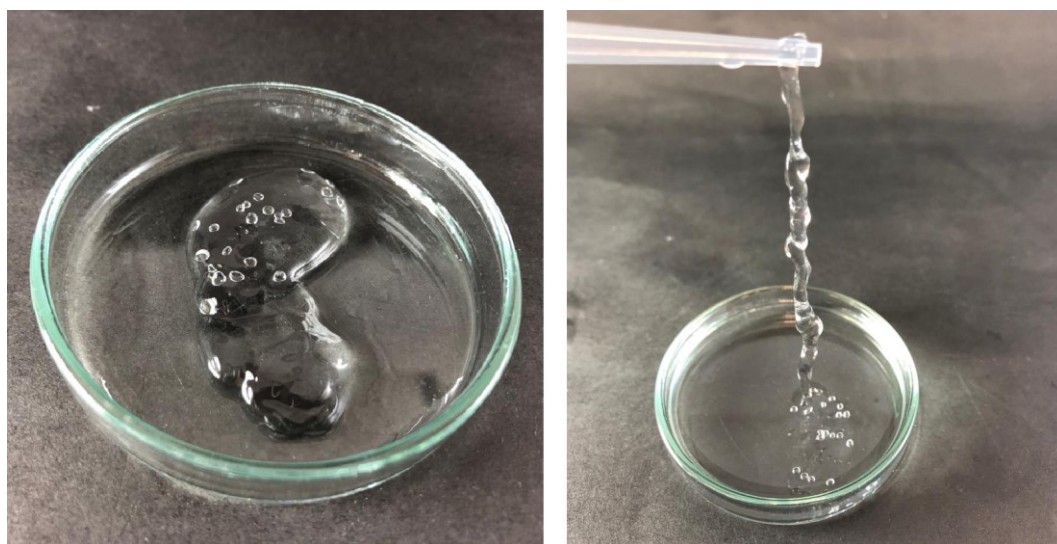


Figure 3.5 Directly crosslinked QSH samples without lyophilization

hydrogels were obtained under these parameters which were durable as shown in Figure 3.5. To dry the samples, evaporator and freeze-dryer were used. The gels that were dried in evaporator created a thin brittle film on the bottom of the vial that was not possible to process. When the lyophilization method was used, scaffold structures were obtained which were suitable for tissue engineering applications.

Although crosslinked hydrogel structures were obtained between 0.03 M and 0.5 M GTA concentrations, the porous structure could not be achieved in the direct hydrogel crosslinking method without lyophilization as shown in Figure 3.6. Therefore, in the following parts of this study, lyophilization was applied prior to GTA crosslinking procedure.

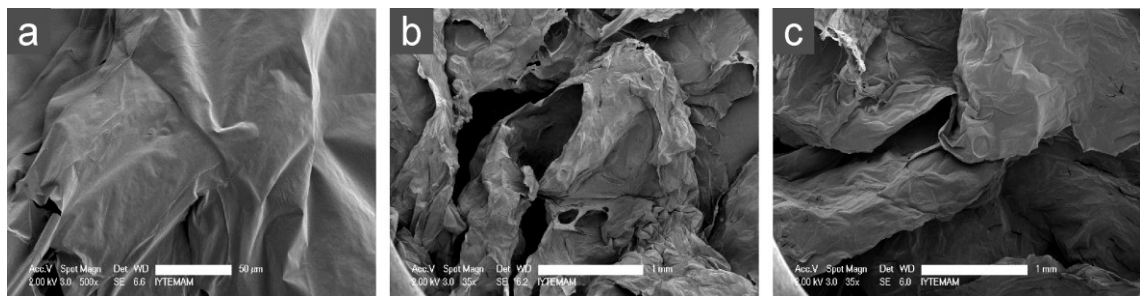


Figure 3.6 SEM images of QSH samples crosslinked via directly crosslinking method with a) 0.03 M , b) 0.1 M and c) 0.5 M GTA solutions

Parallel to the GTA crosslinking, EDC/NHS crosslinking mechanism was also evaluated as described in Figure 3.7. Quince seeds which were gelled into UP H₂O in varying concentrations (2, 10, 20, 50 mg/mL) were filtered and crosslinked with EDS/NHS directly, without lyophilization step. As shown in Figure 3.8, previously used concentration, 2 mg/mL, was not worked for EDC/NHS crosslinking, material saved its flow character even after long crosslinking incubation periods. 10 mg/mL samples only showed viscous flow as a result of partial crosslinking for moderate EDC/NHS concentrations. 20 mg/mL samples got partial crosslink in the first 90 mins and after 3 hours, hydrogels got a proper crosslink. 50 mg/mL samples achieved the fastest crosslink in low hydrogel volumes but in long term, there is no significant difference between 20 mg/mL and 50 mg/mL QSH concentrations in terms of crosslinking ability.



Figure 3.7 The experimental production and design steps of the injectable QSH scaffold; quince fruits were collected, the seeds cored out from the fruits, gelation was achieved in water after 24hours. Then the gels were filtered, crosslinked via EDC/NHS and injected into desired area to reach its final form

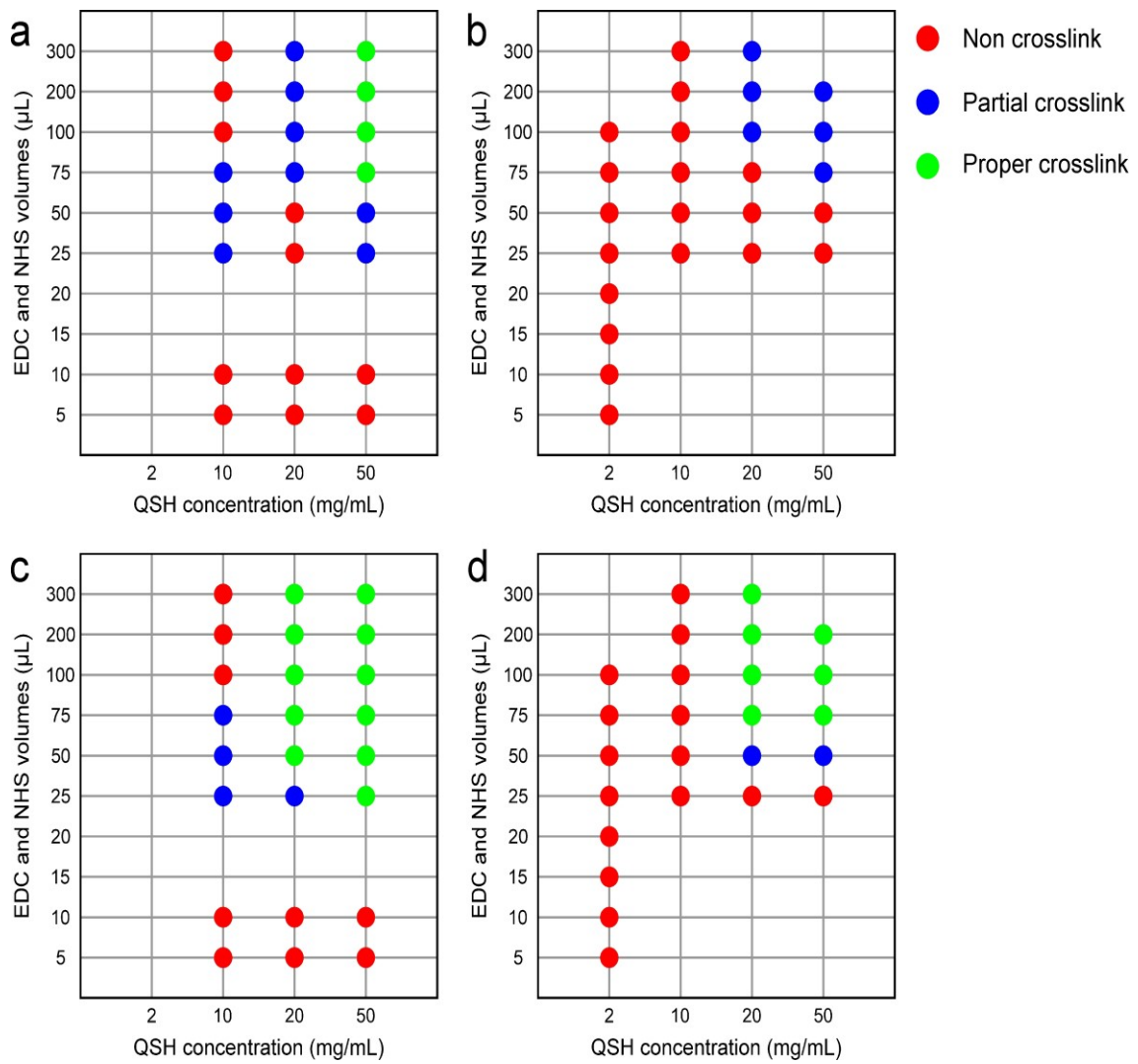


Figure 3.8. Crosslink achievement by sample types of QSH for EDC/NHS crosslinking. EDC and NHS volumes indicate independent, equal volumes for both solutions. 90 min EDC/NHS crosslink period results of a) 500 μL QSH sample volume, b) 1 mL QSH sample volume, 180 min EDC/NHS crosslink period results of c) 500 μL QSH sample volume, d) 1 mL QSH sample volume

3.2. Characterization of QSH

3.2.1. Structural and Morphological Analysis

Macro and micro structural morphology of QSH were investigated by macro imaging and SEM. As shown in Figure 3.9, QSH has an interconnected and porous structure. Porosity is a significant parameter for scaffold design in tissue engineering studies due to the space needed for cell adhesion, proliferation, tissue growth and vascularization.

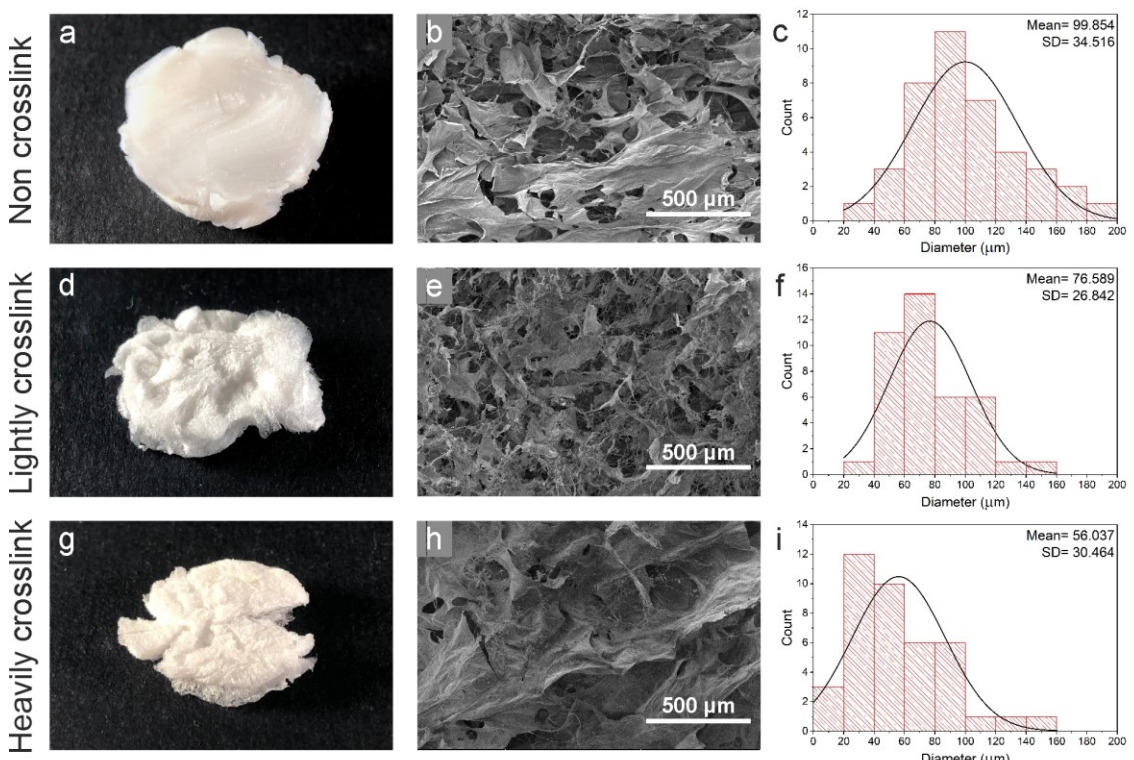


Figure 3.9. Morphological characterization of QSH scaffolds. Macro images of QSH for a) non-crosslinked, d) lightly crosslinked and, g) heavily crosslinked scaffolds, SEM images of porous QSHs for b) non-crosslinked, e) lightly crosslinked and, h) heavily crosslinked scaffolds (scale bar=500 μm), average pore size distribution histograms of QSH for c) non-crosslinked, f) lightly crosslinked and, i) heavily crosslinked scaffolds

Before crosslinking, QSH samples showed 22.52% porosity, and the average pore size was found to be around 99.85 μm . After crosslinking, 18.36% porosity and 76.59 μm average pore size were observed in lightly crosslinking concentrations (0.03 M GTA). When we evaluated the heavily crosslinking concentration (0.5 M GTA) samples, porosity decreased to 13.58%, and the average pore size was also decreased to 56.04 μm (Figure 3.9.). The chemical crosslinking step facilitated formation of a firm structure. Previous studies showed that pore size between 75-300 μm is suitable for bone tissue formation [25; 93; 94]. According to these findings, in this study, the scaffolds that were crosslinked with 0.03 M GTA, showed the most suitable values to be evaluated as a scaffold for bone tissue engineering applications.

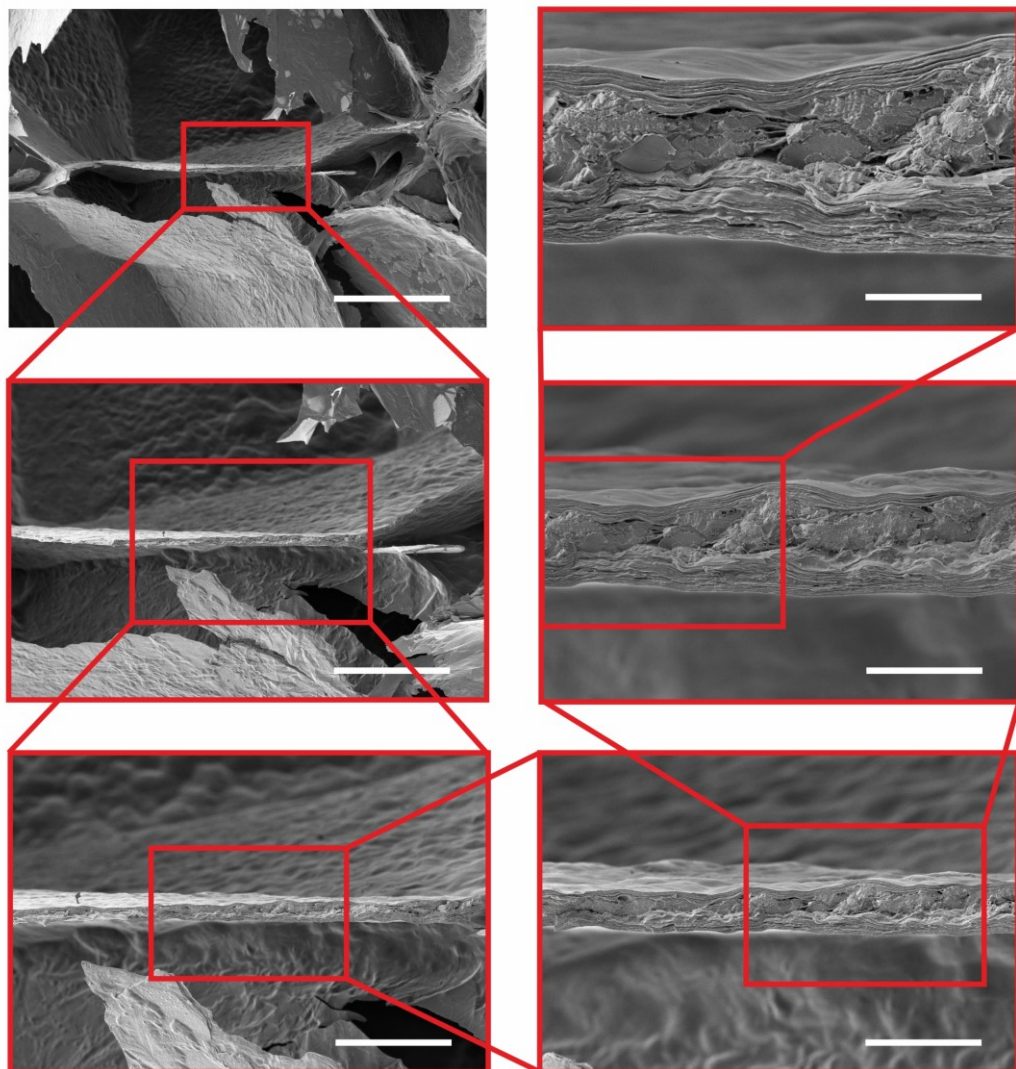


Figure 3.10. Cross-section SEM images of QSH (scale bars=400 μm , 200 μm , 100 μm , 40 μm , 20 μm , 10 μm respectively)

Porous structure of QSH was closely investigated through SEM imaging and QSHs showed layer-by-layer formation at outer layers and a sponge-like structure at inner parts, as shown in Figure 3.10. Layer-by-layer stacking is observed on the walls of inner pores. It has been observed that this layer-by-layer stacking mechanically enforces the scaffold structure that these findings were also supported by mechanical analysis via AFM.

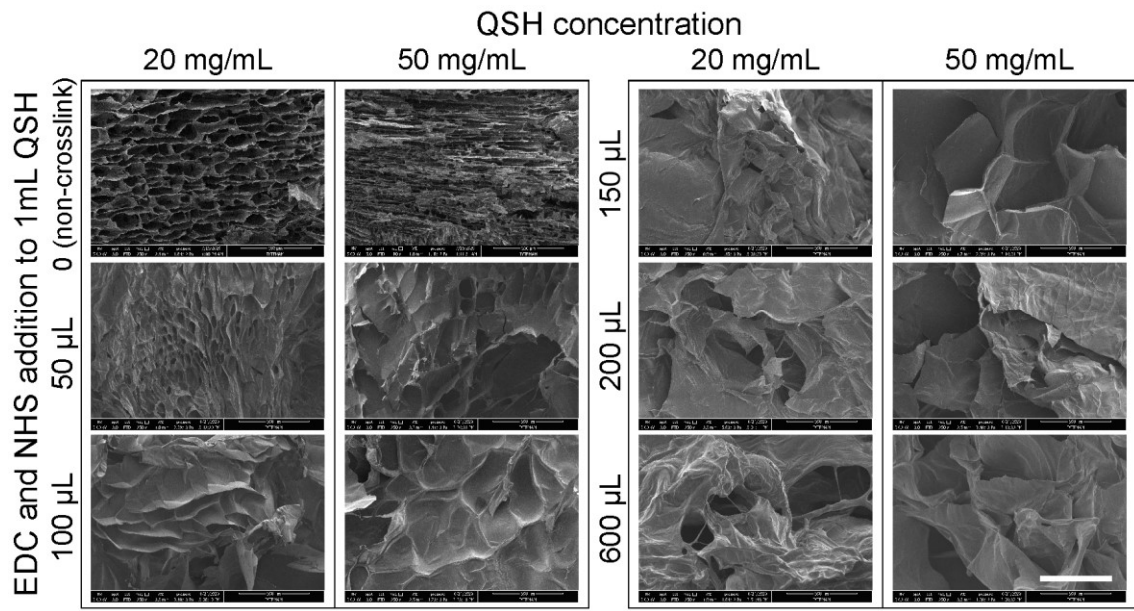


Figure 3.11. Morphological characterization of EDC/NHS crosslinked QSH scaffolds via SEM analysis (scale bar=500 μm)

Also, morphology of EDC/NHS crosslinked QSH was investigated by SEM imaging. As shown in the Figure 3.11, the interconnected and porous structure was remained after crosslinking. QSH has a similar structure with GTA crosslinked samples when crosslinked with EDC/NHS. The porosity of the scaffold remained in lower crosslinker conditions. As crosslinker concentration increased, pore size also getting bigger respectively and the original structure of the material changed.

3.2.2. Swelling Analysis

QSH's capacity to hold water is given in Figure 3.13. QSH samples were immersed into UP H₂O for 2, 8, and 48 hours, and the water holding capacities were evaluated

independently. The maximum water holding capacity was achieved at lower concentrations of the crosslinking reagent. As the concentration of GTA was increased, material firmness increased as well, and this condition decreased the water holding capacity of the material, which is parallel to the literature [95]. QSH crosslinked with 0.03 GTA held water 56.8 times more than its own mass when immersed for 2 hours, while 56.3 and 56.1 folds were reached in 8 and 48 hours immersion. On the other hand, 0.05M GTA crosslinked samples gave 53.7, 66 and 58.7 folds water holding capacities in 2, 8 and 48 hours incubation respectively. Among all GTA and immersing periods, 2 hours of water immersion and 0.03 M GTA concentration were selected as the optimum time frame and concentration for further experiments with the motivation of using the minimum amount of toxic chemical.

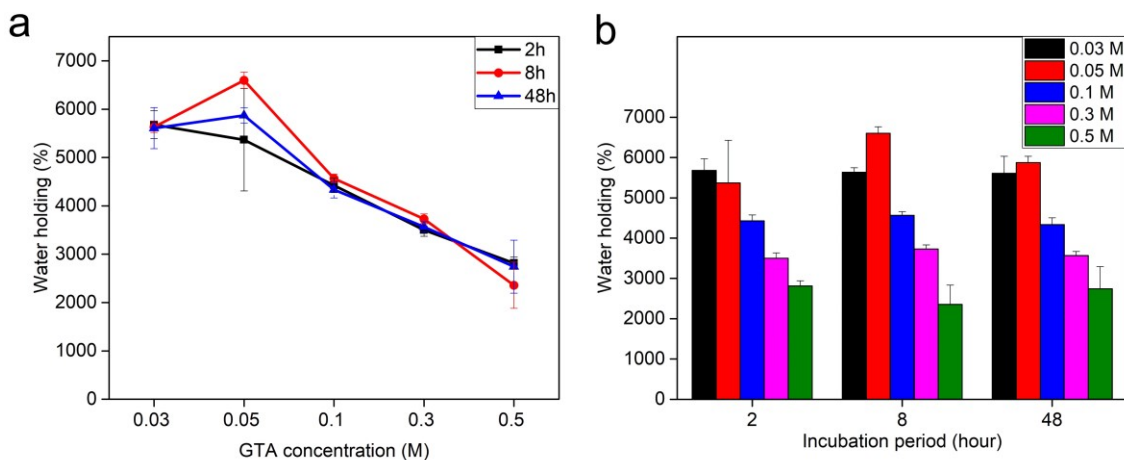


Figure 3.12. Water holding capacity graphs of QSH samples crosslinked with different GTA concentrations. Based on a) crosslink reagent concentration and b) incubation period into water

3.2.3. Degradation Analysis

The degradation rate of the scaffold should be appropriate for the host tissue and its demands. Degradation of QSH was evaluated in DMEM complete medium. In the first experimental set, samples were examined in terms of the effects of different crosslinking parameters on the degradation profile. Samples that were crosslinked with

0.1 M GTA, degraded quite early while 0.03 M GTA crosslinked samples conserved their structure during 22-day experiment (Figure 3.13.). No significant difference was observed regarding degradation between varying crosslinking periods which was 30 min and 1-hour immersion in GTA solution. The optimal parameter for degradation test was defined as 30 min of immersion in 0.03 M GTA solution, and further experiments were completed with this parameter. The second criterion for degradation tests was potential degradation side effects of UV sterilization. Non-sterilized, 15 min and 30 min (for both sides) UV- sterilized samples were compared. 15 min sterilization samples had the same profile with a non-sterilized control group in terms of degradation rate, while 30 min of sterilization samples degraded on day 20, which is not adequate time for neo-tissue formation.

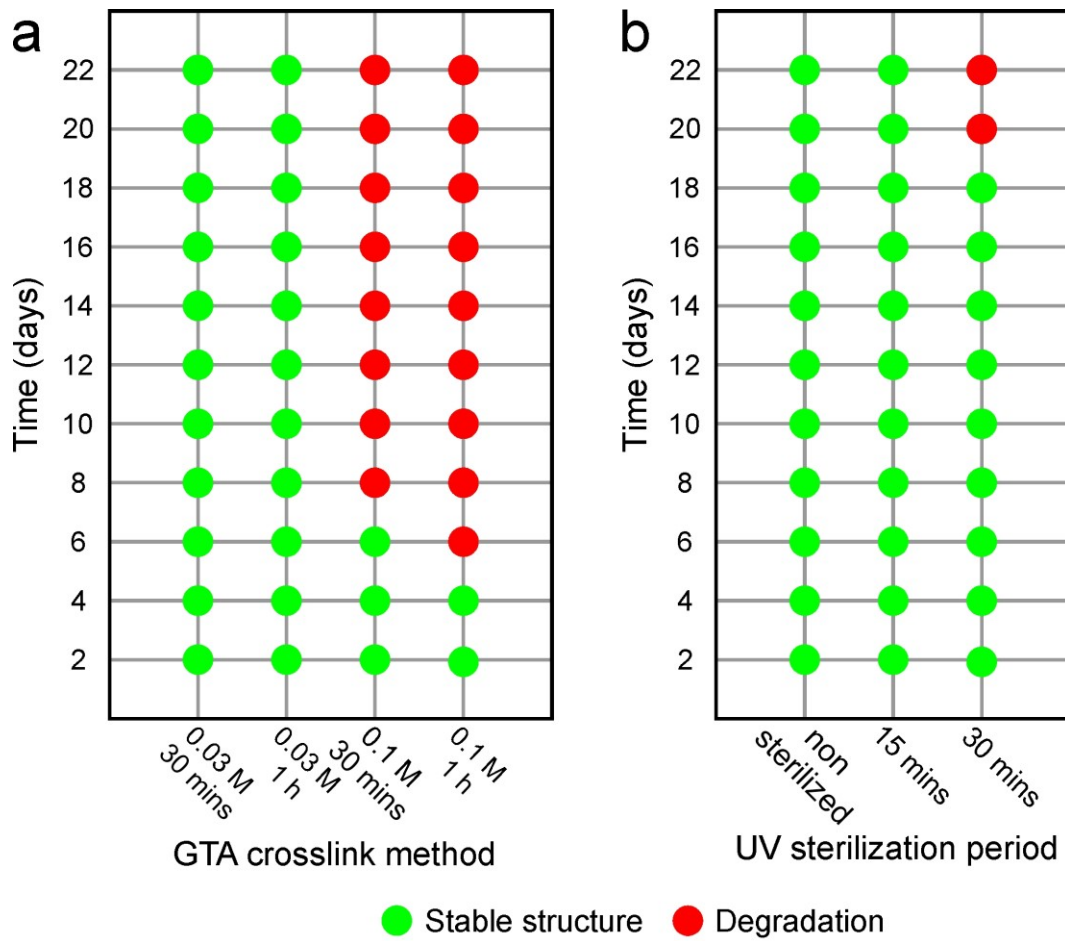


Figure 3.13. Degradation profiles based on a) crosslink solution concentration and incubation period and b) UV sterilization period

3.2.4. FTIR Analysis

Figure 3.14.a shows ATR-FTIR spectra of non-crosslinked, lightly crosslinked (0.03 M), and heavily crosslinked (0.5 M) QSHs. The wide-band appeared between 3600-

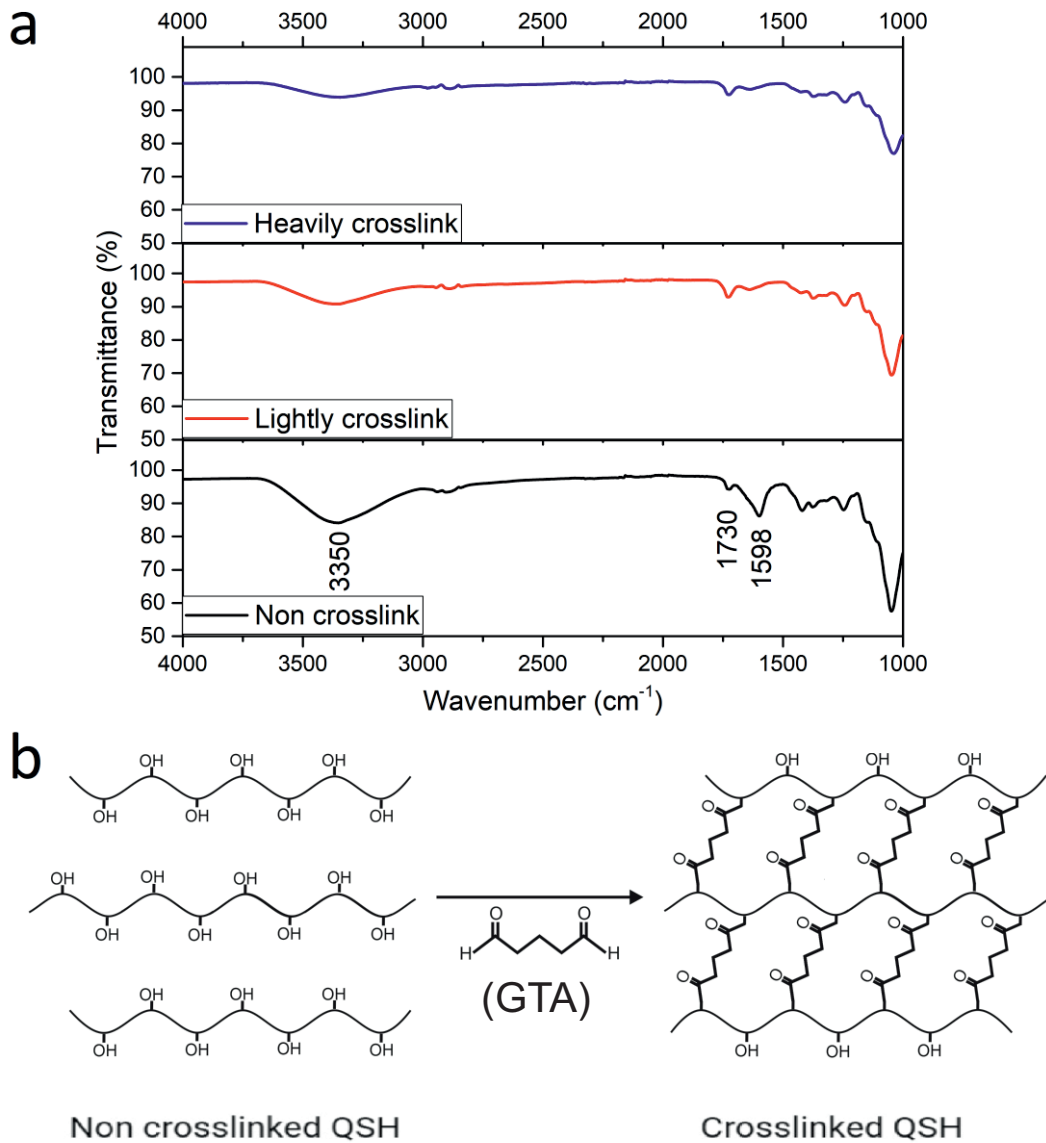


Figure 3.14. a) FTIR spectrum of non-crosslinked, lightly GTA crosslinked, and heavily GTA crosslinked QSH scaffolds. The shoulders appearing around 3350 cm^{-1} , 1730 cm^{-1} and 1598 cm^{-1} correspond to the OH groups, acetate bridge, and carboxyl groups bonds respectively, b) GTA crosslinking mechanism of QSH

3000 cm^{-1} is the characteristic stretching peak of hydrogen bonding regarding the hydroxyl groups of QSH [73; 76; 82; 83; 96-98]. A preferably deep peak observed in non-crosslinked QSH samples around this region compared to crosslinked QSHs, attributed to the formation of the intra/inter hydrogen bonds between QSH hydroxyl groups and GTA aldehyde groups as described in Figure 3.14.b [99; 100]. Because of the presence of CH and CH_2 groups in cellulose and hemicellulose parts, weak CH stretching vibration peaks appear between 2950 and 2800 cm^{-1} [73; 76; 83; 96; 101; 102]. Characteristic peaks around 1600 and 1420 cm^{-1} indicate asymmetric and symmetric stretching of the carbonyl group (C=O) which shows uronic acid presence [90; 98; 103-105]. Furthermore, band at 1730 cm^{-1} indicates the presence of carboxylic group grafting [73] or esterification [76; 82; 83]. Moreover, an increased peak at 1730 cm^{-1} can be defined as the acetate bridge by combining GTA dialdehyde and QSH cellulose content's hydroxyl group [99; 106; 107]. Typical polysaccharide bands are recorded around 1200 - 1000 cm^{-1} shows the C-OH bending and C-O-C stretching of glycosidic linkage [90; 92; 101-103]. FTIR findings suggest effective crosslinking of QSH via GTA.

Next, FTIR analysis was done for EDC/NHS crosslinked QSH samples. Characteristic peaks that correspond to the crosslinking were observed as seen in Figure 3.15. Around 1042 cm^{-1} , C-O-C and C-O-H vibrations [105] were clearly seen in the figure. Also, wide peaks around 3343 cm^{-1} corresponded to OH groups in the structure were observed.

EDC/NHS can efficiently create conjugates between proteins. EDC by itself is normally sufficient for amide bond creating. NHS addition increases the coupling efficiency and stability of amine-reactive intermediates. The mechanism of EDC/NHS crosslinking firstly starts with the activation of carboxyl groups. Activated carboxyl groups figure amine-reactive O-acylisourea intermediates. These intermediates give reaction with primary amines and amide bonds are created. A newly formed peak observed around 1640 cm^{-1} which is related to the amide bonds. Also, the intensity of the peak around 1250 cm^{-1} was highly increased which is related with another amide bond confirm the crosslinking via EDC/NHS [108; 109]. These peaks suggest crosslinking mechanism was successfully worked in both EDC/NHS concentrations.

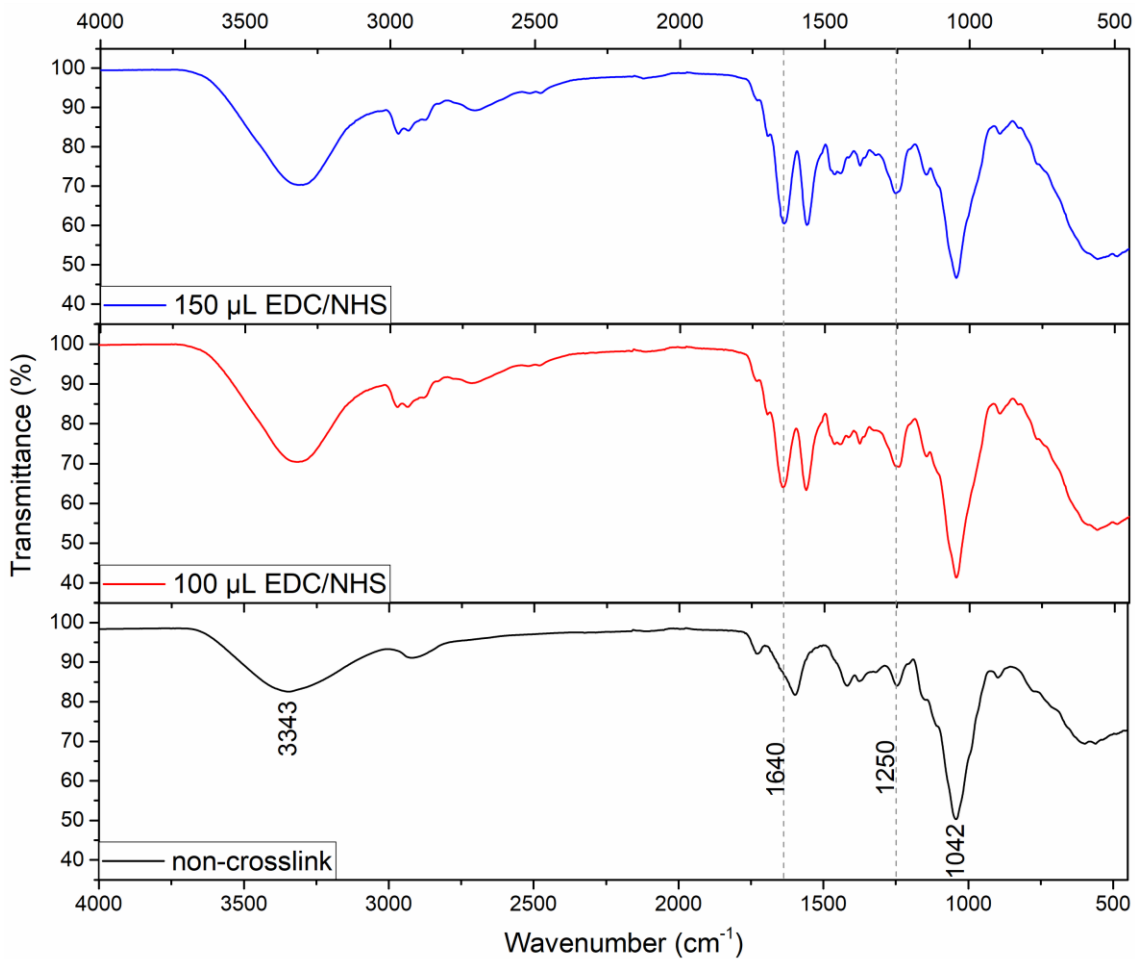


Figure 3.15. FTIR spectrum of non-crosslinked, 100 μL EDC/NHS crosslinked, and 150 μL EDC/NHS crosslinked QSH scaffolds. The shoulders appearing around 1640 cm^{-1} and 1250 cm^{-1} correspond to the amide bonds formed after crosslinking.

3.2.5. AFM Analysis

Surface of a material critically affects the interaction between cell and biomaterial. Surface topography, chemistry, porosity, and wetting are important factors in cell attachment and proliferation [110; 111]. In this study, both surface roughness analysis and mechanical tests were done via AFM [112]. Surface topography and roughness of QSH samples were analyzed by AFM measurements for non-crosslinked and

crosslinked (0.03 M GTA) scaffolds as shown in Figure 3.16. The surface roughness of QSH scaffolds was respectively measured as 613.5 nm and 2 μm for non-crosslinked and crosslinked samples. It is obvious that, after the crosslinking process, the surface roughness increased around 3.5 times. In addition to this, Young's modulus points toward the rigidity of the material such that bigger Young's Modulus refers to more rigid material. Young's modulus distribution of non crosslinked and crosslinked QSH samples analyzed with AFM measurements which were shown in Figure 3.16b,d respectively. Young's modulus of QSH material was increased from 53 MPa to 76 MPa with crosslinking. Because of the chemical crosslinking, the number of entanglements in polymer chains was increased and these newly formed entanglements mediate dissipation of energy [113-115]. Thus, the difference between non crosslinked and crosslinked samples was observed. Young's modulus mapping was used to show

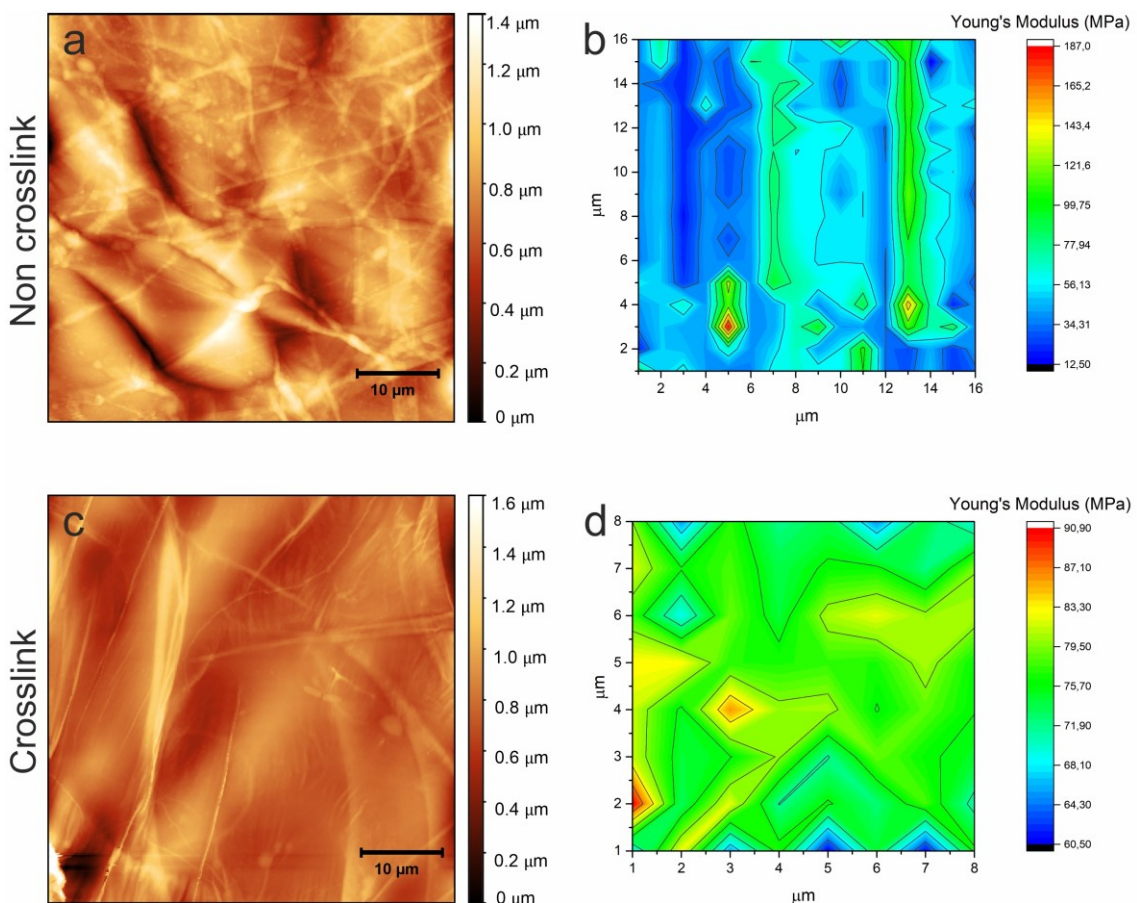


Figure 3.16. AFM analysis showing the surface characteristics of QSH surface topography of a) non-crosslinked and c) crosslinked scaffolds; force-distance profiles of b) non-crosslinked and d) crosslinked scaffolds

Young's (elastic) modulus distribution in a unit area of QSH samples. Young's modulus distribution of QSH was mainly spread between 12 and 60 MPa (from blue to green area) with a heterogeneous profile in non-crosslinked samples as shown in Figure 3.16b. After crosslinking, distribution gained homogeneity between 70 and 80 MPa (green area) as indicated in Figure 3.16d. Crosslinking with GTA was gained a firmer structure to the material and increase Young's modulus parallel to the literature [111] as AFM results showed.

3.2.6. Protein Adsorption Assay

Protein adsorption results give an explicit hint regarding the material's biocompatibility since it shows the attachment capability of the cells on the scaffold surface. Serum albumin is the most abundant protein in the blood, thus has a significant role in foreign body reaction at the early stages of material-blood contact [116]. As the proteins on the cell membrane interact and attach to the biomaterials, material's interaction with serum albumin led to cell-material adhesion profile. Our findings indicated that a considerably higher BSA adsorption was observed at 1000 $\mu\text{g/mL}$ BSA concentration as seen in Figure 3.17. High protein adsorption shows that cells would tend to attach the material.

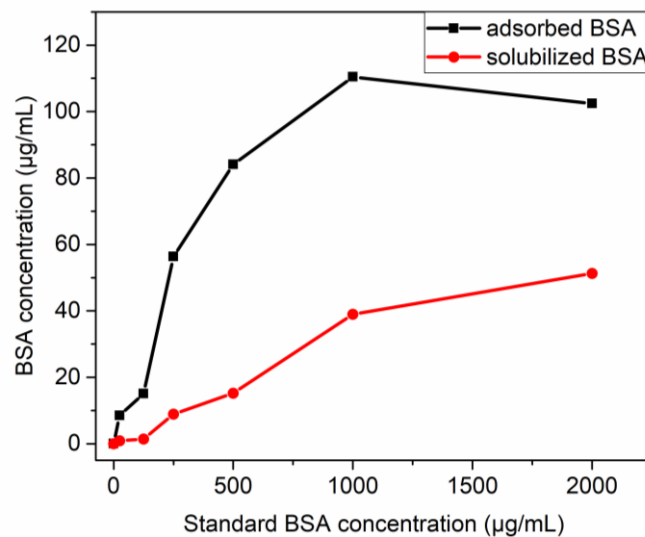


Figure 3.17. Protein adsorption graph of QSH. Adsorbed (black) and solubilized (red) BSA proteins were illustrated in the graph

3.3. 3D Cell Culture Studies, Cell Viability and Proliferation

In vitro 3D cell culture studies were carried out with NIH-3T3 and SaOS-2 cells. These cell lines represent the model tissues in focus and they are one of the most commonly used cell lines in the field. NIH-3T3 cell line was used as a cellular model for scaffold characterization while SaOS-2 cell line was used as a bone tissue model. Cell viability and proliferation analyses were done with AlamarBlue and MTT assay, Live/Dead analysis and live cell imaging via fluorescent dyes.

3.3.1. Cell Viability and Proliferation Analyses

Cell viability analyses of NIH-3T3 cells were accomplished with AlamarBlue assay. QSHs were prepared for all cell viability and proliferation analyses in aqueous solutions at 2mg/mL concentration. QSHs were crosslinked in 0.03M and 0.5 M GTA after lyophilization to assess the effects of GTA concentration on viability as given in Figure 3.18.a. Later, viability tests (Figure 3.18.b,) were performed just by using 0.03 M GTA concentration as this concentration gave the highest cell viability results as given in the Figure 3.18.a

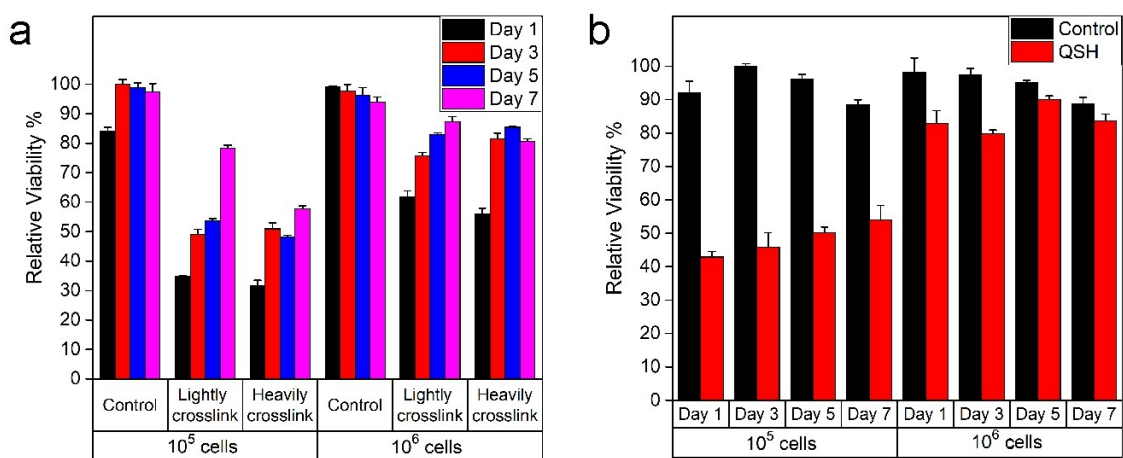


Figure 3.18. Cell viability results of NIH-3T3 cells on QSH scaffolds evaluated by AlamarBlue assay, a) cell viability against crosslinking parameters, b) cell viability against cell number

In both sets in Figure 3.18 and either low or high cell seeding concentrations, due to the inadequate surface area, the proliferation of 2D control groups was limited and cells began to die from the first days of the experiments. Among all QSH samples, the finest results were obtained in the lightly crosslinked scaffold and high cell density which are 0.03 M GTA and 2×10^6 cells per scaffold as seen in Figure 3.18.

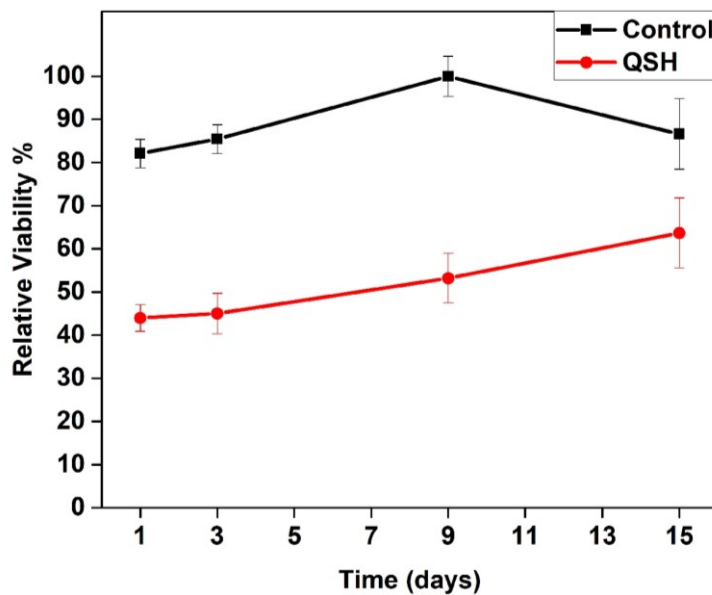


Figure 3.19. Cell viability results of NIH-3T3 cells on QSH scaffolds evaluated by AlamarBlue assay, cell viability for long term culturing

Cell contact is restricted in the complex 3D growth area when compared to traditional 2D cell cultures due to the seeding of the same number of cells to the increased total volume [117-119]. Higher cell number in the unit area increased the cell-cell interactions and this situation influence proliferation positively. Therefore, high cell seeding concentration gave better results in terms of cell viability. As there was cellular loss while seeding on the scaffolds due to partial washout problem because of the porous structure and liquid environment, starting points is lower than 2D control but this gap was closed by proliferating cells even in the short term.

Further, 2×10^6 NIH 3T3 cells were seeded on the 1300 μ L QSHs for long term viability analysis (Figure 3.19.). Cells were cultured up to 14 days to analyze long term viability results to observe proliferation profiles of cells on the QSH scaffold. The proliferation of 2D control group showed a decreasing profile from day 9 as seen in Figure 3.19.

Because of the insufficient surface area related to contact inhibition of cells. In long term analysis of the QSH scaffold, cellular proliferation in the experiment group had an accelerated profile when we compared the growth rate among the day 1-3, 3-9 and 9-15. This regular acceleration gain was related to the adaptation of cells to the QSH. Complex 3D scaffold structure limits cellular communication in early stages [117-119] In overall, the adaptation phase in 3D cell culture takes longer because of slow adsorption and infiltration of cells in the 3D microenvironment. Nevertheless, increasing acceleration of the viability as described in Figure 3.19 shows that as the cell number increase, QSH scaffold promotes proliferation of cells in long term.

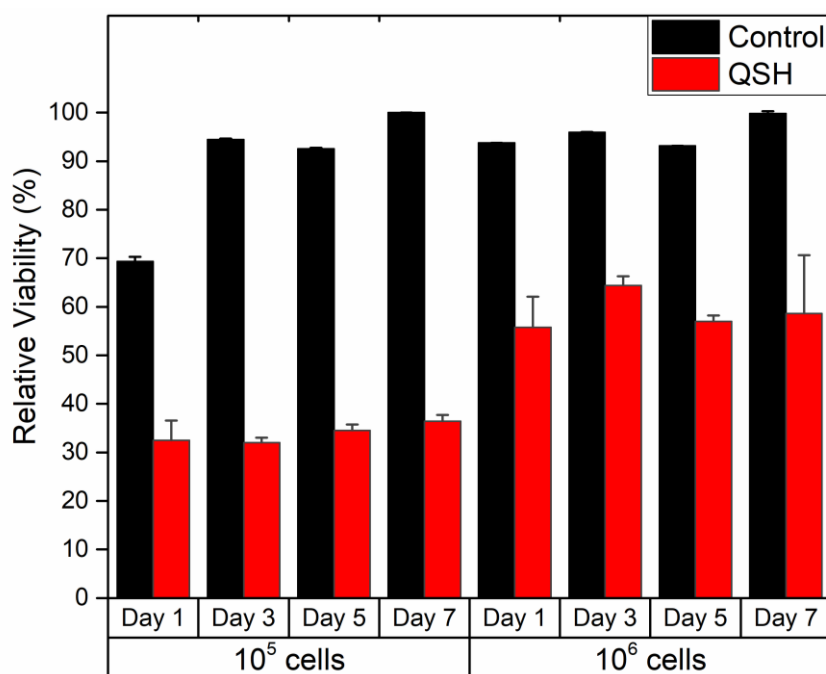


Figure 3.20. Cell viability results of SaOS-2 cells on QSH scaffolds evaluated by AlamarBlue assay, cell viability against cell number

AlamarBlue and MTT assays were carried out to investigate cell viability of SaOS-2 cells that were seeded on QSHs. QSHs were prepared in 2mg/mL concentration in aqueous solutions and crosslinked with 0.03 M GTA. First of all, low density (2×10^5) and high density (2×10^6) SaOS-2 cells were seeded on QSHs, which were crosslinked with 0.03 M GTA and cells were cultured for 7 days for cell number optimization. High

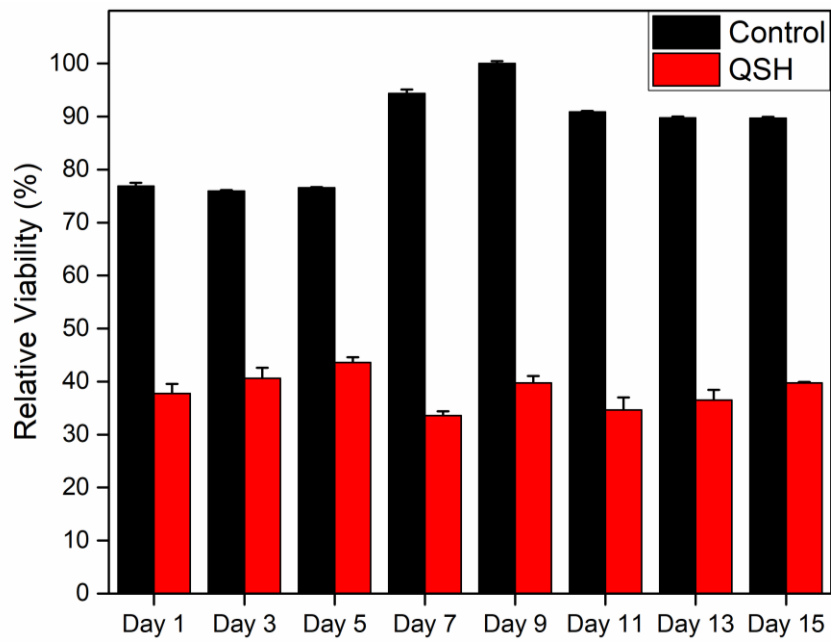


Figure 3.21. Cell viability results of SaOS-2 cells on QSH scaffolds evaluated by AlamarBlue assay, cell viability for long term culturing

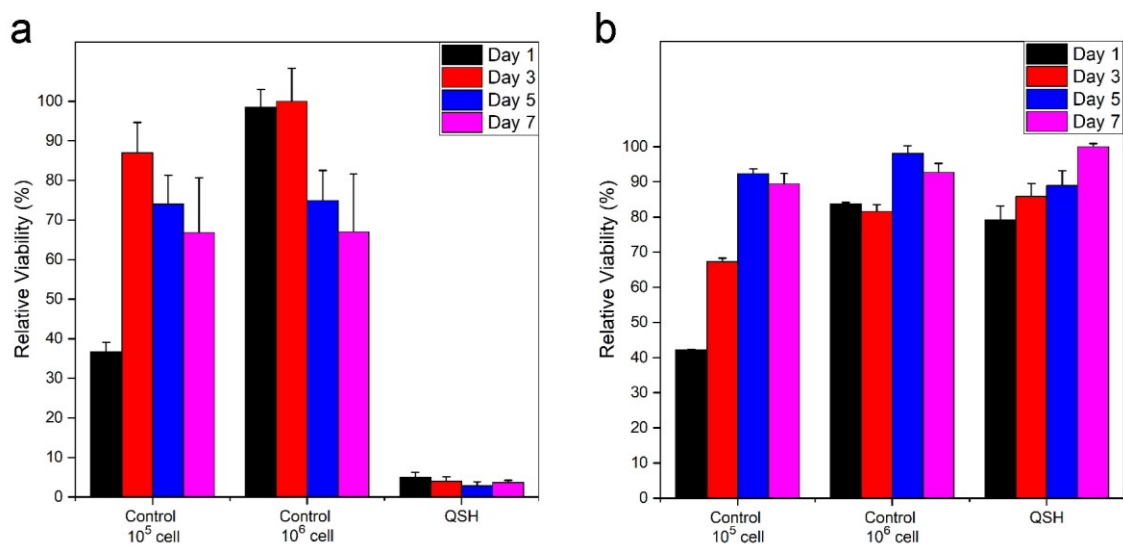


Figure 3.22. Cell viability results of SaOS-2 cells on QSH scaffolds evaluated by a) MTT, b) AlamarBlue assay in shaking method

cell seeding concentrations provided better adsorption and proliferation rates as described in Figure 3.20.

To investigate long term effects, 8×10^5 cells were seeded onto QSHs which were crosslinked with 0.03 M GTA and cultured up to 15 days for long term viability assay as seen in Figure 3.21. AlamarBlue experimental results showed lower cell viability than expected when compared with the microscopy images. This problem might be caused by the diffusion problem of AlamarBlue reagent from supernatant to cells or vice versa. Color change inside the gel constructs was not homogeneous. Therefore, to overcome this problem, alternative analysis methods were tried. First MTT analysis was examined to compare with AlamarBlue analysis, however MTT method did not provide proper results (Figure 3.22.a.). Later, samples were incubated in thermo shaker after AlamarBlue reagent addition at 37°C and 50 rpm for 3.5 hours to overcome the diffusion problem. Shaking of the plates during dye incubation provided colorimetric homogeneity. These homogenous distributions also led to significant cell viability results as shown in Figure 3.22.b.

Short and long term viability analysis of QSH scaffolds with SaOS-2 cells showed that QSH has a proliferation promotive effect with no toxic effects on SaOS-2 cells. Proliferation profiles of 2D control groups were high at the beginning but limited in longer incubation periods because of the insufficient surface area. Cells started to die or detach from the surface both in low and high cell concentrations. When QSHs were used, increased cell number in unit area reinforced cell-cell interactions which made a positive effect on cell proliferation. Thus high cell seeding concentrations provided better results.

Lastly, AlamarBlue analysis with EDC/NHS crosslinked QSH samples was done for SaOS-2 cells. 100 and 150 μL EDC and NHS solutions added to 1mL QSH. Samples prepared in two different methods as crosslink with cells method and seeding of cells after crosslinking method. In both experiment methods, experimental groups gave higher viability results than control, and no toxicity was observed related to QSH material or EDC/NHS crosslinking. Protocol based on seeding of cells before crosslinking (crosslink with cells) gave better results with a slight difference with cell seeding after crosslinking based method. Crosslinking with the cells with 150 μL EDC and NHS solutions gave the best result which was 60% more than 2D and 44% more than 3D controls in terms of viability.

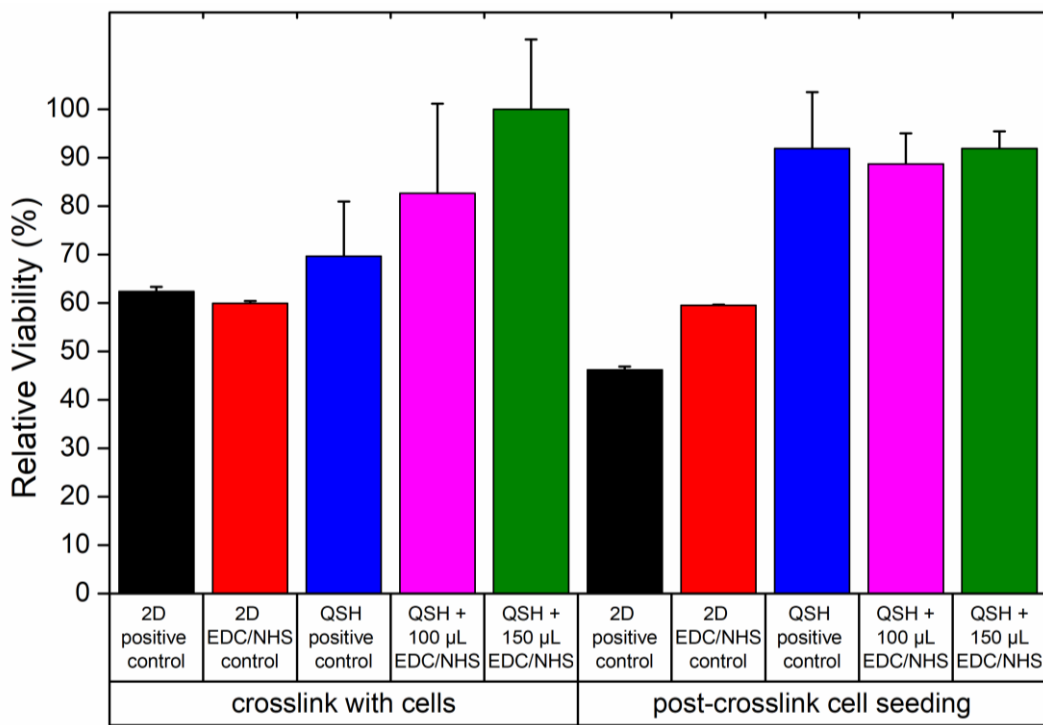


Figure 3.23. Cell viability results of SaOS-2 cells on EDC/NHS crosslinked injectable QSH scaffolds, evaluated by AlamarBlue assay, cell viability for short term culturing

Live/Dead assay was also accomplished for cell viability observation of cells on the QSH scaffold. The assay was run at the day 1, 3, 5 and 7 of the 3D cell culturing period. The limited surface area in the 2D caused contact inhibition [120] and cells were neither dying nor proliferating as seen in Figure 3.24. QSH scaffold that is crosslinked with 0.03 M GTA and has a high cell density gave higher cell viability results when compared with the samples that were crosslinked with 0.5 M GTA and have low cell densities. Also, more spheroid formations were observed in these configurations. These findings suggest that increased GTA concentration in crosslinking solution may have toxic effects on cells and firmer structure does not allow cellular infiltration thus cell viability decreases which is correlated with the literature [121-123]. Also, high cell seeding concentrations provide better results due to high cell-cell interaction. Later, 4×10^5 SaOS-2 cells were seeded on the 2D surface as positive control, and the same amount of cells were seeded onto QSHs, which were crosslinked with 0.03 M GTA as seen in Figure 3.25, Figure 3.26 and Figure 3.27. The assay was conducted over a

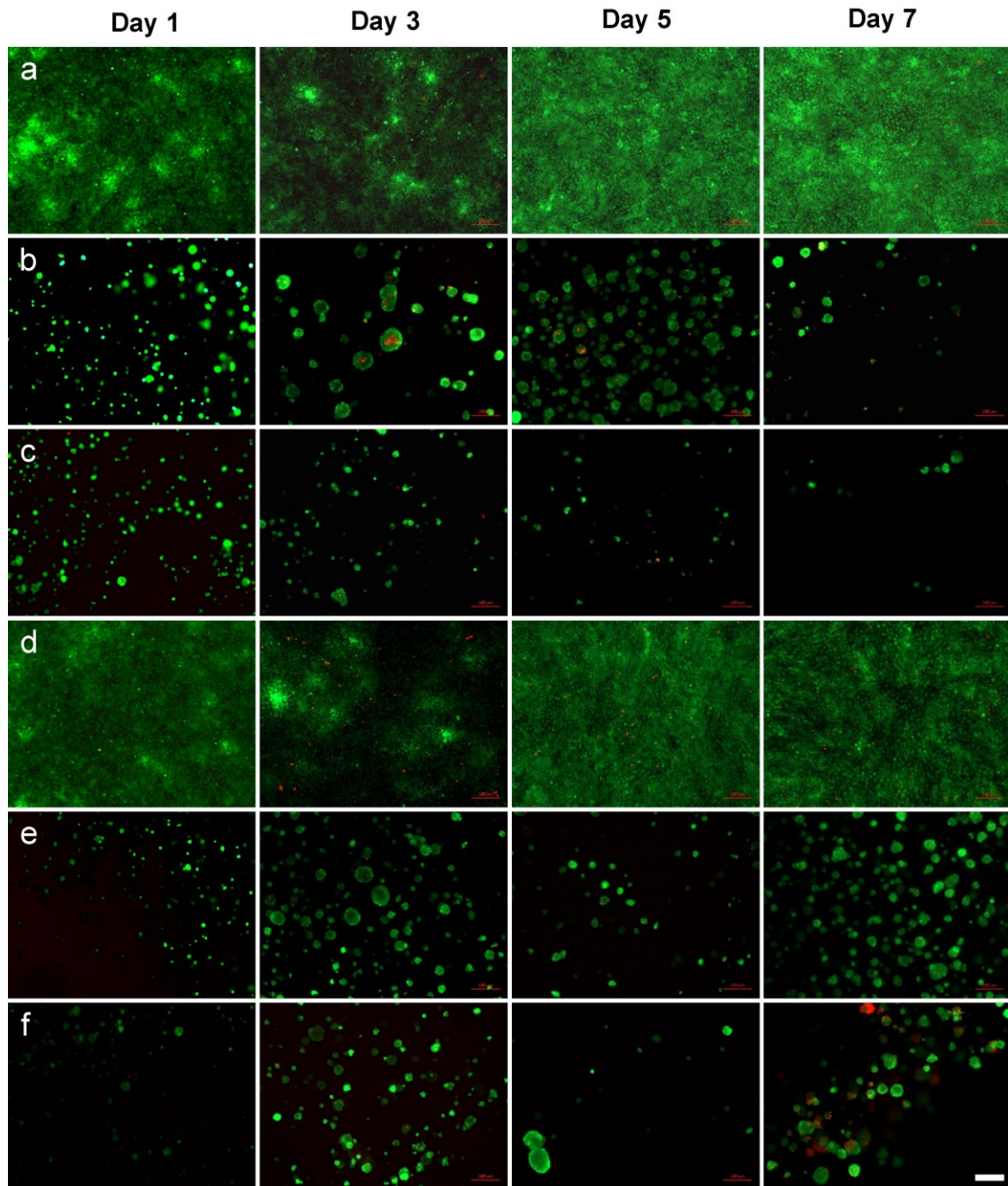


Figure 3.24. Fluorescence microscope images of Live/Dead assay of NIH-3T3 cells in a-c) 10^5 and d-f) 10^6 concentration on a,d) 2D control, QSH scaffolds which are crosslinked with b,e) 0.03 M GTA and c,f) 0.5 M GTA (scale bar 100 μm)

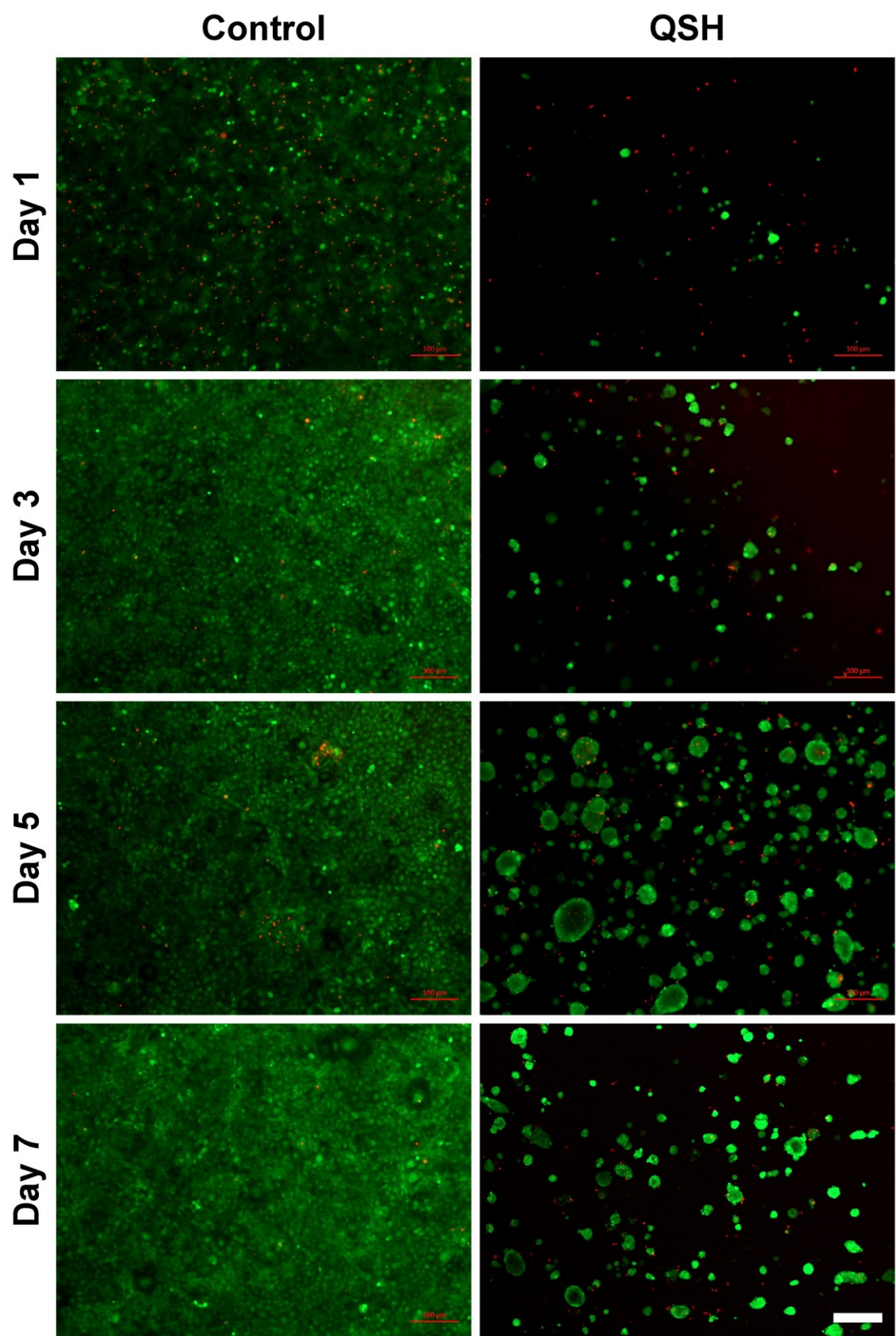


Figure 3.25. Fluorescence microscope images of Live/Dead assay of SaOS-2 cells on 2D control and QSH scaffold from day 1 to 7 (scale bar 100 μ m)

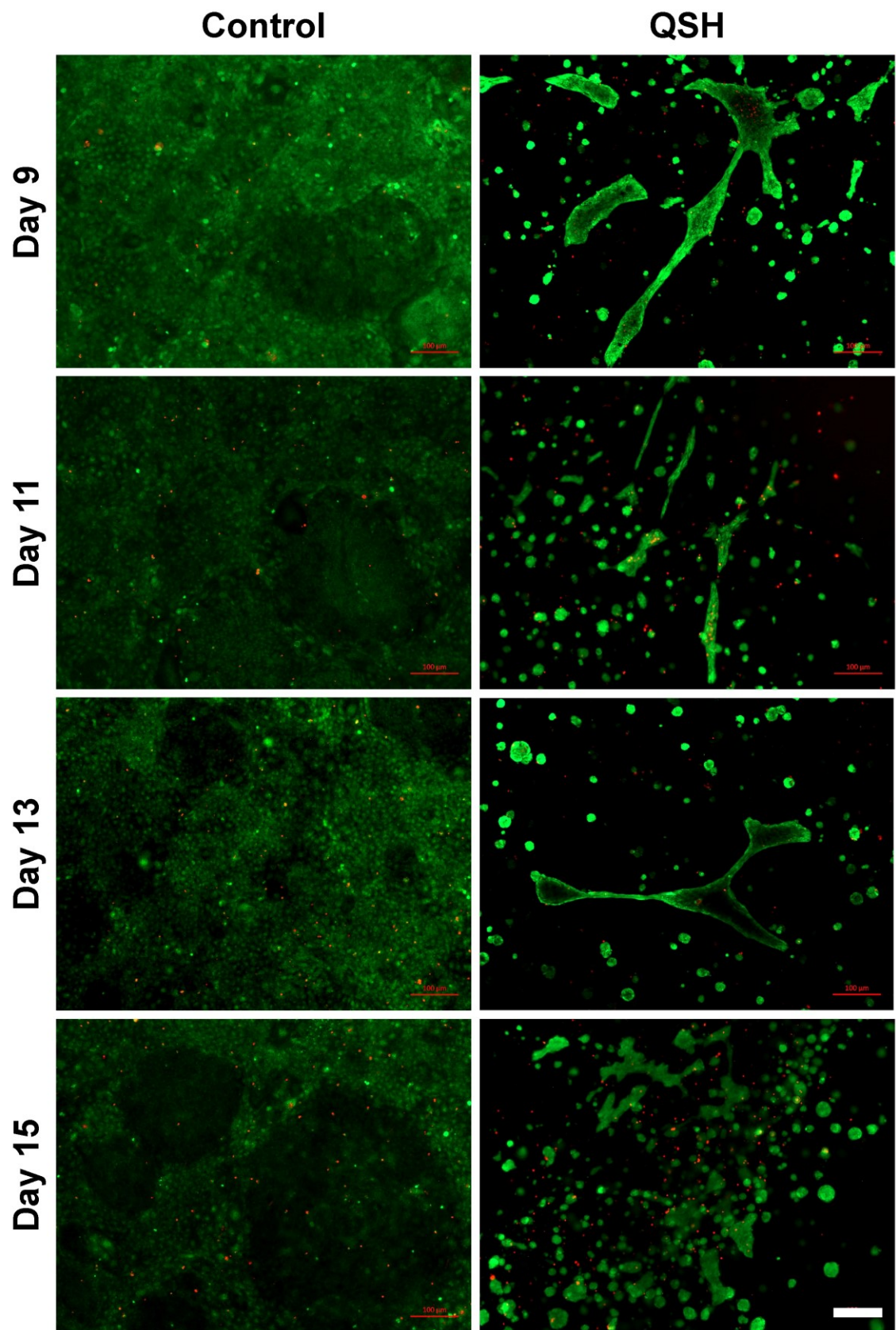


Figure 3.26. Fluorescence microscope images of Live/Dead assay of SaOS-2 cells on 2D control and QSH scaffold from day 9 to 15 (scale bar 100 μm)

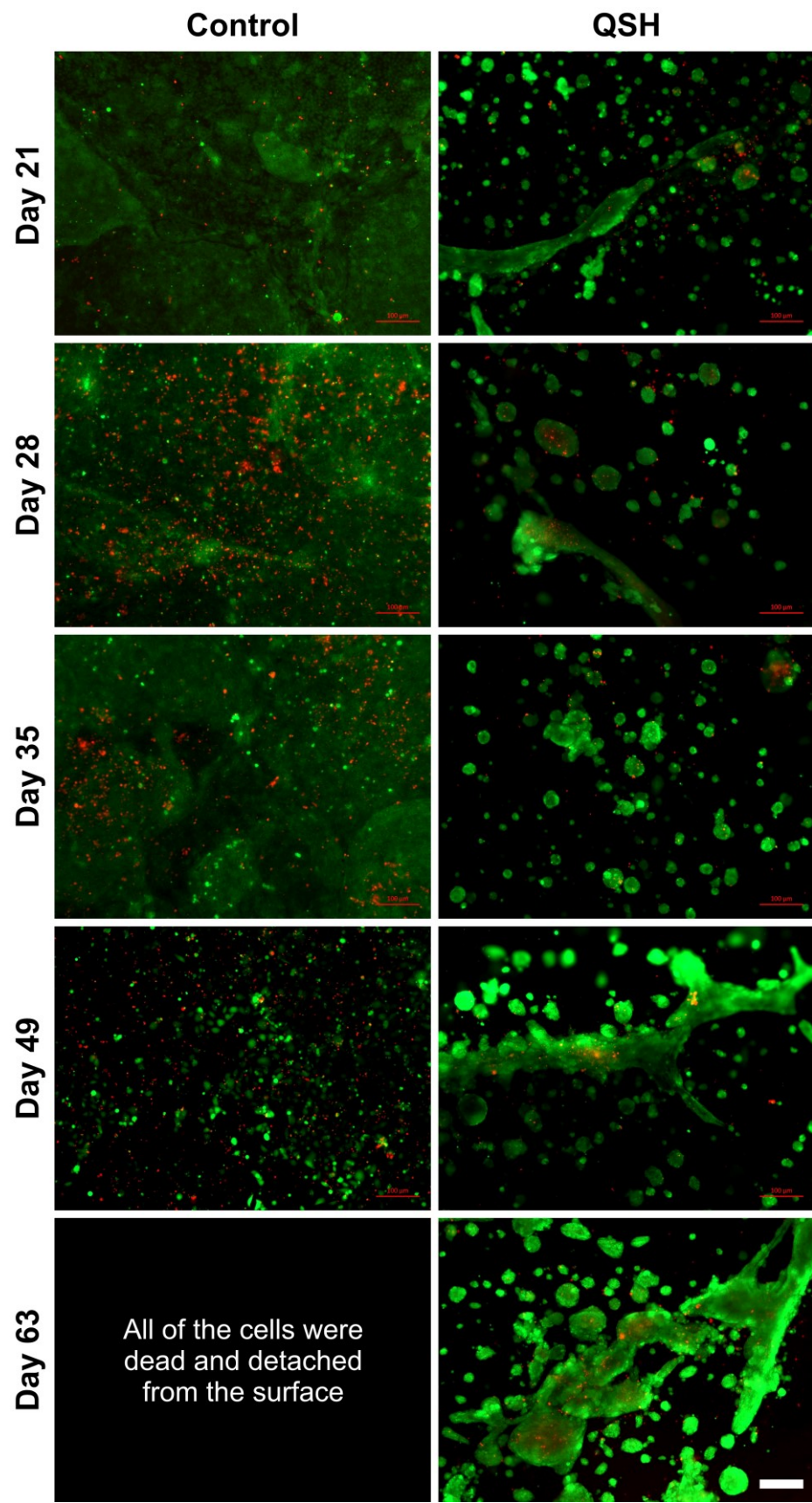


Figure 3.27. Fluorescence microscope images of Live/Dead assay of SaOS-2 cells on 2D control and QSH scaffold from day 21 to 63 (scale bar 100 μ m)

period of 9 weeks, and the cells were observed every second day during the first 2 weeks of the experiment. As a characteristic behavior of carcinogenic cells, cells started to proliferate over each other layer by layer but from day 9, similarly as observed in NIH-3T3 cells, a limited culture area in the 2D control group resulted in negative results even with carcinogenic cells; and cells were detached from the surface or died due to contact inhibition (Figure 3.26, Figure 3.27). Cells on the QSH scaffolds firstly formed spheroids but then, they created bigger interconnected tissue formations starting from day 9 (Figure 3.26). In the long term observation, cells in 2D could not survive on the plates and detach from the surface after 7th week while the cells on the QSH scaffolds continued to proliferate (Figure 3.27). Obtained results were promising and showing that ECM secretion might be taking place and the cells start to create a neo-tissue.

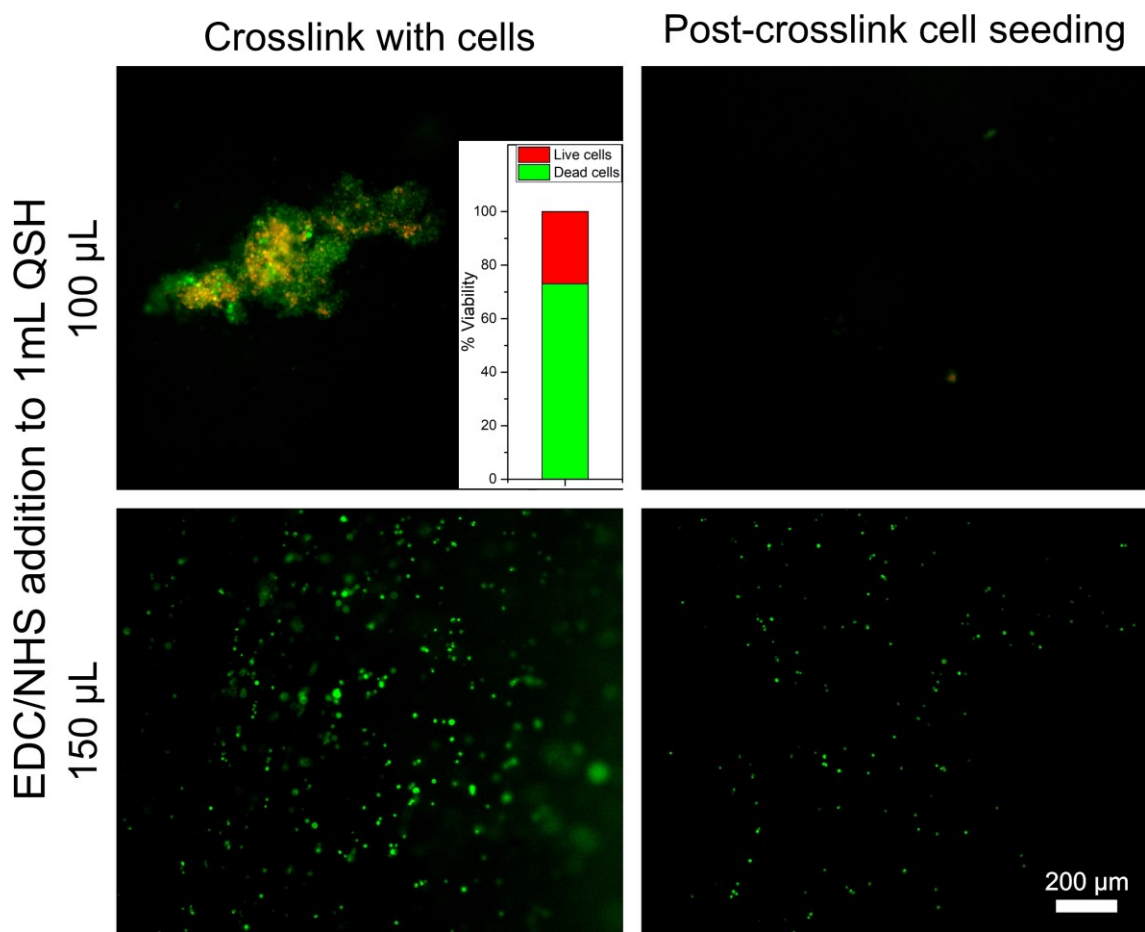


Figure 3.28. Fluorescence microscope images of Live/Dead assay of SaOS-2 cells on EDC/NHS crosslinked injectable QSH scaffolds (scale bar 200 μm)

Therefore, ECM components were analyzed further to investigate the microenvironment of newly formed 3D structures in the preformed scaffolds.

Lastly, the Live-Dead assay with EDC/NHS crosslinked QSH samples was done for SaOS-2 cells (Figure 3.28). 100 and 150 μ L EDC and NHS solutions added to 1mL QSH. Samples prepared in two different methods as crosslink with cells and seeding of cells after crosslinking. In both experiment sets, no toxicity was observed related to QSH material or EDC/NHS crosslinking. When we compared the protocols with each other, seeding of cells before crosslinking gave better results. As cells mixed with the material before crosslinking, cells easily located while there would be penetration problems in the second method. Crosslinking with the cells with 100 μ L EDC and NHS solutions gave the best results with a 73% viability rate.

3.3.2. 3D Cell Culture Morphology and ECM Secretion Analyses

3D cell culture formation and spheroids were visualized with SEM. Later, to observe the formation of ECM and 3D tissue-like structures DAPI and collagen staining were done.

3.3.2.1. SEM Analyses

Long term proliferation of NIH-3T3 cells on QSH scaffolds were observed via SEM for 2 months cultured scaffolds (Figure 3.29). Cells were strongly adhered to the scaffold and created spheroids among interconnected pores of the QSH scaffold. Originally, NIH-3T3 cells indicate monolayer characteristics in 2D, however; they were inducted to create 3D spheroids on QSH scaffolds. Adherence and spreading of spheroids all along the scaffold show that QSH scaffold has biocompatible character and a suitable scaffold material for tissue engineering applications.

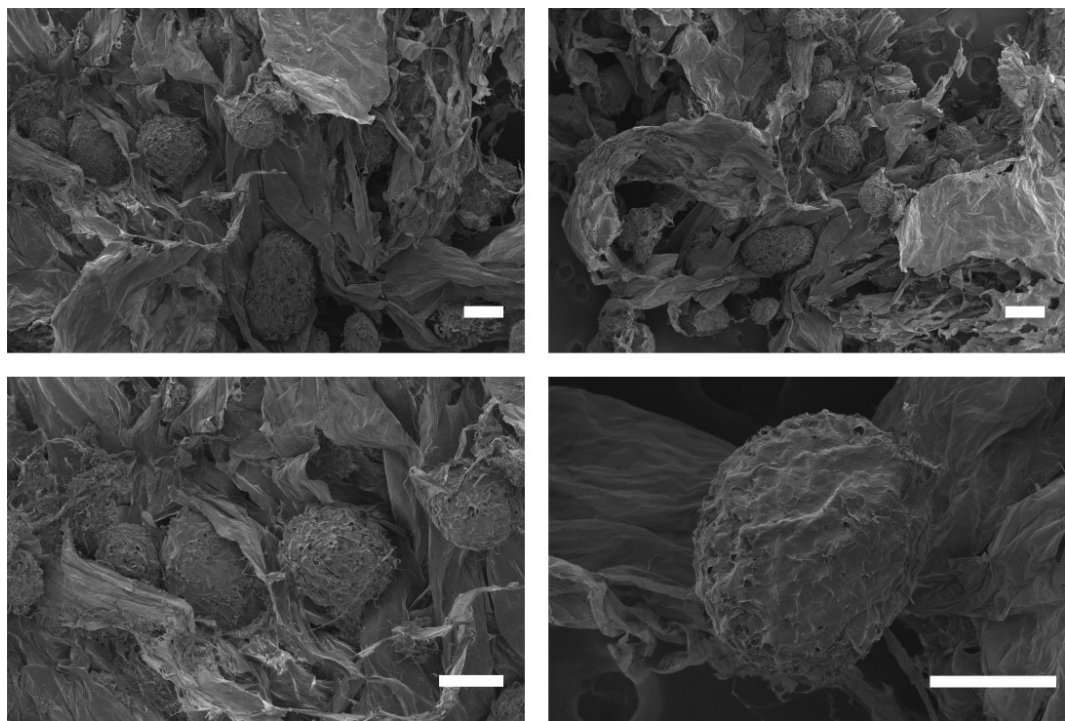


Figure 3.29. SEM images of NIH-3T3 cells on QSH scaffolds for long term incubation (scale bar: 200 μm)

3.3.2.2. ECM Formation Analyses

Long term proliferation results that were shown on SEM imaging were supported with immunostaining experiments. After DAPI staining spheroid formations were observed which about 300 μm in diameter were spread over the hydrogel as seen in Figure 3.30. ECM secretion is an important step in neo-tissue formation. A scaffold material should be replaced with own ECM of the cells during tissue formation [124; 125]. Production of ECM was analyzed via analysis of Collagen secretion. 1-month cultured 3D spheroids were analyzed via Anti-collagen Type-I FITC staining (Figure 3.31). Collagen secretion was clearly observed for all spheroid structures that shows ECM formation by cells.

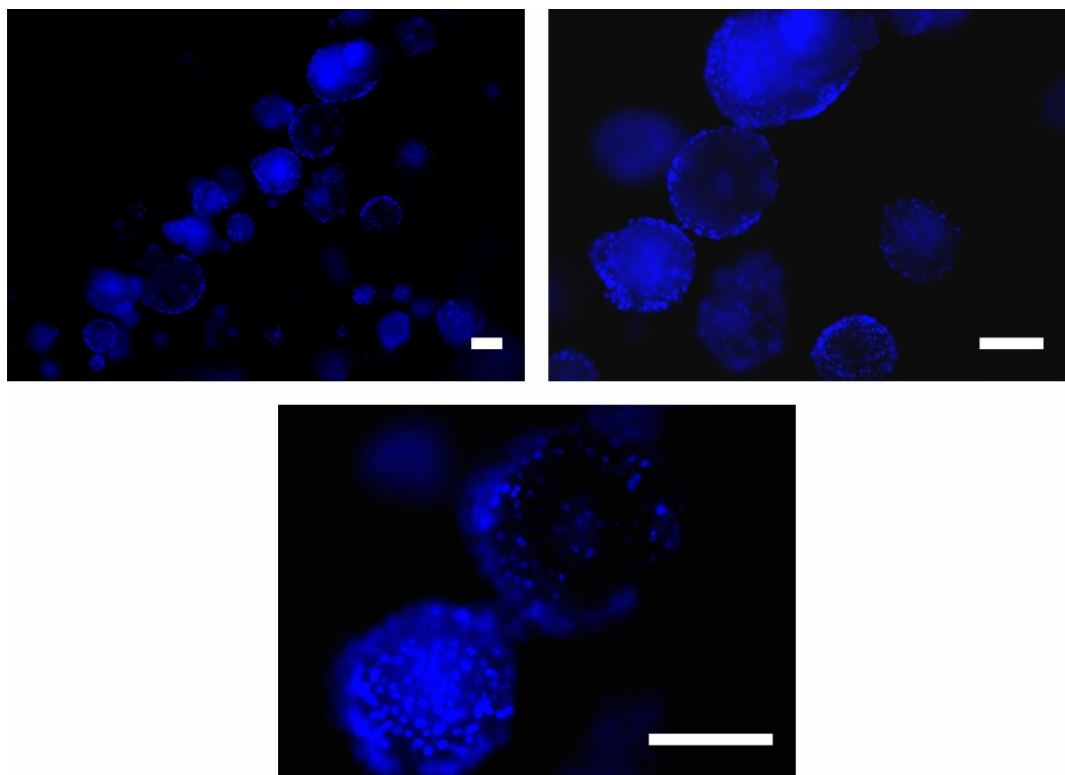


Figure 3.30. DAPI staining images of NIH-3T3 cells on QSH scaffolds
for long term incubation (scale bar: 200 μ m)

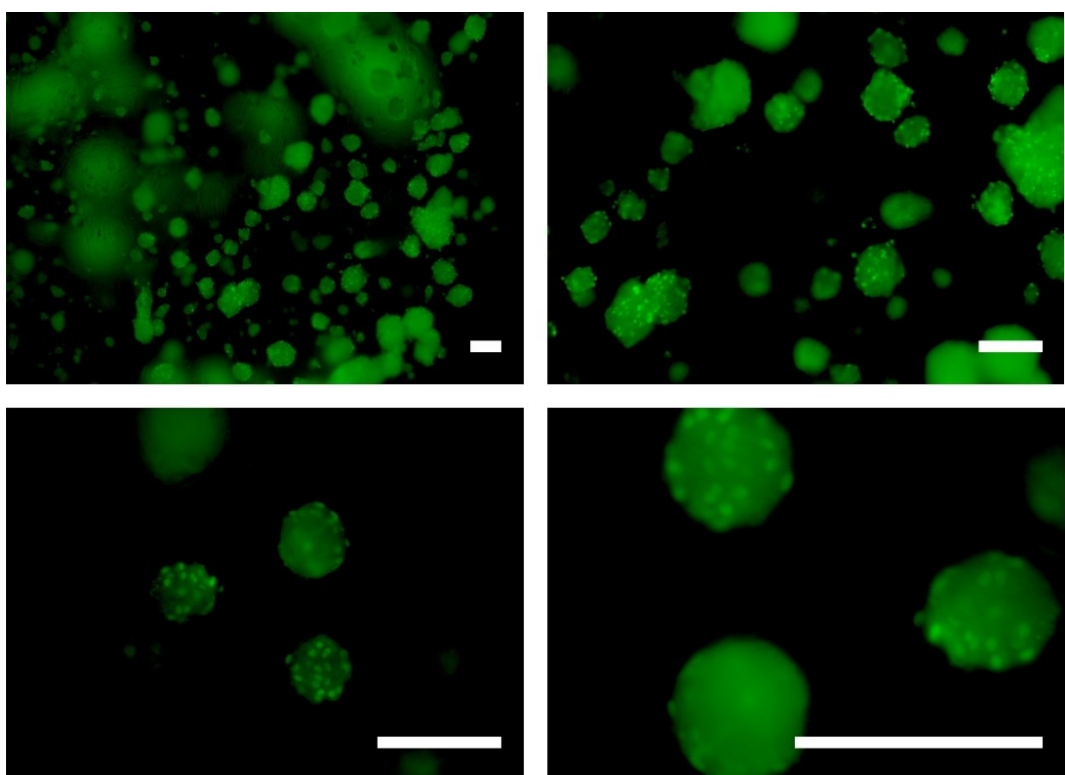


Figure 3.31. Collagen staining images of NIH-3T3 cells on QSH
scaffolds for long term incubation (scale bar: 200 μ m)

CHAPTER 4

CONCLUSION

In recent years, bone tissue engineering has become one of the most important research areas Worldwide. The presented thesis has provided an innovative approach to contribute this developing field. This thesis represents proof of concept study to develop a novel scaffold material that can be used in therapeutic applications, which has the potential to be used in clinical studies.

There have been several studies related to structural, physicochemical, and mechanical properties of the QSH and its utilization as a wound-healing cream, antioxidant-antibacterial reagent, or drug delivery system. In this study, the potential of the QSH as a tissue engineering scaffold was comprehensively evaluated in terms of chemical and mechanical properties, as well as biological suitability. QSH production approach was accomplished and compared with similar studies in the literature. An optimized product was evaluated for 3D cell culture studies. Porosity and swelling ratio, crosslinking parameters, and protein adsorption capacity were investigated to characterize the material. In the light of obtained results, 2 mg/mL QSH provided the most appropriate results in terms of porosity, durability, and mechanical strength. Afterward, the best results in terms of biodegradation in long term were observed for the crosslinking conditions with 0.03 M GTA. The final form of the QSH scaffold has 76.59 μm average pore size and an excellent water holding capacity, which is 56.8 times of its own weight. Later on, QSH characterized as an injectable hydrogel. 20 mg/mL quince seed-water ratio gave the most appropriate results with EDC/NHS crosslinking method as an injectable hydrogel.

Cellular viability, proliferation, and ECM secreting capacity were analyzed with two different cell lines to verify the biocompatibility of QSH as a biomaterial. NIH-3T3 cell line was used as a cell model and then SaOS-2 cell line was used as bone tissue model. 2 mg/mL QSH crosslinked with 0.03 M GTA provided the highest cell viability with the minimum toxic effect for both cell lines. Spheroids around 300 μm and integrated cell clusters were observed among interconnected QSH scaffold. These integrated cellular structures confirm that QSH promotes cells to create 3D tissue-like structures. Also,

ECM formation and collagen secretion was investigated for 3D spheroids in long term incubation. Lastly, cellular viability and proliferation were analyzed with SaOS-2 cell line to verify the biocompatibility of injectable QSH, and no toxic effect was observed. To conclude the work, these results reveal that the obtained findings were compromised with literature data and QSH has a big potential as a scaffold to be used in tissue engineering studies. High-level porosity and water holding capacity, appropriate mechanical properties, and excellent biocompatibility of the QSH verify that, this material could highly support tissue regeneration. Moreover, the affordable price of the raw material of the QSH thrust itself forward in terms of accessibility. Outputs of the study are aimed to reduce the cost of tissue engineering research and treatment in terms of material related expenses while increasing patient welfare at medical, commercial, and social scale.

REFERENCES

1. Fuchs, Julie R.; Nasseri, Boris A.; and Vacanti, Joseph P. 2001. "Tissue engineering: a 21st century solution to surgical reconstruction." *The Annals of Thoracic Surgery* 72 (2): 577-591. [https://doi.org/https://doi.org/10.1016/S0003-4975\(01\)02820-X](https://doi.org/https://doi.org/10.1016/S0003-4975(01)02820-X).
<http://www.sciencedirect.com/science/article/pii/S000349750102820X>.
2. Chandra, Prafulla K.; Soker, Shay; and Atala, Anthony. 2020. "Chapter 1 - Tissue engineering: current status and future perspectives." In *Principles of Tissue Engineering (Fifth Edition)*, edited by Robert Lanza, Robert Langer, Joseph P. Vacanti and Anthony Atala, 1-35. Academic Press.
3. Tibbitt, Mark W.; and Anseth, Kristi S. 2009. "Hydrogels as extracellular matrix mimics for 3D cell culture." *Biotechnology and Bioengineering* 103 (4): 655-663. <https://doi.org/10.1002/bit.22361>. <https://doi.org/10.1002/bit.22361>.
4. Kang, Yunqing; Jabbari, Esmaiel; and Yang, Yunzhi. 2013. "Integrating Top-Down and Bottom-Up Scaffolding Tissue Engineering Approach for Bone Regeneration." *Micro and Nanotechnologies in Engineering Stem Cells and Tissues*: 142-158. <https://doi.org/doi:10.1002/9781118574775.ch6>.
<https://doi.org/10.1002/9781118574775.ch6>.
5. Jaiswal, N.; Haynesworth, S. E.; Caplan, A. I.; and Bruder, S. P. 1997. "Osteogenic differentiation of purified, culture-expanded human mesenchymal stem cells in vitro." *J Cell Biochem* 64 (2): 295-312.
6. Schnaper, H. W.; Grant, D. S.; Stetler-Stevenson, W. G.; Fridman, R.; D'Orazi, G.; Murphy, A. N.; Bird, R. E.; Hoythya, M.; Fuerst, T. R.; French, D. L.; and et al. 1993. "Type IV collagenase(s) and TIMPs modulate endothelial cell morphogenesis in vitro." *J Cell Physiol* 156 (2): 235-46. <https://doi.org/10.1002/jcp.1041560204>.
7. Engler, A. J.; Sen, S.; Sweeney, H. L.; and Discher, D. E. 2006. "Matrix elasticity directs stem cell lineage specification." *Cell* 126 (4): 677-89. <https://doi.org/10.1016/j.cell.2006.06.044>.
8. Engler, A. J.; Rehfeldt, F.; Sen, S.; and Discher, D. E. 2007. "Microtissue elasticity: measurements by atomic force microscopy and its influence on cell

- differentiation." *Methods Cell Biol* 83: 521-45. [https://doi.org/10.1016/s0091-679x\(07\)83022-6](https://doi.org/10.1016/s0091-679x(07)83022-6).
9. Petersen, O. W.; Ronnov-Jessen, L.; Howlett, A. R.; and Bissell, M. J. 1992. "Interaction with basement membrane serves to rapidly distinguish growth and differentiation pattern of normal and malignant human breast epithelial cells." *Proceedings of the National Academy of Sciences* 89 (19): 9064-9068. <https://doi.org/10.1073/pnas.89.19.9064>. <https://dx.doi.org/10.1073/pnas.89.19.9064>.
 10. Liu Tsang, Valerie; and Bhatia, Sangeeta N. 2004. "Three-dimensional tissue fabrication." *Advanced Drug Delivery Reviews* 56 (11): 1635-1647. <https://doi.org/https://doi.org/10.1016/j.addr.2004.05.001>. <http://www.sciencedirect.com/science/article/pii/S0169409X04001449>.
 11. Zhang, Xiaoying; and Zhang, Yangde. 2015. "Tissue Engineering Applications of Three-Dimensional Bioprinting." *Cell Biochemistry and Biophysics* 72 (3): 777-782.<https://doi.org/10.1007/s12013-015-0531-x>. <https://doi.org/10.1007/s12013-015-0531-x>.
 12. Lott, Juliana; De Carvalho, Pablo Herthel; Assis, Dawidson; and De Goes, Alfredo Miranda. 2013. "Innovative Strategies for Tissue Engineering." InTech.
 13. Saltzman, W. Mark; and Kyriakides, Themis R. 2020. "Chapter 16 - Cell interactions with polymers." In *Principles of Tissue Engineering (Fifth Edition)*, edited by Robert Lanza, Robert Langer, Joseph P. Vacanti and Anthony Atala, 275-293. Academic Press.
 14. Liu, Jie; Jiang, Zhaozhong; Zhang, Shengmin; Liu, Chen; Gross, Richard A.; Kyriakides, Themis R.; and Saltzman, W. Mark. 2011. "Biodegradation, biocompatibility, and drug delivery in poly(ω -pentadecalactone-co-p-dioxanone) copolymers." *Biomaterials* 32 (27): 6646-6654. <https://doi.org/10.1016/j.biomaterials.2011.05.046>. <https://dx.doi.org/10.1016/j.biomaterials.2011.05.046>.
 15. Liu, Xiaohua; and Ma, Peter X. 2004. "Polymeric Scaffolds for Bone Tissue Engineering." *Annals of Biomedical Engineering* 32 (3): 477-486. <https://doi.org/10.1023/b:abme.0000017544.36001.8e>. <https://dx.doi.org/10.1023/b:abme.0000017544.36001.8e>.
 16. Pietrzak, W.S.; and Vacanti, C.A. 2014. *Musculoskeletal Tissue Regeneration: Biological Materials and Methods*. Humana Press.

17. Bose, Prasenjit. 2018. "EXTRACELLULAR MATRIX ARCHITECTURE AND BIOMECHANICS OF 3D ENGINEERED MICROTISSUES."
18. Theocharis, Achilleas D.; Skandalis, Spyros S.; Gialeli, Chrysostomi; and Karamanos, Nikos K. 2016. "Extracellular matrix structure." *Advanced Drug Delivery Reviews* 97: 4-27. <https://doi.org/https://doi.org/10.1016/j.addr.2015.11.001>. <http://www.sciencedirect.com/science/article/pii/S0169409X15002574>.
19. Frantz, C.; Stewart, K. M.; and Weaver, V. M. 2010. "The extracellular matrix at a glance." *Journal of Cell Science* 123 (24): 4195-4200. <https://doi.org/10.1242/jcs.023820>. <https://dx.doi.org/10.1242/jcs.023820>.
20. Hynes, Richard O. 2009. "The Extracellular Matrix: Not Just Pretty Fibrils." *Science* 326 (5957): 1216-1219. <https://doi.org/10.1126/science.1176009>. <https://dx.doi.org/10.1126/science.1176009>.
21. Shuttleworth, Adrian. 1998. "Extracellular Matrix." In *Encyclopedia of Immunology (Second Edition)*, edited by Peter J. Delves, 861-866. Oxford: Elsevier.
22. Rozario, Tania; and Desimone, Douglas W. 2010. "The extracellular matrix in development and morphogenesis: A dynamic view." *Developmental Biology* 341 (1): 126-140. <https://doi.org/10.1016/j.ydbio.2009.10.026>. <https://dx.doi.org/10.1016/j.ydbio.2009.10.026>.
23. Kusindarta, Dwi Liliek; and Wihadmadyatami, Hevi. 2018. "The Role of Extracellular Matrix in Tissue Regeneration." InTech.
24. Fernandes, Hugo; Moroni, Lorenzo; van Blitterswijk, Clemens; and de Boer, Jan. 2009. "Extracellular matrix and tissue engineering applications." *Journal of Materials Chemistry* 19 (31): 5474-5484. <https://doi.org/10.1039/B822177D>. <http://dx.doi.org/10.1039/B822177D>.
25. Cheung, Hoi-Yan; Lau, Kin-Tak; Lu, Tung-Po; and Hui, David. 2007. "A critical review on polymer-based bio-engineered materials for scaffold development." *Composites Part B: Engineering* 38 (3): 291-300. <https://doi.org/10.1016/j.compositesb.2006.06.014>. <https://dx.doi.org/10.1016/j.compositesb.2006.06.014>.
26. Maurus, Peter B.; and Kaeding, Christopher C. 2004. "Bioabsorbable implant material review." *Operative Techniques in Sports Medicine* 12 (3): 158-160.

- <https://doi.org/https://doi.org/10.1053/j.otsm.2004.07.015>.
<http://www.sciencedirect.com/science/article/pii/S1060187204000541>.
27. Tang, Xiaoyan; Thankappan, Shalumon Kottappally; Lee, Paul; Fard, Sahar E.; Harmon, Matthew D.; Tran, Katelyn; and Yu, Xiaojun. 2014. "Chapter 21 - Polymeric Biomaterials in Tissue Engineering and Regenerative Medicine." In *Natural and Synthetic Biomedical Polymers*, edited by Sangamesh G. Kumbar, Cato T. Laurencin and Meng Deng, 351-371. Oxford: Elsevier.
28. Iqbal, Naseer; Khan, Abdul Samad; Asif, Anila; Yar, Muhammad; Haycock, John W.; and Rehman, Ihtesham Ur. 2019. "Recent concepts in biodegradable polymers for tissue engineering paradigms: a critical review." *International Materials Reviews* 64 (2): 91-126.
<https://doi.org/10.1080/09506608.2018.1460943>.
<https://dx.doi.org/10.1080/09506608.2018.1460943>.
29. Dhandayuthapani, Brahatheeswaran; Yoshida, Yasuhiko; Maekawa, Toru; and Kumar, D. Sakthi. 2011. "Polymeric Scaffolds in Tissue Engineering Application: A Review." *International Journal of Polymer Science* 2011: 1-19.
<https://doi.org/10.1155/2011/290602>. <https://dx.doi.org/10.1155/2011/290602>.
30. Aravamudhan, Aja; Ramos, Daisy M.; Nada, Ahmed A.; and Kumbar, Sangamesh G. 2014. "Chapter 4 - Natural Polymers: Polysaccharides and Their Derivatives for Biomedical Applications." In *Natural and Synthetic Biomedical Polymers*, edited by Sangamesh G. Kumbar, Cato T. Laurencin and Meng Deng, 67-89. Oxford: Elsevier.
31. Gomes, Manuela; Azevedo, Helena; Malafaya, Patrícia; Silva, Simone; Oliveira, Joaquim; Silva, Gabriela; João Mano, Rui Sousa; and Reis, Rui. 2013. "16 - Natural Polymers in Tissue Engineering Applications." In *Handbook of Biopolymers and Biodegradable Plastics*, edited by Sina Ebnesajjad, 385-425. Boston: William Andrew Publishing.
32. Liu, Mei; Zeng, Xin; Ma, Chao; Yi, Huan; Ali, Zeeshan; Mou, Xianbo; Li, Song; Deng, Yan; and He, Nongyue. 2017. "Injectable hydrogels for cartilage and bone tissue engineering." *Bone Research* 5 (1): 17014.
<https://doi.org/10.1038/boneres.2017.14>.
<https://dx.doi.org/10.1038/boneres.2017.14>.
33. Hernández-González, Aurora C.; Téllez-Jurado, Lucía; and Rodríguez-Lorenzo, Luis M. 2020. "Alginate hydrogels for bone tissue engineering, from injectables

- to bioprinting: A review." *Carbohydrate Polymers* 229: 115514. <https://doi.org/https://doi.org/10.1016/j.carbpol.2019.115514>. <http://www.sciencedirect.com/science/article/pii/S0144861719311828>.
34. Lou, Junzhe; Stowers, Ryan; Nam, Sungmin; Xia, Yan; and Chaudhuri, Ovijit. 2018. "Stress relaxing hyaluronic acid-collagen hydrogels promote cell spreading, fiber remodeling, and focal adhesion formation in 3D cell culture." *Biomaterials* 154: 213-222. <https://doi.org/10.1016/j.biomaterials.2017.11.004>. <https://dx.doi.org/10.1016/j.biomaterials.2017.11.004>.
35. Lee, H. Janice; Lee, Jin-Soo; Chansakul, Thanissara; Yu, Christopher; Elisseeff, Jennifer H.; and Yu, Seungju M. 2006. "Collagen mimetic peptide-conjugated photopolymerizable PEG hydrogel." 27 (30): 5268-5276. <https://doi.org/10.1016/j.biomaterials.2006.06.001>. <https://dx.doi.org/10.1016/j.biomaterials.2006.06.001>.
36. Ibrahim, Nabil; Nada, Ahmed; and Eid, Basma. 2018. "Polysaccharide-Based Polymer Gels and Their Potential Applications: Synthesis and Characterization." 97-126.
37. Jain, Dharmendra; and Bar-Shalom, Daniel. 2014. "Alginate drug delivery systems: application in context of pharmaceutical and biomedical research." *Drug Development and Industrial Pharmacy* 40 (12): 1576-1584. <https://doi.org/10.3109/03639045.2014.917657>. <https://doi.org/10.3109/03639045.2014.917657>.
38. Sancilio, Silvia; Gallorini, Marialucia; Di Nisio, Chiara; Marsich, Eleonora; Di Pietro, Roberta; Schweikl, Helmut; and Cataldi, Amelia. 2018. "Alginate/Hydroxyapatite-Based Nanocomposite Scaffolds for Bone Tissue Engineering Improve Dental Pulp Biomineralization and Differentiation." *Stem Cells International* 2018: 1-13. <https://doi.org/10.1155/2018/9643721>. <https://dx.doi.org/10.1155/2018/9643721>.
39. Marsich, Eleonora; Borgogna, Massimiliano; Donati, Ivan; Mozetic, Pamela; Strand, Berit L.; Salvador, Santiago Gomez; Vittur, Franco; and Paoletti, Sergio. 2008. "Alginate/lactose-modified chitosan hydrogels: A bioactive biomaterial for chondrocyte encapsulation." *Journal of Biomedical Materials Research Part A* 84A (2): 364-376. <https://doi.org/10.1002/jbm.a.31307>. <https://onlinelibrary.wiley.com/doi/abs/10.1002/jbm.a.31307>.

40. Ma, Lie; Gao, Changyou; Mao, Zhengwei; Zhou, Jie; Shen, Jiacong; Hu, Xueqing; and Han, Chunmao. 2003. "Collagen/chitosan porous scaffolds with improved biostability for skin tissue engineering." *Biomaterials* 24 (26): 4833-4841. [https://doi.org/https://doi.org/10.1016/S0142-9612\(03\)00374-0](https://doi.org/https://doi.org/10.1016/S0142-9612(03)00374-0). <http://www.sciencedirect.com/science/article/pii/S0142961203003740>.
41. Chvapil, Milos; Kronenthal, Richard L.; and van Winkle, Walton. 1973. "Medical and Surgical Applications of Collagen." In *International Review of Connective Tissue Research*, edited by David A. Hall and D. S. Jackson, 1-61. Elsevier.
42. Peng, Y.; Glattauer, V.; Werkmeister, J. A.; and Ramshaw, J. A. M. 2004. "Evaluation for collagen products for cosmetic application." *International Journal of Cosmetic Science* 26 (6): 313-313. https://doi.org/10.1111/j.1467-2494.2004.00245_2.x. https://onlinelibrary.wiley.com/doi/abs/10.1111/j.1467-2494.2004.00245_2.x.
43. Avila Rodríguez, María Isabela; Rodríguez Barroso, Laura G; and Sánchez, Mirna Lorena. 2018. "Collagen: A review on its sources and potential cosmetic applications." *Journal of Cosmetic Dermatology* 17 (1): 20-26. <https://doi.org/10.1111/jocd.12450>. <https://onlinelibrary.wiley.com/doi/abs/10.1111/jocd.12450>.
44. Li, G. Y.; Fukunaga, S.; Takenouchi, K.; and Nakamura, F. 2005. "Comparative study of the physiological properties of collagen, gelatin and collagen hydrolysate as cosmetic materials." *International Journal of Cosmetic Science* 27 (2): 101-106. <https://doi.org/10.1111/j.1467-2494.2004.00251.x>. <https://onlinelibrary.wiley.com/doi/abs/10.1111/j.1467-2494.2004.00251.x>.
45. Dong, Chanjuan; and Lv, Yonggang. 2016. "Application of Collagen Scaffold in Tissue Engineering: Recent Advances and New Perspectives." *Polymers* 8 (2): 42. <https://doi.org/10.3390/polym8020042>. <https://dx.doi.org/10.3390/polym8020042>.
46. Cen, Lian; Liu, Wei; Cui, Lei; Zhang, Wenjie; and Cao, Yilin. 2008. "Collagen Tissue Engineering: Development of Novel Biomaterials and Applications." *Pediatric Research* 63 (5): 492-496. <https://doi.org/10.1203/pdr.0b013e31816c5bc3>. <https://dx.doi.org/10.1203/PDR.0b013e31816c5bc3>.

47. Parenteau-Bareil, Rémi; Gauvin, Robert; and Berthod, François. 2010. "Collagen-Based Biomaterials for Tissue Engineering Applications." *Materials* 3 (3): 1863-1887. <https://doi.org/10.3390/ma3031863>. <https://dx.doi.org/10.3390/ma3031863>.
48. Zimmermann, Jörg; Bittner, Katharina; Stark, Björn; and Mülhaupt, Rolf. 2002. "Novel hydrogels as supports for in vitro cell growth: poly(ethylene glycol)- and gelatine-based (meth)acrylamidopeptide macromonomers." *Biomaterials* 23 (10): 2127-2134. [https://doi.org/https://doi.org/10.1016/S0142-9612\(01\)00343-X](https://doi.org/https://doi.org/10.1016/S0142-9612(01)00343-X). <http://www.sciencedirect.com/science/article/pii/S014296120100343X>.
49. Johnston-Banks, FA. 1990. "Gelatin: Food Gels." *Elsevier Applied Science, London* 26: 885-891.
50. Djagny, Kodjo Boady; Wang, Zhang; and Xu, Shiying. 2001. "Gelatin: A Valuable Protein for Food and Pharmaceutical Industries: Review." *Critical Reviews in Food Science and Nutrition* 41 (6): 481-492. <https://doi.org/10.1080/20014091091904>. <https://dx.doi.org/10.1080/20014091091904>.
51. Mari, C. Echave; Laura Saenz del Burgo; Jose, L. Pedraz; and Gorka, Orive. 2017. "Gelatin as Biomaterial for Tissue Engineering." *Current Pharmaceutical Design* 23 (24): 3567-3584. <https://doi.org/http://dx.doi.org/10.2174/0929867324666170511123101>. <http://www.eurekaselect.com/node/152373/article>.
52. Monroy, Daniella Alejandra Pompa; Bravo, José Manuel Cornejo; Mercado, Irma Esthela Soria; and Gómez, Luis Jesús Villarreal. 2018. "Gelatin and Collagen Nanofiber Scaffolds for Tissue Engineering." InTech.
53. Sánchez, P.; Pedraz, J. L.; and Orive, G. 2017. "Biologically active and biomimetic dual gelatin scaffolds for tissue engineering." *International Journal of Biological Macromolecules* 98: 486-494. <https://doi.org/https://doi.org/10.1016/j.ijbiomac.2016.12.092>. <http://www.sciencedirect.com/science/article/pii/S014181301631707X>.
54. Su, Kai; and Wang, Chunming. 2015. "Recent advances in the use of gelatin in biomedical research." *Biotechnology Letters* 37 (11): 2139-2145. <https://doi.org/10.1007/s10529-015-1907-0>. <https://doi.org/10.1007/s10529-015-1907-0>.

55. Felt, Olivia; Buri, Pierre; and Gurny, Robert. 1998. "Chitosan: A Unique Polysaccharide for Drug Delivery." *Drug Development and Industrial Pharmacy* 24 (11): 979-993. <https://doi.org/10.3109/03639049809089942>.
<https://doi.org/10.3109/03639049809089942>.
56. Mhurchu, C. Ni; Dunshea-Mooij, C.; Bennett, D.; and Rodgers, A. 2005. "Effect of chitosan on weight loss in overweight and obese individuals: a systematic review of randomized controlled trials." *Obesity Reviews* 6 (1): 35-42. <https://doi.org/10.1111/j.1467-789X.2005.00158.x>.
<https://onlinelibrary.wiley.com/doi/abs/10.1111/j.1467-789X.2005.00158.x>.
57. Croisier, Florence; and Jérôme, Christine. 2013. "Chitosan-based biomaterials for tissue engineering." *European Polymer Journal* 49 (4): 780-792. <https://doi.org/10.1016/j.eurpolymj.2012.12.009>.
<https://dx.doi.org/10.1016/j.eurpolymj.2012.12.009>.
58. Francis Suh, J. K.; and Matthew, Howard W. T. 2000. "Application of chitosan-based polysaccharide biomaterials in cartilage tissue engineering: a review." *Biomaterials* 21 (24): 2589-2598. [https://doi.org/10.1016/s0142-9612\(00\)00126-5](https://doi.org/10.1016/s0142-9612(00)00126-5). [https://dx.doi.org/10.1016/S0142-9612\(00\)00126-5](https://dx.doi.org/10.1016/S0142-9612(00)00126-5).
59. Paul, Willi; and Sharma, Chandra. 2004. "Chitosan and Alginate Wound Dressings: A Short Review." *Trends in Biomaterials and Artificial Organs* 18.
60. Madihally, Sundararajan V.; and Matthew, Howard W. T. 1999. "Porous chitosan scaffolds for tissue engineering." *Biomaterials* 20 (12): 1133-1142. [https://doi.org/10.1016/s0142-9612\(99\)00011-3](https://doi.org/10.1016/s0142-9612(99)00011-3).
[https://dx.doi.org/10.1016/S0142-9612\(99\)00011-3](https://dx.doi.org/10.1016/S0142-9612(99)00011-3).
61. Ong, Shin-Yeu; Wu, Jian; Moochhala, Shabbir M.; Tan, Mui-Hong; and Lu, Jia. 2008. "Development of a chitosan-based wound dressing with improved hemostatic and antimicrobial properties." *Biomaterials* 29 (32): 4323-4332. <https://doi.org/10.1016/j.biomaterials.2008.07.034>.
<https://dx.doi.org/10.1016/j.biomaterials.2008.07.034>.
62. Kumbar, S. G.; Kulkarni, A. R.; and Aminabhavi, T. M. 2002. "Crosslinked chitosan microspheres for encapsulation of diclofenac sodium: effect of crosslinking agent." *Journal of Microencapsulation* 19 (2): 173-180. <https://doi.org/10.1080/02652040110065422>.
<https://doi.org/10.1080/02652040110065422>.

63. Overstreet, Derek J.; Dutta, Dipankar; Stabenfeldt, Sarah E.; and Vernon, Brent L. 2012. "Injectable hydrogels." *Journal of Polymer Science Part B: Polymer Physics* 50 (13): 881-903. <https://doi.org/10.1002/polb.23081>. <https://dx.doi.org/10.1002/polb.23081>.
64. Zhao, Liang; Weir, Michael D.; and Xu, Hockin H. K. 2010. "An injectable calcium phosphate-alginate hydrogel-umbilical cord mesenchymal stem cell paste for bone tissue engineering." *Biomaterials* 31 (25): 6502-6510. <https://doi.org/10.1016/j.biomaterials.2010.05.017>. <https://dx.doi.org/10.1016/j.biomaterials.2010.05.017>.
65. Hemmrich, Karsten; Van De Sijpe, Karlien; Rhodes, Nicholas P.; Hunt, John A.; Di Bartolo, Chiara; Pallua, Norbert; Blondeel, Phillip; and Von Heimburg, Dennis. 2008. "Autologous In Vivo Adipose Tissue Engineering in Hyaluronan-Based Gels—A Pilot Study." *Journal of Surgical Research* 144 (1): 82-88. <https://doi.org/10.1016/j.jss.2007.03.017>. <https://dx.doi.org/10.1016/j.jss.2007.03.017>.
66. Li, Jiawei; Chen, Guojun; Xu, Xingquan; Abdou, Peter; Jiang, Qing; Shi, Dongquan; and Gu, Zhen. 2019. "Advances of injectable hydrogel-based scaffolds for cartilage regeneration." *Regenerative Biomaterials* 6 (3): 129-140. <https://doi.org/10.1093/rb/rbz022>. <https://dx.doi.org/10.1093/rb/rbz022>.
67. Ashraf, Muhammad U.; Muhammad, Gulzar; Hussain, Muhammad A.; and Bukhari, Syed N. A. 2016. "Cydonia oblonga M., A Medicinal Plant Rich in Phytonutrients for Pharmaceuticals." *Frontiers in Pharmacology* 7. <https://doi.org/10.3389/fphar.2016.00163>. <https://dx.doi.org/10.3389/fphar.2016.00163>.
68. Fattouch, Sami; Caboni, Pierluigi; Coroneo, Valentina; Tuberoso, Carlo I. G.; Angioni, Alberto; Dessi, Sandro; Marzouki, Nejib; and Cabras, Paolo. 2007. "Antimicrobial Activity of Tunisian Quince (Cydonia oblonga Miller) Pulp and Peel Polyphenolic Extracts." *Journal of Agricultural and Food Chemistry* 55 (3): 963-969. <https://doi.org/10.1021/jf062614e>. <https://doi.org/10.1021/jf062614e>.
69. Wang, Xiaoyan; Jia, Wei; Zhao, Aihua; and Wang, Xiaorong. 2006. "Anti-influenza agents from plants and traditional Chinese medicine." *Phytotherapy Research* 20 (5): 335-341. <https://doi.org/10.1002/ptr.1892>. <https://onlinelibrary.wiley.com/doi/abs/10.1002/ptr.1892>.

70. Jouki, Mohammad; Mortazavi, Seyed Ali; Yazdi, Farideh Tabatabaei; and Koocheki, Arash. 2014. "Characterization of antioxidant–antibacterial quince seed mucilage films containing thyme essential oil." *Carbohydrate Polymers* 99: 537-546. <https://doi.org/10.1016/j.carbpol.2013.08.077>.
<https://dx.doi.org/10.1016/j.carbpol.2013.08.077>.
71. Jouki, Mohammad; Tabatabaei Yazdi, Farideh; Mortazavi, Seyed Ali; and Koocheki, Arash. 2013. "Physical, barrier and antioxidant properties of a novel plasticized edible film from quince seed mucilage." 62: 500-507. <https://doi.org/10.1016/j.ijbiomac.2013.09.031>.
<https://dx.doi.org/10.1016/j.ijbiomac.2013.09.031>.
72. Hamauzu, Yasunori; Irie, Miho; Kondo, Makoto; and Fujita, Tomoyuki. 2008. "Antiulcerative properties of crude polyphenols and juice of apple, and Chinese quince extracts." *Food Chemistry* 108 (2): 488-495. <https://doi.org/https://doi.org/10.1016/j.foodchem.2007.10.084>.
<http://www.sciencedirect.com/science/article/pii/S0308814607011363>.
73. Jouki, Mohammad; Mortazavi, Seyed Ali; Yazdi, Farideh Tabatabaei; and Koocheki, Arash. 2014. "Optimization of extraction, antioxidant activity and functional properties of quince seed mucilage by RSM." 66: 113-124. <https://doi.org/10.1016/j.ijbiomac.2014.02.026>.
<https://dx.doi.org/10.1016/j.ijbiomac.2014.02.026>.
74. Hamauzu, Yasunori; Inno, Takanori; Kume, Chihiro; Irie, Miho; and Hiramatsu, Kohzy. 2006. "Antioxidant and Antiulcerative Properties of Phenolics from Chinese Quince, Quince, and Apple Fruits." *Journal of Agricultural and Food Chemistry* 54 (3): 765-772. <https://doi.org/10.1021/jf052236y>.
<https://doi.org/10.1021/jf052236y>.
75. Jouki, Mohammad; Mortazavi, Seyed Ali; Yazdi, Farideh Tabatabaei; and Koocheki, Arash. 2014. "Optimization of extraction, antioxidant activity and functional properties of quince seed mucilage by RSM." *International Journal of Biological Macromolecules* 66: 113-124. <https://doi.org/https://doi.org/10.1016/j.ijbiomac.2014.02.026>.
<http://www.sciencedirect.com/science/article/pii/S014181301400110X>.
76. Wang, Li; Liu, Hua-Min; and Qin, Guang-Yong. 2017. "Structure characterization and antioxidant activity of polysaccharides from Chinese quince seed meal." *Food Chemistry* 234: 314-322.

- <https://doi.org/10.1016/j.foodchem.2017.05.002>.
<https://dx.doi.org/10.1016/j.foodchem.2017.05.002>.
77. Silva, Branca M.; Andrade, Paula B.; Ferreres, Federico; Seabra, Rosa M.; Beatriz, M.; Oliveira, P. P.; and Ferreira, Margarida A. 2005. "Composition of Quince (*Cydonia oblonga* Miller) seeds: phenolics, organic acids and free amino acids." *Natural Product Research* 19 (3): 275-281.
<https://doi.org/10.1080/14786410410001714678>.
<https://doi.org/10.1080/14786410410001714678>.
78. Silva, Branca M.; Andrade, Paula B.; Valentão, Patrícia; Ferreres, Federico; Seabra, Rosa M.; and Ferreira, Margarida A. 2004. "Quince (*Cydonia oblonga*Miller) Fruit (Pulp, Peel, and Seed) and Jam: Antioxidant Activity." *Journal of Agricultural and Food Chemistry* 52 (15): 4705-4712.
<https://doi.org/10.1021/jf040057v>. <https://dx.doi.org/10.1021/jf040057v>.
79. Tamri, Pari; Hemmati, Aliasghar; and Boroujerdnia, Mehri Ghafourian. 2014. "Wound healing properties of quince seed mucilage: In vivo evaluation in rabbit full-thickness wound model." *International Journal of Surgery* 12 (8): 843-847.
<https://doi.org/10.1016/j.ijsu.2014.06.016>.
<https://dx.doi.org/10.1016/j.ijsu.2014.06.016>.
80. Hemmati, Ali A.; and Mohammadian, Fariba. 2000. "An Investigation into the Effects of Mucilage of Quince Seeds on Wound Healing in Rabbit." 7 (4): 41-46. https://doi.org/10.1300/j044v07n04_05.
https://dx.doi.org/10.1300/J044v07n04_05.
81. Hemmati, Ali Asghar; Kalantari, Hibatoallah; Jalali, Amir; Rezai, Somie; and Zadeh, Hossein Haghghi. 2012. "Healing effect of quince seed mucilage on T-2 toxin-induced dermal toxicity in rabbit." *Experimental and Toxicologic Pathology* 64 (3): 181-186. <https://doi.org/10.1016/j.etp.2010.08.004>.
<https://dx.doi.org/10.1016/j.etp.2010.08.004>.
82. Ashraf, Muhammad Umer; Hussain, Muhammad Ajaz; Bashir, Sajid; Haseeb, Muhammad Tahir; and Hussain, Zakir. 2018. "Quince seed hydrogel (glucuronoxylan): Evaluation of stimuli responsive sustained release oral drug delivery system and biomedical properties." *Journal of Drug Delivery Science and Technology* 45: 455-465. <https://doi.org/10.1016/j.jddst.2018.04.008>.
<https://dx.doi.org/10.1016/j.jddst.2018.04.008>.

83. Wang, Li; Liu, Hua-Min; Xie, Ai-Jun; Wang, Xue-De; Zhu, Chun-Yan; and Qin, Guang-Yong. 2018. "Chinese quince (*Chaenomeles sinensis*) seed gum: Structural characterization." *Food Hydrocolloids* 75: 237-245. <https://doi.org/10.1016/j.foodhyd.2017.08.001>. <https://dx.doi.org/10.1016/j.foodhyd.2017.08.001>.
84. Cielecka, Izabela; Szustak, Marcin; Gendaszewska-Darmach, Edyta; Kalinowska, Halina; Ryngajło, Małgorzata; Manukiewicz, Waldemar; and Bielecki, Stanisław. 2018. "Novel Bionanocellulose/κ-Carrageenan Composites for Tissue Engineering." *Applied Sciences* 8 (8): 1352. <https://doi.org/10.3390/app8081352>. <https://dx.doi.org/10.3390/app8081352>.
85. Schrecker, S. T.; and Gostomski, P. A. 2005. "Determining the Water Holding Capacity of Microbial Cellulose." *Biotechnology Letters* 27 (19): 1435-1438. <https://doi.org/10.1007/s10529-005-1465-y>. <https://doi.org/10.1007/s10529-005-1465-y>.
86. Bedell, Matthew L.; Guo, Jason L.; Xie, Virginia Y.; Navara, Adam M.; and Mikos, Antonios G. 2020. "Chapter 17 - Polymer scaffold fabrication." In *Principles of Tissue Engineering (Fifth Edition)*, edited by Robert Lanza, Robert Langer, Joseph P. Vacanti and Anthony Atala, 295-315. Academic Press.
87. Chesterman, Julian; Zhang, Zheng; Ortiz, Ophir; Goyal, Ritu; and Kohn, Joachim. 2020. "Chapter 18 - Biodegradable polymers." In *Principles of Tissue Engineering (Fifth Edition)*, edited by Robert Lanza, Robert Langer, Joseph P. Vacanti and Anthony Atala, 317-342. Academic Press.
88. Luo, Ying. 2020. "Chapter 19 - Three-dimensional scaffolds." In *Principles of Tissue Engineering (Fifth Edition)*, edited by Robert Lanza, Robert Langer, Joseph P. Vacanti and Anthony Atala, 343-360. Academic Press.
89. Ermis, Menekse; Calamak, Semih; Calibasi Kocal, Gizem; Guven, Sinan; Durmus, Naside G.; Rizvi, Imran; Hasan, Tayyaba; Hasirci, Nesrin; Hasirci, Vasif; and Demirci, Utkan. 2018. "Chapter 15 - Hydrogels as a New Platform to Recapitulate the Tumor Microenvironment." In *Handbook of Nanomaterials for Cancer Theranostics*, edited by João Conde, 463-494. Elsevier.
90. Manrique, Guillermo D.; and Lajolo, Franco M. 2002. "FT-IR spectroscopy as a tool for measuring degree of methyl esterification in pectins isolated from ripening papaya fruit." *Postharvest Biology and Technology* 25 (1): 99-107.

- [https://doi.org/https://doi.org/10.1016/S0925-5214\(01\)00160-0](https://doi.org/https://doi.org/10.1016/S0925-5214(01)00160-0).
<http://www.sciencedirect.com/science/article/pii/S0925521401001600>.
91. Vidal, S.; Williams, P.; O'Neill, M. A.; and Pellerin, P. 2001. "Polysaccharides from grape berry cell walls. Part I: tissue distribution and structural characterization of the pectic polysaccharides." *Carbohydrate Polymers* 45 (4): 315-323. [https://doi.org/https://doi.org/10.1016/S0144-8617\(00\)00285-X](https://doi.org/https://doi.org/10.1016/S0144-8617(00)00285-X).
<http://www.sciencedirect.com/science/article/pii/S014486170000285X>.
92. Kačuráková, M.; Čapek, P.; Sasinková, V.; Wellner, N.; and Ebringerová, A. 2000. "FT-IR study of plant cell wall model compounds: pectic polysaccharides and hemicelluloses." *Carbohydrate Polymers* 43 (2): 195-203.
[https://doi.org/https://doi.org/10.1016/S0144-8617\(00\)00151-X](https://doi.org/https://doi.org/10.1016/S0144-8617(00)00151-X).
<http://www.sciencedirect.com/science/article/pii/S014486170000151X>.
93. Karageorgiou, Vassilis; and Kaplan, David. 2005. "Porosity of 3D biomaterial scaffolds and osteogenesis." *Biomaterials* 26 (27): 5474-5491.
<https://doi.org/https://doi.org/10.1016/j.biomaterials.2005.02.002>.
<http://www.sciencedirect.com/science/article/pii/S0142961205001511>.
94. Tsuruga, E.; Takita, H.; Itoh, H.; Wakisaka, Y.; and Kuboki, Y. 1997. "Pore Size of Porous Hydroxyapatite as the Cell-Substratum Controls BMP-Induced Osteogenesis." *Journal of Biochemistry* 121 (2): 317-324.
<https://doi.org/10.1093/oxfordjournals.jbchem.a021589>.
<https://dx.doi.org/10.1093/oxfordjournals.jbchem.a021589>.
95. Kruif, C. G. De; Anema, Skelte G.; Zhu, Changjun; Havea, Palatasa; and Coker, Christina. 2015. "Water holding capacity and swelling of casein hydrogels." 44: 372-379. <https://doi.org/10.1016/j.foodhyd.2014.10.007>.
<https://dx.doi.org/10.1016/j.foodhyd.2014.10.007>.
96. Rezagholi, Fatemeh; Hashemi, Seyed Mohammad Bagher; Gholamhosseinpour, Aliakbar; Sherahi, Mousa Hamidabadi; Hesarinejad, Mohammad Ali; and Ale, Marcel T. 2019. "Characterizations and rheological study of the purified polysaccharide extracted from quince seeds." *Journal of the Science of Food and Agriculture* 99 (1): 143-151. <https://doi.org/10.1002/jsfa.9155>.
<https://dx.doi.org/10.1002/jsfa.9155>.
97. Sharma, Vipin K.; and Mazumdar, B. 2013. "Feasibility and characterization of gummy exudate of *Cochlospermum religiosum* as pharmaceutical excipient."

- Industrial Crops & Products* 50 (Complete): 776-786.
<https://doi.org/10.1016/j.indcrop.2013.08.041>.
98. Xie, Ai-Jun; Yin, Hui-Shuang; Liu, Hua-Min; Zhu, Chun-Yan; and Yang, Ya-Jie. 2018. "Chinese quince seed gum and poly (N,N -diethylacryl amide-co-methacrylic acid) based pH-sensitive hydrogel for use in drug delivery." *Carbohydrate Polymers* 185: 96-104.
<https://doi.org/10.1016/j.carbpol.2018.01.007>.
<https://dx.doi.org/10.1016/j.carbpol.2018.01.007>.
99. Mansur, Herman S.; Sadahira, Carolina M.; Souza, Adriana N.; and Mansur, Alexandra A. P. 2008. "FTIR spectroscopy characterization of poly (vinyl alcohol) hydrogel with different hydrolysis degree and chemically crosslinked with glutaraldehyde." *Materials Science and Engineering: C* 28 (4): 539-548.
<https://doi.org/10.1016/j.msec.2007.10.088>.
<https://dx.doi.org/10.1016/j.msec.2007.10.088>.
100. Rahmi, Rahmi. 2015. "Comparative adsorption of Fe(III) and Cd(II) ions on glutaraldehyde crosslinked chitosan-coated cristobalite." *Oriental Journal of Chemistry* 31: 2071-2076. <https://doi.org/10.13005/ojc/310427>.
101. Archana, G.; Sabina, K.; Babuskin, S.; Radhakrishnan, K.; Fayidh, Mohammed A.; Babu, P. Azhagu Saravana; Sivarajan, M.; and Sukumar, M. 2013. "Preparation and characterization of mucilage polysaccharide for biomedical applications." *Carbohydrate Polymers* 98 (1): 89-94.
<https://doi.org/10.1016/j.carbpol.2013.04.062>.
<https://dx.doi.org/10.1016/j.carbpol.2013.04.062>.
102. Ritzoulis, Christos; Marini, Emmanouela; Aslanidou, Alexandra; Georgiadis, Nikolaos; Karayannakidis, Panayotis D.; Koukiotis, Christos; Filotheou, Andreas; Lousinian, Sylvie; and Tzimpilis, Evangelos. 2014. "Hydrocolloids from quince seed: Extraction, characterization, and study of their emulsifying/stabilizing capacity." *Food Hydrocolloids* 42: 178-186.
<https://doi.org/10.1016/j.foodhyd.2014.03.031>.
<https://dx.doi.org/10.1016/j.foodhyd.2014.03.031>.
103. Cai, Weirong; Xu, Huiling; Xie, Liangliang; Sun, Jian; Sun, Taotao; Wu, Xiaoyan; and Fu, Qinbao. 2016. "Purification, characterization and in vitro anticoagulant activity of polysaccharides from Gentiana scabra Bunge roots." *Carbohydrate Polymers* 140: 308-313.

- [https://doi.org/https://doi.org/10.1016/j.carbpol.2015.12.054.](https://doi.org/https://doi.org/10.1016/j.carbpol.2015.12.054)
[http://www.sciencedirect.com/science/article/pii/S0144861715012321.](http://www.sciencedirect.com/science/article/pii/S0144861715012321)
104. Hosseinzadeh, Hossein; and Mohammadi, Sina. 2015. "Quince seed mucilage magnetic nanocomposites as novel bioadsorbents for efficient removal of cationic dyes from aqueous solutions." *Carbohydrate polymers* 134: 213-221.
[https://doi.org/10.1016/j.carbpol.2015.08.008.](https://doi.org/10.1016/j.carbpol.2015.08.008)
<http://europepmc.org/abstract/MED/26428118>
105. Razavi, Seyed Mohammad Ali; Cui, Steve W.; Guo, Qingbin; and Ding, Huihang. 2014. "Some physicochemical properties of sage (*Salvia macrosiphon*) seed gum." *Food Hydrocolloids* 35: 453-462.
[https://doi.org/https://doi.org/10.1016/j.foodhyd.2013.06.022.](https://doi.org/https://doi.org/10.1016/j.foodhyd.2013.06.022)
[http://www.sciencedirect.com/science/article/pii/S0268005X13002002.](http://www.sciencedirect.com/science/article/pii/S0268005X13002002)
106. Rimdusit, Sarawut; Somsaeng, Korapat; Kewsuan, Prartana; Jubsilp, Chanchira; and Tiptipakorn, Sunan. 2012. "Comparison of Gamma Radiation Crosslinking and Chemical Crosslinking on Properties of Methylcellulose Hydrogel." *Engineering Journal* 16 (4): 15-28.
[https://doi.org/10.4186/ej.2012.16.4.15.](https://doi.org/10.4186/ej.2012.16.4.15)
[https://dx.doi.org/10.4186/ej.2012.16.4.15.](https://dx.doi.org/10.4186/ej.2012.16.4.15)
107. Zhu, Hongli; Narakathu, Binu Baby; Fang, Zhiqiang; Tausif Aijazi, Ahmed; Joyce, Margaret; Atashbar, Massood; and Hu, Liangbing. 2014. "A gravure printed antenna on shape-stable transparent nanopaper." *Nanoscale* 6 (15): 9110.
[https://doi.org/10.1039/c4nr02036g.](https://doi.org/10.1039/c4nr02036g) [https://dx.doi.org/10.1039/c4nr02036g.](https://dx.doi.org/10.1039/c4nr02036g)
108. Yu, Shu-Huei; Wu, Yu-Bey; Mi, Fwu-Long; and Shyu, Shin-Shing. 2008. "Polysaccharide-based artificial extracellular matrix: Preparation and characterization of three-dimensional, macroporous chitosan, and heparin composite scaffold." *Journal of Applied Polymer Science* 109 (6): 3639-3644.
[https://doi.org/10.1002/app.28494.](https://doi.org/10.1002/app.28494)
[https://onlinelibrary.wiley.com/doi/abs/10.1002/app.28494.](https://onlinelibrary.wiley.com/doi/abs/10.1002/app.28494)
109. Acevedo, Cristian A.; Sánchez, Elizabeth; Díaz-Calderón, Paulo; Blaker, Jonny J.; Enrione, Javier; and Quero, Franck. 2017. "Synergistic effects of crosslinking and chitosan molecular weight on the microstructure, molecular mobility, thermal and sorption properties of porous chitosan/gelatin/hyaluronic acid scaffolds." *Journal of Applied Polymer Science* 134 (18).

- [https://doi.org/10.1002/app.44772.](https://doi.org/10.1002/app.44772)
[https://onlinelibrary.wiley.com/doi/abs/10.1002/app.44772.](https://onlinelibrary.wiley.com/doi/abs/10.1002/app.44772)
110. Zheng, Zhenhuan; Zhang, Ling; Kong, Lijun; Wang, Aijun; Gong, Yandao; and Zhang, Xiufang. 2009. "The behavior of MC3T3-E1 cells on chitosan/poly-L-lysine composite films: Effect of nanotopography, surface chemistry, and wettability." *Journal of Biomedical Materials Research Part A* 89A (2): 453-465. [https://doi.org/10.1002/jbm.a.31979.](https://doi.org/10.1002/jbm.a.31979)
[https://onlinelibrary.wiley.com/doi/abs/10.1002/jbm.a.31979.](https://onlinelibrary.wiley.com/doi/abs/10.1002/jbm.a.31979)
111. Yang, Lanti; Fitié, Carel F. C.; Van Der Werf, Kees O.; Bennink, Martin L.; Dijkstra, Pieter J.; and Feijen, Jan. 2008. "Mechanical properties of single electrospun collagen type I fibers." *Biomaterials* 29 (8): 955-962. [https://doi.org/10.1016/j.biomaterials.2007.10.058.](https://doi.org/10.1016/j.biomaterials.2007.10.058)
[https://dx.doi.org/10.1016/j.biomaterials.2007.10.058.](https://dx.doi.org/10.1016/j.biomaterials.2007.10.058)
112. Sridhar, Radhakrishnan; Madhaiyan, Kalaipriya; Sundarajan, Subramanian; Góra, Aleksander; Venugopal, Jayarama Reddy; and Ramakrishna, Seeram. 2014. "Cross-linking of protein scaffolds for therapeutic applications: PCL nanofibers delivering riboflavin for protein cross-linking." *J. Mater. Chem. B* 2 (12): 1626-1633. [https://doi.org/10.1039/c3tb21789b.](https://doi.org/10.1039/c3tb21789b)
[https://dx.doi.org/10.1039/C3TB21789B.](https://dx.doi.org/10.1039/C3TB21789B)
113. Jeon, Oju; Song, Su Jin; Lee, Kee-Jung; Park, Moon Hyang; Lee, Soo-Hong; Hahn, Sei Kwang; Kim, Sungjee; and Kim, Byung-Soo. 2007. "Mechanical properties and degradation behaviors of hyaluronic acid hydrogels cross-linked at various cross-linking densities." *Carbohydrate Polymers* 70 (3): 251-257. [https://doi.org/10.1016/j.carbpol.2007.04.002.](https://doi.org/10.1016/j.carbpol.2007.04.002)
114. PourAkbar Saffar, Kaveh; Arshi, Ahmad Reza; JamilPour, Nima; Najafi, Ahmad Raeisi; Rouhi, Gholamreza; and Sudak, Les. 2010. "A cross-linking model for estimating Young's modulus of artificial bone tissue grown on carbon nanotube scaffold." *Journal of Biomedical Materials Research Part A* 94A (2): 594-602. [https://doi.org/10.1002/jbm.a.32737.](https://doi.org/10.1002/jbm.a.32737)
[https://onlinelibrary.wiley.com/doi/abs/10.1002/jbm.a.32737.](https://onlinelibrary.wiley.com/doi/abs/10.1002/jbm.a.32737)
115. Suto, S.; and Yoshinaka, M. 1993. "Chemical cross-linking of cholesteric liquid-crystalline hydroxypropyl cellulose with dialdehydes." *Journal of Materials Science* 28 (17): 4644-4650. [https://doi.org/10.1007/bf00414253.](https://doi.org/10.1007/bf00414253)
[https://dx.doi.org/10.1007/BF00414253.](https://dx.doi.org/10.1007/BF00414253)

116. Seredych, Mykola; Mikhalovska, Lyuba; Mikhalovsky, Sergey; and Gogotsi, Yury. 2018. "Adsorption of Bovine Serum Albumin on Carbon-Based Materials." *C* 4 (1). <https://doi.org/10.3390/c4010003>.
117. Fallica, Brian; Maffei, Joseph S.; Villa, Shaun; Makin, Guy; and Zaman, Muhammad. 2012. "Alteration of Cellular Behavior and Response to PI3K Pathway Inhibition by Culture in 3D Collagen Gels." *PLoS ONE* 7 (10): e48024. <https://doi.org/10.1371/journal.pone.0048024>.
<https://dx.doi.org/10.1371/journal.pone.0048024>.
118. Luca, Anna C.; Mersch, Sabrina; Deenen, René; Schmidt, Stephan; Messner, Isabelle; Schäfer, Karl-Ludwig; Baldus, Stephan E.; Huckenbeck, Wolfgang; Piekorz, Roland P.; Knoefel, Wolfram T.; Krieg, Andreas; and Stoecklein, Nikolas H. 2013. "Impact of the 3D Microenvironment on Phenotype, Gene Expression, and EGFR Inhibition of Colorectal Cancer Cell Lines." *PLoS ONE* 8 (3): e59689. <https://doi.org/10.1371/journal.pone.0059689>.
<https://dx.doi.org/10.1371/journal.pone.0059689>.
119. Türker, Esra; Yildiz, Ümit Hakan; and Arslan Yildiz, Ahu. 2019. "Biomimetic hybrid scaffold consisting of co-electrospun collagen and PLLCL for 3D cell culture." *International Journal of Biological Macromolecules* 139: 1054-1062. <https://doi.org/10.1016/j.ijbiomac.2019.08.082>.
<https://dx.doi.org/10.1016/j.ijbiomac.2019.08.082>.
120. Holley, R. W.; and Kiernan, J. A. 1968. ""Contact inhibition" of cell division in 3T3 cells." *Proceedings of the National Academy of Sciences* 60 (1): 300-304. <https://doi.org/10.1073/pnas.60.1.300>. <https://dx.doi.org/10.1073/pnas.60.1.300>.
121. Zeiger, Errol; Gollapudi, Bhaskar; and Spencer, Pamela. 2005. "Genetic toxicity and carcinogenicity studies of glutaraldehyde—a review." *Mutation Research/Reviews in Mutation Research* 589 (2): 136-151. <https://doi.org/https://doi.org/10.1016/j.mrrev.2005.01.001>.
<http://www.sciencedirect.com/science/article/pii/S1383574205000049>.
122. Fürst, Walter; and Banerjee, Asmita. 2005. "Release of Glutaraldehyde From an Albumin-Glutaraldehyde Tissue Adhesive Causes Significant In Vitro and In Vivo Toxicity." *The Annals of Thoracic Surgery* 79 (5): 1522-1528. <https://doi.org/https://doi.org/10.1016/j.athoracsur.2004.11.054>.
<http://www.sciencedirect.com/science/article/pii/S0003497504023264>.

123. Sung, Hsing-Wen; Huang, Rong-Nan; Huang, Lynn L. H.; and Tsai, Chen-Chi. 1999. "In vitro evaluation of cytotoxicity of a naturally occurring cross-linking reagent for biological tissue fixation." *Journal of Biomaterials Science, Polymer Edition* 10 (1): 63-78. <https://doi.org/10.1163/156856299x00289>.
<https://dx.doi.org/10.1163/156856299X00289>.
124. Kisiday, J.; Jin, M.; Kurz, B.; Hung, H.; Semino, C.; Zhang, S.; and Grodzinsky, A. J. 2002. "Self-assembling peptide hydrogel fosters chondrocyte extracellular matrix production and cell division: Implications for cartilage tissue repair." *Proceedings of the National Academy of Sciences* 99 (15): 9996-10001.
<https://doi.org/10.1073/pnas.142309999>.
<https://dx.doi.org/10.1073/pnas.142309999>.
125. Park, Sang-Hyug; Gil, Eun Seok; Shi, Hai; Kim, Hyeyon Joo; Lee, Kyongbum; and Kaplan, David L. 2010. "Relationships between degradability of silk scaffolds and osteogenesis." *Biomaterials* 31 (24): 6162-6172.
<https://doi.org/10.1016/j.biomaterials.2010.04.028>.
<https://dx.doi.org/10.1016/j.biomaterials.2010.04.028>.